



MoS₂-based nanocomposites: synthesis, structure, and applications in water remediation and energy storage: a review

M. I. A. Abdel Maksoud¹ · Ahmed G. Bedir² · Mohamad Bekhit¹ · Marwa Mohamed Abouelela^{2,3} · Ramy Amer Fahim¹ · A. S. Awed⁴ · Sayed Y. Attia⁵ · Said M. Kassem¹ · M. Abd Elkodous^{3,6} · Gharieb S. El-Sayyad⁷ · Saad G. Mohamed⁵ · Ahmed I. Osman⁸ · Ala'a H. Al-Muhtaseb⁹ · David W. Rooney⁸

Received: 24 June 2021 / Accepted: 9 July 2021 / Published online: 20 July 2021
© The Author(s) 2021

Abstract

The world is currently facing critical water and energy issues due to the growing population and industrialization, calling for methods to obtain potable water, e.g., by photocatalysis, and to convert solar energy into fuels such as chemical or electrical energy, then storing this energy. Energy storage has been recently improved by using electrochemical capacitors and ion batteries. Research is actually focusing on the synthesis of materials and hybrids displaying improved electronic, physiochemical, electrical, and optical properties. Here, we review molybdenum disulfide (MoS₂) materials and hybrids with focus on synthesis, electronic structure and properties, calculations of state, bandgap and charge density profiles, and applications in energy storage and water remediation.

Keywords Water treatment · MoS₂ · MoS₂-based hybrids · Energy storage · Supercapacitors · Two-dimensional layered nanomaterials

Abbreviations

EDLCs	Electrochemical double-layer capacitors
HOMO	Highest occupied molecular orbital
LUMO	Lowest unoccupied molecular orbital
MHCS	Mesoporous hollow carbon spheres
NDMA	N-Nitrosodimethylamine
DOS	Projected density of states

Introduction

Two-dimensional layered nanomaterials have drawn much research consideration from their interesting physicochemical properties such as the extraordinary electrical, optical, and physical characteristics that arose from their ultra-thin construction and their quantum size impact. Among these two-dimensional layered materials, transition metal dichalcogenides are a set of substances with several attractive

✉ M. I. A. Abdel Maksoud
muhamadmqsod@gmail.com

✉ Ahmed I. Osman
aosmanahmed01@qub.ac.uk

¹ National Center for Radiation Research and Technology (NCRRT), Egyptian Atomic Energy Authority (EAEA), Nasr City, Cairo, Egypt

² Egyptian Petroleum Research Institute (EPRI), Nasr City, Cairo 11727, Egypt

³ Department of Electrical and Electronic Information Engineering, Toyohashi University of Technology, 1-1 Hibarigaoka, Tempaku-cho, Toyohashi, Aichi 441-8580, Japan

⁴ Higher Institute for Engineering and Technology at Manzala, Manzala, Egypt

⁵ Tabbin Institute for Metallurgical Studies (TIMS), Tabbin, Helwan 109, Cairo 11421, Egypt

⁶ Center for Nanotechnology (CNT), School of Engineering and Applied Sciences, Nile University, Sheikh Zayed, Giza 16453, Egypt

⁷ Drug Radiation Research Department, National Center for Radiation Research and Technology (NCRRT), Egyptian Atomic Energy Authority (EAEA), Nasr City, Cairo, Egypt

⁸ School of Chemistry and Chemical Engineering, Queen's University Belfast, Belfast BT9 5AG, Northern Ireland, UK

⁹ Department of Petroleum and Chemical Engineering, College of Engineering, Sultan Qaboos University, Muscat, Oman

characteristics for fundamental research and promising applicability. The transition metal dichalcogenides have the general formulation notated as MX_2 , in which M stands for the transition metal atom, and X represents the chalcogen. They consist of weakly joined sandwich-like layers (X-M-X). The neighboring layers are connected via van der Waals forces. In each layer, M is bonded to X atoms by covalent bonds. Exfoliation of the bulk substances into a few layers mostly conserves their characteristics and also leads to additional features due to restriction impacts. These materials have sparked numerous interest due to their unique physical characteristics and special applications (Jayabal et al. 2017; Chhowalla et al. 2013; Arshad et al. 2019). In opposition to graphene possessing a zero bandgap, transition metal dichalcogenides have a bandgap comparable to Si or GaAs and offer an interesting ability for reducing the size of the technology and semiconductor to the nanoscale. Additionally, many years ago, transition metal dichalcogenides affirmed their applications in many fields like solid-state lubricants, rechargeable batteries and photovoltaic devices (Gourmelon et al. 1997; Fortin and Sears 1982; Gupta et al. 2020; Abdel Maksoud et al. 2021).

Among the family of transition metal dichalcogenides, molybdenum disulfide (MoS_2) has recently been broadly studied in many research fields such as: lubrication, supercapacitors, lithium-ion batteries and drug delivery, because of its extraordinary activity and its perfect two-dimensional structure. MoS_2 has also exhibited excellent performance in environmental remediation applications such as electro- or photocatalysis, adsorption of heavy metals, ammonium nitrogen removal, and membrane-based separation (Kalin et al. 2012; Lin et al. 2015; Chang et al. 2016; Wang and Mi 2017; Zhang et al. 2017a; Fan et al. 2019; Liu et al. 2018a; Xing et al. 2018; Sheng et al. 2019; Zhou et al. 2020).

Herein, we reported the recent advances in MoS_2 material and its hybrid forms for energy applications in detail. Firstly, the controllable synthesis of MoS_2 , divided into top-down and bottom-up approaches, was reviewed. Then, its unique electronic structure and its associated characteristics were analyzed. After that, the density-functional theory calculations were utilized to identify MoS_2 density of state, bandgap, charge density profiles, and work function. Later, MoS_2 -based hybrids for water remediation were presented. Then, MoS_2 -based hybrids for energy storage applications were presented, which started with supercapacitors and were then followed by three types of ion batteries.

Structure and controllable synthesis of MoS_2

MoS_2 structure is a trigonal prismatic of S–Mo–S arrangement having two atomic planes of S surrounding an atomic plane of Mo in a sandwich-like structure. The length of

the Mo–S bond is 1.54 Å, while the S–S bond is 3.08 Å in length. Accordingly, the MoS_2 single-layer thickness is about 0.62 nm (Late et al. 2012). The MoS_2 semiconductor has an indirect bandgap of 1.2 eV, while the direct bandgap of a single-layered MoS_2 semiconductor is 1.8 eV (Arshad et al. 2019). In addition, although multilayer MoS_2 is not photoluminescent, exfoliation-induced changes in its electronic structure lead to photoluminescent behavior in exfoliated monolayers (Splendiani et al. 2010).

MoS_2 has three main phases (Ding et al. 2016; Ali et al. 2018): 1 T MoS_2 , 2H MoS_2 and 3R MoS_2 (Fig. 1). In the 1 T MoS_2 unit cell, the sulfur atoms coordinate the molybdenum atoms octahedrally; 2H MoS_2 has the molybdenum atom coordinated by two S–Mo–S units in a trigonal prismatic geometry for each elemental cell; and with the same geometry as the 2H MoS_2 , coming to the third phase the 3R MoS_2 but three units of S–Mo–S are directed along the c-axis instead of two. The 1 T phase has metallic properties, while the 2H and the 3R phases are semiconductors (Acerce et al. 2015a; Toh et al. 2017; Wang et al. 2017a). Natural MoS_2 exists as the thermodynamically favored 2H phase, while the 1 T phase does not occur naturally and is usually obtained from lithium-intercalated 2H- MoS_2 interlayers by chemical exfoliation (Lukowski et al. 2013; Eda et al. 2011; Wang et al. 2012; Fan et al. 2015). Furthermore, the monolayered 1 T- MoS_2 is metastable from the thermodynamic perspective, which tends to restructure to form the more stable phase, 2H- MoS_2 . Consequently, the 1 T phase commonly happens in a multiphase form along with the 2H phase (Chhowalla et al. 2013; Chua et al. 2016; Chou et al. 2015; Song et al. 2015).

2H- MoS_2 and their composites were extensively studied for energy-related applications, especially supercapacitors, due to their fascinating electronic, optical, catalytic characteristics, and considered the most common form in nature. (Ding et al. 2016; Xiao et al. 2017a; Liu et al. 2016; Shi et al. 2016). However, 2H- MoS_2 is less competitive to graphene-based materials in energy storage applications due to their semiconductivity and bandgap (≈ 1.3 – 1.9 eV) (Yang et al., 2013; Chen and McDonald 2016). From another point of view, 1 T- MoS_2 is metallic and superior to 2H- MoS_2 in electronic conductivity (nearly higher 107 times) that making 1 T- MoS_2 deliver an excellent platform or stage for electron transfer; this is the first point. Secondly, the abundance of in-plane active sites (in contrast to that in 2H phase, which assembled on the edges) affords an improved reactivity. Thirdly, the improved interlayer spacing (≈ 1 nm) offers fast and wide ion-diffusion channels. Owing to the previous qualities, enhanced energy materials can be fabricated and designed by amendable structures of MoS_2 (1 T phase) via doping, stress, deflection, intercalation, or heterojunction (Acerce et al. 2015b; Wang et al. 2017b; Ambrosi et al. 2015).

Where in the 1T MoS₂ unit cell, the sulfur atoms coordinate the molybdenum atoms octahedrally, in 2H MoS₂, the molybdenum atom is coordinated by two S–Mo–S units in a trigonal prismatic geometry for each elemental cell; with the same geometry as the 2H MoS₂, coming to the third phase the 3R MoS₂ but three units of S–Mo–S are directed along the c-axis instead of two.

Many approaches have been established to synthesize MoS₂ nanostructures. Generally, the methods for synthesizing MoS₂ nanoparticles can usually involve either a “top-down” approach or a “bottom-up” approach.

Top-down

The “top-down” strategy is an exfoliation process of bulk layered materials which widely includes mechanical, liquid, and electrochemical exfoliation.

Mechanical exfoliation

Mechanical exfoliation or simply “micromechanical cleavage” was first used as an approach to prepare two-dimensional nanosheets from bulk layered materials by mechanical fragmentation as was applied to graphene (Late et al. 2012; Novoselov et al. 2004; Novoselov et al. 2005). Mechanical exfoliation, also known as the Scotch-tape method, means “detaching” or “peeling” of bulk crystals with adhesive tape or bulk crystals rubbing against a solid surface (Novoselov 2011; Li et al. 2014). The cleaning of the substrate before sticking the tape onto it gives better results (Huang et al., 2015a). Often, using a film of gold as an intermediary substrate enhances mechanical exfoliation because gold has a good tolerance for chalcogens, which effectively overcomes the van der Waals force among the top layer and the residue of the crystal (Magda et al. 2015; Desai et al. 2016).

Mechanical exfoliation, which does not require costly or specialized machinery, is the most effective way to create the cleanest, most crystalline, and atomically thin nanosheets of layered materials. (Kolobov and Tominaga 2016). Nevertheless, since this technique cannot be used for large-scale processing, it can only be used to prepare samples for research purposes.

Nanomechanical exfoliation, an expansion of mechanical exfoliation, has recently been documented to generate high-quality MoS₂ nanosheets having a definite layer. A particularly acute tungsten probe of a tip diameter of about 10 nm is used in nanomechanical exfoliation to peel nanosheets of a thick flake of MoS₂ stacked on the substrate with an edge-on alignment. Piezoelectric actuators power the tungsten probe, and the entire process is observed in real-time using a high-resolution transmission electron microscope (Tang et al. 2014). Miyake and Wang used an atomic force microscope

to conduct nanometer-scale mechanical processing on a Si chip of less than 50 nm in radius (Miyake and Wang 2015).

Liquid exfoliation

There are two types of liquid exfoliation: sonication and shear force-assisted.

Sonication-assisted liquid exfoliation Sonication has also been shown to aid in the exfoliation of layered substances in liquid suspensions that may assist in intercalating the barrier of activation (Nicolosi et al. 2013). Based on high sonication power and constituents (ions, polymers, surfactants) that reinforce the adhesion on the stratified MoS₂ surface and facilitate their exfoliation, the process yields an excellent yield of the level of dispersion of few-layered MoS₂.

A wide variety of organic solvents identified the top 20 solvents for sonication-assisted MoS₂ exfoliation was investigated. In ultraviolet–visible spectra, the absorbance values for solvents are at 672 nm (which is excitonic peak characteristic for a few layered MoS₂) divided by the length of the cell. The $A/l = \epsilon C$ relationship, also identified as Beer–Lambert law, shows that the absorbance value is directly linear with concentration, where ϵ is the extinction coefficient (Coleman et al. 2011). On the other hand, transition metal dichalcogenides nanosheets prefer to accumulate unless a surfactant or polymer is used since they are still hydrophobic even after being exfoliated in H₂O (i.e., through a long sonication period) (Samadi et al. 2018).

With the assistance of polyvinylpyrrolidone, (Liu et al. 2012) published a simple method to exfoliate and disperse MoS₂. Polyvinylpyrrolidone-coated MoS₂ nanosheets that result are distributed in the ethanol, making preparation and system fabrication of thin film using the technique of solution processing much more straightforward.

To exfoliate MoS₂, (Xuan et al. 2017) used sodium alginate as a natural polysaccharide. The sonicating process lasted for 5.5 h, and during this period, a stirring was occurred for 1 min every 20 min to make the suspensions homogeneous.

To synthesize MoS₂ nanosheets, (Liu et al. 2018b) demonstrated a simple exfoliation process with salt in the liquid phase. They used isopropyl alcohol as a medium for exfoliation and salts like sodium tartrate, potassium sodium tartrate, and potassium ferrocyanide as assistants. These salts have an effective impact on the exfoliation of MoS₂ in isopropyl alcohol. In the isopropyl alcohol-K₄Fe(CN)₆ method, it was discovered that (K₄Fe(CN)₆) could increase the efficiency of exfoliation by about 73 times, accompanied by obtaining MoS₂ nanosheets dispersion with concentrations of 0.240 mg mL⁻¹.

Yuwen et al. (2016) claimed that via normal butyllithium as a lithiation mediator, ultrasonically enhanced Li

intercalation could generate MoS₂ nanosheets of matching morphology and features like conventional methods of lithium intercalation, which was produced by the work of (Joensen et al. 1986). Furthermore, ultrasonication-enhanced lithium intercalation will significantly reduce reaction time and yield high-yielding materials (Yuwen et al. 2016).

Nevertheless, the exfoliation method based on normal butyllithium intercalation has many drawbacks, including a long lithiation time, little yield, and the size of the flake is in the submicron range. Using lithium, potassium, and sodium naphthalenide, (Zheng et al. 2014) established a better methodology to exfoliate MoS₂ monolayered. The hydrazine (N₂H₄) along with sodium naphthalenide was used as double intercalants in this study to widen the gaps between interlayers of bulk MoS₂, which is then exfoliated in water. A redox rearrangement model may describe the expansion process, in which part of the N₂H₄ is oxidized to N₂H₅⁺ during intercalation. The intercalated N₂H₅⁺ is thermally unstable and will decompose into N₂, NH₃, and H₂ when the intercalated MoS₂ films are heated to high temperatures. As intercalated N₂H₄ molecules decompose and gasify, the sheets of MoS₂ extend by 100 times more than their initial length. The expanded crystal of MoS₂ is then undergoing intercalation with naphthalenide alkaline solution in a second step. Finally, to prevent sheet fragmentation, the intercalated MoS₂ is exfoliated by submerging it in low-power ultrasonic water. Sodium ions have a much greater ionic radius than lithium ions, allowing for a more significant expansion of interlayer space.

Furthermore, compared to Li_x MoS₂, Na_x MoS₂ reacts more aggressively with water, resulting in extra H₂ emitted in a shorter period, promoting exfoliation. This method achieved high-efficiency exfoliation, with lateral widths of around 10 μm in 80 percent of single-layer MoS₂ sheets, approximately ten times greater than flakes identified using standard butyl lithium procedures. Some sodium-containing surfactants, such as sodium dodecyl benzene sulfonate, can be used as intercalation agents for MoS₂ exfoliation besides sodium naphthalenide (Guan et al. 2018).

Guan et al. (2015) published a method for exfoliating MoS₂ in an aqueous solution with high yields using a particular protein, bovine serum albumin. They discovered that bovine serum albumin could serve as an efficient exfoliating agent as well as a stabilizer, preventing monolayer nanosheets from reaggregating (Guan et al. 2015). The yield of MoS₂ nanosheets (1.36 mg/mL) was significantly higher than 0.3 mg/mL of N-methylpyrrolidone agent (Coleman et al. 2011) and 0.5 mg/mL in case of use of surfactants (Smith et al. 2011).

Owing to the long period of induced scission and the creation of non-homogeneous MoS₂ layers, the resulting MoS₂ nanosheets have a relatively small dimension, which is a disadvantage in sonication-assisted exfoliation. Recently, a

blend of bath and probe sonication results in a significantly faster exfoliation than bath sonication alone recorded by (Kaushik et al. 2020).

It is important to mention another method based on the sonication process and water expansion upon freezing called the water freezing–thawing approach. This approach is focused on the freezing behavior of water (Matsumoto et al. 2002), whereby when water freezes, it exerts a powerful extrusion force, causing pressures of about 2500 bar in a closed structure (Yoo et al. 2009), which can resolve the van der Waals interaction among neighboring layers in two-dimensional materials. The expansion of layered materials structure occurs as they thaw, ascribing to liquid water absorption. Exfoliation of two-dimensional nanosheets would be enhanced by repeated freezing and thawing cycles. H₂O can soak into the interlayers of graphite, according to (Algara-Siller et al. 2015). A moderate H₂O freeze–thaw method and polyvinylpyrrolidone as a stabilizer were used to prepare a few and monolayer two-dimensional nanosheets with no creation of scrolls or flaws. The results show that this method is efficient for exfoliating MoS₂ and MoO₃ nanosheets with fewer than 5 atomic layers, yielding around 32, 42, and 25 percent, respectively, upon 30 cycles of freeze–thaw. While time wasting, this method is economical and requires simple instrumentation, and it has much potential for two-dimensional exfoliating materials on a large scale (Zhu et al. 2019).

Shear force-assisted liquid exfoliation In this method, bulk MoS₂ is exfoliated in suitable surfactant solutions or organic solvents using mechanical mixers with a high speed, like shearing laboratory mixers, ball milling, and even kitchen blenders produce local shear rate in a mixing vessel (usually with 1 L or higher capacity). A mixture of ball milling with low-energy besides sonication was used to report a simple, effective, and scalable method for MoS₂ exfoliation. Ball milling produces compression and shear forces on layered materials, causing their exfoliation to form two-dimensional nanosheets from the edge outer surfaces. The MoS₂ suspension as-fabricated was 0.8 mg/mL. The nanosheets of MoS₂ with sizes in the range of 50–700 nm and thicknesses range of 1.2–8 nm were imaged using atomic force microscopy (Yao et al. 2012).

Sun et al. (2018) successfully fabricated MoS₂/graphene nanosheets using hydrate salts of potassium sodium tartrate to ball mill both bulk MoS₂ and graphite. Intercalating agent potassium sodium tartrate dissociates into K⁺, Na⁺, and tartrate linker, which could then be intercalated into graphite and bulky MoS₂, facilitating exfoliation (Sun et al. 2018). It is illustrated the exfoliated MoS₂ nanosheets with a size ≈ of 100 nm and thickness of about 2–5 layers.

A kitchen blender was used to demonstrate exfoliation shear of MoS₂ nanosheets on a large scale in a surfactant.

They achieved 0.4 mg/mL concentrations and 1.3 mg/min output rates by optimizing mixing factors (time of mixing, rotor speed, MoS₂ concentration, and solution volume). Both length and thickness could be regulated from 40–220 nm in length and about 2–12 layers in thickness by changing the surfactant concentration (Varrla et al. 2015).

Electrochemical exfoliation

The electrochemical exfoliation method is a promising process, usually carried out in mild conditions, simple, repeatable, and appropriate for large-scale production (Ji et al. 2019). An electrochemical method of lithium intercalation was used to exfoliate bulk layered MoS₂ (cathodic exfoliation of MoS₂). Metal foils of lithium and MoS₂ were used for cathodic and anodic poles, respectively, in this process. Lithium ions are intercalated within the bulk layered MoS₂ when discharging at constant current, weakening the van der Waals force among layers. After being washed with acetone, the intercalated compounds are ultrasonicated in H₂O or C₂H₅OH to exfoliate and extract the two-dimensional nanosheets (Zeng et al. 2011). While this procedure can exfoliate multi-layered compounds into monolayers (for example, single-layer MoS₂), it is hard to extract the residual lithium doping effect, which causes the MoS₂ nanosheets to lose their semiconducting properties. (Eda et al. 2011; Py and Haering 1983). Liu et al. have used electrochemical anodic exfoliation of bulk MoS₂ to obtain thin nanosheets of MoS₂ with high quality (Liu et al. 2014a). The anode, counter electrode, and electrolyte were made up of a bulk layered MoS₂ crystal, a Pt thread, and a 0.5 M aqueous Na₂SO₄ solution, respectively. Exfoliated monolayer and few-layer MoS₂ nanosheets with lateral sizes up to 50 nm have excellent consistency and intrinsic structure.

Bottom-up methods

Among these bottom-up methods, the hydro/solvothermal, microwave, and chemical vapor deposition synthesis routes are widely applied in MoS₂ nanosheets synthesis.

Hydro/solvothermal synthesis

This method is a traditional wet-chemical synthesis technique that operates at a high temperature of vapor pressure in a sealed autoclave to produce high yield, controllable size, and homogeneous layer thickness of nanomaterial. The only difference between hydrothermal and solvothermal synthesis is that the former uses an aqueous precursor (Gupta et al. 2015; Tan et al. 2017). The hydro/solvothermal synthesis method can be preceded with the assistant of ionic liquids. (Ma et al. 2008) used a hydrothermal process with 1-butyl-3-methylimidazolium tetrafluoroborate to

make micro-spheres of MoS₂ with 2.1 μm in diameter. (Du et al. 2015) prepared MoS₂ nanospheres via a solvothermal method with the assistance of an ionic liquid. In dimethyl formamide/water mixed solvents, they used a template of 1-ethyl-3-methylimidazolium bromide. The ratio of dimethyl formamide to H₂O has an important influence on the morphology and size of MoS₂ produced. (Pirath et al. 2021) used a surfactant-assisted hydrothermal system to make few-layered MoS₂ nanosheets. The results indicated that the synthesized MoS₂ nanosheets had a petal-like morphology.

Microwave synthesis

The microwave synthesis technique for synthesizing MoS₂ is simple, secure, and time and energy-efficient (Lee et al. 2019; Baghbanzadeh et al. 2011). Nanotubes and fullerene-like MoS₂ nanoparticles were created using a method of microwave-assisted processing path. The amorphous powders of MoS₂ were calcined for 2 h at 600 °C in an argon atmosphere. Structural analysis shows that after 200 s of microwave irradiation, the synthesized MoS₂ is like fullerene in its structure with orientated at random, strongly doubled up layers of MoS₂ ordered in short range, whereas a longer time (600 s) of irradiation provided nanostructures similar to nanotube and fullerene in their morphology (Panigrahi and Pathak 2011). A microwave-assisted hydrothermal route was used to build MoS₂/poly(ethylene glycol) nanoflowers. For 10 min, the precursors of MoS₂ were subjected to microwave irradiation at 220 °C. The nanoflowers form of MoS₂/poly(ethylene glycol) comprises multi-layers of MoS₂ nanosheets (Sun et al. 2019).

A direct MoS₂ growth on graphene substrate was reported by employing a safe, simple, scalable ultrafast, and efficient microwave-initiated method that did not involve inert gas (Sarwar et al. 2020). The dried blend of (NH₄)₂MoS₄-graphene-CS₂ was microwave irradiated for 60 s in a microwave oven for home use (2.45 GHz, 1250 W). Graphene was used as a substrate, absorbing microwave energy and converting it to heat, which caused the reduction of (NH₄)₂MoS₄ to MoO₂, which was then transformed to MoS₂ dispersed on the graphene substrate (Sarwar et al. 2020).

MoS₂ nanosheets use conventional hydrothermal and microwave methods and compares their electrocatalytic performance for hydrogen evolution. The obtained MoS₂ from both ways has similar crystal structural characteristics despite the 24-h hydrothermal synthesis process; microwave-assisted synthesis takes just 30 min. Both techniques give thin and combined nanosheets, but the microwave-formed MoS₂ nanosheets have a smoother edge and less crumpled shape. Both MoS₂ nanosheets were in nearly similar electrocatalytic performance (Solomon et al. 2020).

Chemical vapor deposition methods

On substrates such as SiO₂/Si (Kang et al. 2015), sapphire (Yu et al. 2017), and glass (Yang et al. 2018; Yang et al. 2019), the chemical vapor deposition method is a promising bottom-up synthesizing of controllable size and thickness of MoS₂ with high quality. The correct precursors, MoO₃ and S, are first evaporated at a certain temperature in the chemical vapor deposition technique. The S vapor then gains access to the MoO₃ by passing through an inert gas such as argon (Lee et al. 2017). MoO₃ film is sulfurized in this case, and MoS₂ is formed on a SiO₂ substrate. It should be noted that the chemical vapor deposition condition can be used to monitor the thickness and size of the as-synthesized MoS₂ film. MoS₂ films made by chemical vapor deposition have a high degree of crystalline structure (Lee et al. 2017).

However, the small surface area of traditional chemical vapor deposition growth strategies makes mass development of monolayer or few layers MoS₂ impossible. The MoS₂ nanosheets have been synthesized by using micro-sized cubic NaCl crystal powders as a template. They chose NaCl as a substrate because it is inexpensive and scalable, with high chemical stability, allowing batch production of highly crystalline MoS₂ powders. With raising the temperature from 500 to 650 °C, the average nanosheets thickness of MoS₂ increases from 1.93 to 2.62 nm, and the suitable growth range was set as 550–650 °C (Zhu et al. 2020).

Density-functional theory calculations of MoS₂

The electronic characteristics of MoS₂, such as the bandgap, density of state, highest occupied molecular orbital HOMO and lowest unoccupied molecular orbital LUMO, charge density diagram, and work function, were studied via density-functional theory. The density-functional theory estimate of square nanotubes of MoS₂ was investigated by (Zhang et al. 2021). They discovered two groups of 4 bands near the Fermi level having identical energies. States at the square's 4 corners are defined by the conduction band minimum and valence band limit of nanotubes (see Fig. 2). The direct bandgap of the square nanotube is 0.23 eV in armchair structure and having an indirect bandgap of 0.28 eV in zigzag structure as a semiconductor. As the diameter grows, the bandgap grows as well. These values are much smaller than those of cylinder-shaped nanotubes: 0.4 eV, and monolayers MoS₂: 1.738 eV (Seifert et al. 2000) due to the electronic states close to the 5-coordinated molybdenum atoms and the 2-coordinated sulfur atoms at the corners. In the top view and side view of a two-dimensional deformation charge density map of both cylinder and square nanotubes, thick and thin circles reflect Mo and S atoms, respectively.

In the top view and side view of a two-dimensional deformation charge density map of both cylinder and square nanotubes, thick and thin circles reflect Mo and S atoms, respectively. States at the square's 4 corners are defined by the conduction band minimum and valence band limit of nanotubes.

By the Brillouin zone's high symmetry K point, the direct bandgap of stacked vertically few-layer MoS₂ drastically alters with thicknesses, according to (Majee et al. 2020). The valence band of 0.171 eV splits at the K level, according to a hypothetical band schematic for six layers of MoS₂, yielding two distinct excitons (A and B). The A and B were determined to have values of 1.73 and 1.90 eV, respectively. The existence of indirect transfers between the valence band maxima at high points of symmetry and the conduction band minima among the K points, based on the literature, is also suggested by the band structure estimation.

The optical band gap of MoS₂/ZrO₂ was studied (Eid and Al-Hossainy 2021) in the high absorption area for indirect and direct, allowing transition. The E_g can be computed by plotting (αhν)² versus (hν) and then extrapolation of the linear curve parts to zero absorption (Al-Hossainy et al. 2018). The E_g of [propylene glycol-MoS₂/ZrO₂]^C and [propylene glycol -MoS₂]^C hybrid nanofluid films was 2.355 eV and 2.562 eV, respectively. This decrease in E_g resulted from the formation of new energy levels in E_g, attributed to increased defects that required electrons to be transferred from the valence to the conduction band, lowering bandgap as the loading was 0.50% wt. [ZrO₂]. In universal reactivity descriptors, by using quantum predictions, HOMO and LUMO are essentially standard. The stability of a molecule is determined by the difference in energy between frontier molecular orbitals. This plays a crucial part in the conductivity measurement of e-s, aiding in understanding electricity transport. The energy of HOMO and LUMO values is often negative, indicating that isolated compounds have stabilized. Aromatic compounds are predicted to target electrophilic locations based on the observed frontier molecular orbitals. These orbitals must be combined in a variety of responses.

The density of states of MoS₂ pristine phases and their intercalated Cs ion equivalents were investigated by (Ali et al. 2021). It is worth noting that the Mo atom's d orbital contributes the most to the density of state total, whereas Cs atom contributes a little. The influence of a Cs atom, on the other hand, was visible in the reorganization of the density of state for the 3 phases. The total density of state for the three phases increased as a result of the Cs intercalation. Furthermore, the intercalation with Cs caused a phase change thermodynamically in the 3R and 2H phases by means of moving Fermi level near the valence band, converting the phase from semiconductor to metallic (Vatamanu et al. 2015; Azmi et al. 2016). Quantum capacitance of the MoS₂ intercalated with Cs would be calculated using the

density of state because it represents the quantum existence of materials. Estimation of quantum capacitance is critical when scheming electrodes for supercapacitor because it provides data about the electronic reaction of material when exposed to voltage and influences the electrode's electrical double-layer action. The useful potential for MoS₂ ranges from -0.5 – 0.5 V in this sample of aq. neutral electrolytes, which is the agreed potential window experimentally (Azmi et al. 2016). The Fermi level is the potential at zero charge, where the supercapacitor is unable to accept any extra charges in quantum capacitance calculations. The computed potential at zero charge shows the capacitance at no applied voltage since rich occupied states will accommodate charges, as shown by their quantum capacitance. The quantum capacitance of the three phases is raised by Cs intercalation to 2530, 3180, and 3257 F/g, respectively, for the 1 T, 2H, and 3R phases. The massive rise in quantum capacitance is due to the change in state density for 3R and 2H phases toward metallic existence.

Furthermore, the quantum capacitance improvement was only observed in the positive potential window, implying that 2H-MoS₂ could be used in asymmetric supercapacitor systems as a positive electrode. Cs-MoS₂ has a quantum capacitance that is 200% greater than doped graphene. In comparison with pristine MoS₂, the difference in charge density was calculated. Charge transfer adsorption between Cs atoms and MoS₂ is signaled by the charges in the bonds between the Cs and S atoms. Bader charge analysis was used to investigate the charge transfer quantitatively (Tang et al. 2009). The Cs ion passes a charge to the MoS₂ system in the 1 T, 3R, and 2H stages, respectively, of 0.85, 0.86, and 0.86 *el*, indicating the creation of ionic bonding.

Subramanian et al. (2020) predicted that the Schottky barrier at the epitaxial graphene/molybdenum disulfide interface would be lesser than that of the metal. To predict the Schottky barrier from first principles, estimates of work functions of the individual components pristine Ti, MoS₂, graphene, and relaxed heterointerfaces (epitaxial graphene/MoS₂ and Ti/MoS₂) are needed. According to previous first-principles calculations, the work functions of undoped Ti, MoS₂, and graphene are 4.38, 4.05, and 4.23 eV, respectively (Singh-Miller and Marzari 2009). The absolute value is significantly lowered by 0.3 eV here due to various parameterizations of the exchange–correlation functional and van der Waals interactions in other works since the choice of parameterizations affects the work function's absolute values.

Also, the density-functional theory was used to investigate the electrical and optical characteristics of N, Co, and Co–N co-doped MoS₂ monolayers for visible light photocatalytic activity by (Cheriyani et al. 2018).

The electrical characteristics of MoS₂ pristine and MoS₂ doped with TM were investigated by (Deng et al. 2019). The energy of formation among S-vacancy of MoS₂ and the

TM is given by $[E_f = E_{vac} + E_{TM} - E_{(TM-MoS_2)}]$, where E_{vac} , E_{TM} , and E_{TM-MoS_2} stand for combined energies of MoS₂ monolayered with S vacant position, a free atom of transition metal, and the MoS₂ doped with the transition metal (Ma et al. 2016). Because of its high forming energy, Ti-doped MoS₂ has the highest binding power as well as the most stable structure (Deng et al. 2019). Since the Fermi level is in the energy gap region, all structures considered have semiconducting properties. The band distance of pristine MoS₂ is 1.70 eV, close to the experimental value of 1.69 eV (Kuc et al. 2011) and the theoretical result of 1.8 eV (Kam and Parkinson 1982). Pt-doped MoS₂ is a semiconductor with the indirect band gap type, while Ti-, Ni-, and Pd-doped MoS₂ are semiconductors with a direct band gap.

MoS₂-based nanocomposites for water remediation application

With the current global economic evolution, tackling prominent pollutants has become a global priority (Abdel Maksoud et al. 2020; Makvandi et al. 2021; Mamba et al. 2007; Singh et al. 2021). Hence, a variance of approaches has been undertaken to promote techniques for removing or decomposing pollutants, such as adsorption (Xiao et al. 2020), membrane separation (Luciano et al. 2020), biological (Oliveira et al. 2020), coagulation (Sillanpää et al. 2018), photo-oxidation (Onga et al. 2020), and photocatalysis technologies (Chenab et al. 2020).

In recent years, MoS₂ has confirmed exceptional utilization potential in the water remediation field. Overall, MoS₂ and its composites possess the capability to degrade and/or remove distinctive pollutants, which affords the potential for water remedy. MoS₂ has been recognized as a proper photocatalyst and/or absorbent in water remediation, ascribing to its extraordinary specific uptake, cost-effective, exceptional specific surface area, and small bandgap. Notwithstanding, the display of absorbent or photocatalyst composed or based on MoS₂ material is still far away from contentment, as it has a low surface area and an intrinsically lower electric conduction (Fageria et al. 2017). To defeat all the above obstacles, MoS₂ incorporated with different proper photocatalysts such as carbonaceous material, metal oxides, and metal sulfides (Shanker et al. 2017).

MoS₂-carbon materials

One efficient strategy incorporates the MoS₂ with carbonaceous materials with extraordinary electric conductivities and unique surface areas (Chen et al. 2017). Amongst them, the reduced graphene oxide possesses attracted great interest to synthesize reduced graphene oxide-based photocatalysts ascribing to its remarkable theoretical specific

area and unique electric and thermo-mechanical features (Wang et al. 2016a; Shen et al. 2017; Jilani et al. 2018; Hebar et al. 2017; Maddinedi et al. 2017; Patel et al. 2020), which can be availed as an electron collector for gaining and donating electrons (Lv et al. 2017). The MoS₂/reduced graphene oxide composites have recently synthesized to degrade the ranitidine under visible light (Zou et al. 2020). The detected diffraction peaks confirmed the successful preparation of MoS₂/reduced graphene oxide. The high resolution-transmission electron microscope image of the MoS₂/reduced graphene oxide composite presents distinctive layer-like structures besides a marked lattice fringe and having a 7.2 Å as an interlayer distance. The photocatalytic potential is to degrade ranitidine via MoS₂/reduced graphene oxide composites under visible radiation. The removal efficiencies of ranitidine via MoS₂ and reduced graphene oxide were reached about 33% and 35%, respectively. At the same time, the MoS₂/reduced graphene oxide composites possess a photodegradation performance that reached 74% after 1 h of visible light exposure.

Further, the photodegradation efficiency toward ranitidine enhances with rising the reduced graphene oxide content. This behavior can be attributed to the incorporation of reduced graphene oxide outstandingly enhanced the separation performance for the generated pairs of photoelectrons in the MoS₂/reduced graphene oxide composites, and it enhances the specific surface area of the composite. Besides, the attraction within the electrons of p-orbital for ranitidine and the reduced graphene oxide conjugated system (π - π) enhances pollutants' adsorption via the utilizing of the MoS₂/reduced graphene oxide composite photocatalyst. Exaggerated coating of reduced graphene oxide on the MoS₂ surface prevents the MoS₂ capacity from absorbing visible radiation. Hence, the MoS₂/reduced graphene oxide composite exhibited a photocatalytic performance lower in contrast to that of pristine MoS₂. The formation potential of N-Nitrosodimethylamine (NDMA) of the ranitidine solution after 60 min under visible-radiation exposure was illustrated. With the rising reduced graphene oxide ratio, the formation potential of NDMA for ranitidine has reduced (6.76%) and then enhanced (45.27%), which complies with the photodegradation behavior and the mineralization degree.

Recently, heavy metals permanently menace human health and global sustainable evolution. The hexavalent chromium Cr (VI) is a very serious mineral pollutant with non-bioreduction and carcinogenic features. Currently, the reduction of Cr(VI) via photodegradation strategies is considered an essential way of efficient approaches to mitigating Cr (VI) contamination (Fang et al. 2018).

Bai et al. (2018) have synthesized Red phosphorus coating on MoS₂/reduced graphene oxide hybrid for removal of Cr (VI) and Rhodamine B. Figure 3a–f demonstrates the comparative surface morphology of the hybrid MoS₂@

reduced graphene oxide and Red phosphorus coating MoS₂/reduced graphene oxide, in addition to their partial magnification, showing the curly layers where the graphene oxide works as a scaffold resulting in an anchoring and stabilizing for the nanostructured sheets of MoS₂ and Red phosphorus. Figure 3g affirms a consistent distribution of carbon, oxygen, phosphorus, molybdenum, and sulfur for the Red phosphorus coating MoS₂/reduced graphene oxide hybrid. The results also revealed that the MoS₂ and graphene oxide layers are owning an unstacked arrangement. In addition, the graphene oxide reduction and the coating of MoS₂ on the surface of reduced graphene oxide layers have been occurred concurrently, ending in a regular and controllable distribution of the nanostructured sheets of MoS₂ on the surface of reduced graphene oxide layers. Further, the results unveiled that the Red phosphorus coating MoS₂/reduced graphene oxide displays a hexagonal crystal arrangement in the nanoscale nature. Finally, the Red phosphorus coating MoS₂/reduced graphene oxide composite was used to remove about 98.0% of Cr (VI) and about 99.3% from the rhodamine B over half-hour only.

The photodegradation performance of Red phosphorus coating MoS₂/reduced graphene oxide hybrid is notably correlated with the e⁻ and h⁺ amount and their activity. Besides, the graphene oxide demonstrated an essential function in collecting, shuttling the generated electrons, and distinguished adsorption. Most remarkably, Cr (VI) and rhodamine B working as a scavenger to each other may absorb e⁻ and h⁺ together, ending to occurring a synergy impact between the Cr (VI) removal and the rhodamine B oxidation as presented in the graphical photodegradation mechanism.

Also, the carbon nanotubes are one-dimensional material, showing excellent merits such as unique electric conduction, exceptional thermal conduction, and remarkable stability in the structure (Kim et al. 2005; Bindumadhavan et al. 2013). So, combining the unique properties of carbon nanotubes and MoS₂, we can get a unique construction of the MoS₂/carbon nanotubes composite that can be utilized as a proper photocatalyst composite for environmental applications. In photocatalytic application, the electrons in carbon nanotubes can be immediately excited to MoS₂ under ultraviolet or visible irradiation, resulting in the robust separation of charge carriers of photoexcitation. Hence, carbon nanotubes with a large diameter are an excellent selection to gain huge photocatalysis if carbon nanotubes are utilized as decorated on the surface of MoS₂ (Zhang et al. 2017b).

The extraordinary adsorption potential for lead (0.9 µg/g) and cadmium (~0.7 µg/g) from manufacturing mine water via a photocatalyst nanocomposite based on MoS₂/multi-wall-carbon nanotubes has been reported by (Gusain et al. 2019). The adsorption of lead/cadmium ions on the surface of photocatalyst nanocomposite ascribing to creating a complex (metal/sulfur) between the lead/cadmium ion

and the sulfur group is on the MoS₂ over the exchange process via H⁺ ions. Also, the negative charges being in the MoS₂/multiwall-carbon nanotubes surface tend to the electrostatic interaction that was occurring among the positive charges for lead/cadmium ions and the negative charges of the adsorbent.

Between the carbonaceous materials, carbon nanofibers have been examined as candidate materials used in many fields, such as catalyst carriers and flexible electrodes (Almeida et al. 2019). These merits are ascribed to its extraordinary electrical conduction, excellent mechanical characteristics, and a broad range of products simply. (Liang et al. 2020) have reported the preparation of composites of MoS₂/carbon nanofibers, which seems as foxtail via the electrospinning technique. The outcomes reveal that the surface morphology of MoS₂ was verified by varying the precursor concentration, as exhibited in Fig. 4. Compared to pure MoS₂, the MoS₂ carbon nanofibers composites showed remarkable photocatalytic potential toward dye degradation. It is ascribed to the synergistic influence between carbon nanofibers and MoS₂, which may be resulting from the heterogeneous interfaces and the excellent conduction properties of carbon nanofibers. Further, the exceptional adsorptive capacity of MoS₂/carbon nanofibers composites can improve the apparent concentration of reactants. Besides, the hierarchical structure morphology can supply additional reactive sites.

It is ascribed to the synergistic influence between carbon nanofibers and MoS₂, which may be resulting from the heterogeneous interfaces. The hierarchical structure morphology can supply additional reactive sites.

Graphitic carbon nitride besides has a two-dimensional layered construction, and it is a layered material like graphite. Recently, graphitic carbon nitride has been shown to advantage exceptionally attractive, ascribed to its proper bandgap and extraordinary stability in tough chemical conditions (Pramoda et al. 2017). Nevertheless, pure graphitic carbon nitride possesses low photocatalytic performance resulting from that the hole–electrons, that photogenerated, suffer from the fast recombination. But, MoS₂ has a demanding structure, including unsaturated atoms of both atoms (Mo and S) at the edges, which give a promising edge activity over the photodegradation process. Combining MoS₂ and graphitic carbon nitride to create heterostructure catalysts has been confirmed to improve the catalytic performance resulting from the effective charge separation (Li et al. 2017; Li et al., 2018a; Lu et al. 2019; Yang and Wang 2021). Recently, (Liu et al. 2020a) have reported enhancing the charge separation in the Z-scheme MoS₂/graphitic carbon nitride composite for improved photodegradation potential toward bisphenol-A. Compared with the graphitic carbon nitride sample, the MoS₂/graphitic carbon nitride composite exhibited exceptionally improved photocatalytic potential.

Also, a significant repression toward bisphenol A degradation was seen ascribed to the scavenging impact.

Also, the MoS₂/graphitic carbon nitride composite exhibited a notable performance toward heavy metals removal. The synthesis of the heterostructure MoS₂/graphitic carbon nitride as a promising catalyst for removing U(VI) has been reported by (Zhang et al. 2020a). The heterostructure advanced the charge transference and improving the separation potential of photogenerated electron–hole pairs. Further, the heterostructure MoS₂/graphitic carbon nitride sample showed extraordinary photoreduction performance toward U(VI), which was notably higher than that obtained of pure graphitic carbon nitride. Besides, the heterostructure MoS₂/graphitic carbon nitride sample exhibited noteworthy stability under visible radiation. The electrons (e⁻) are transported between the conduction bands, whereas the holes (h⁺) were transported between valence bands for both (graphitic carbon nitride and MoS₂). Besides, e⁻ lessen dissolved O₂ while decreasing U(VI), and the declining output interacts synergistically with e⁻ to reduce U(VI).

Furthermore, compared with the earlier published bulk phase of the heterogeneous MoS₂@graphitic carbon nitride, the heterogeneous MoS₂/graphitic carbon nitride phase lessens the transport time and interval photoinduced carriers and therefore lowers the recombination feasibility of the carriers through transfer (Shi et al. 2018).

MoS₂-metals oxides materials

In recent decades, to address the problem of dangerous environmental contamination, photocatalysis based on semiconductor materials has been broadly examined for the photocatalysis of contaminations (Lee and Jang 2014).

Titania or titanium (IV) oxide TiO₂-based photocatalysts have numerous merits, which are ascribed to outstanding benefits such as cost-effectiveness, excellent chemical stability, and friendliness to the environment. Nevertheless, the TiO₂ catalysts display excellent photocatalytic activity in the near UV attributable to its broad bandgap energy (3.2 eV) that is incapable of being used in the visible light region (Xiao et al. 2014). On the other hand, MoS₂/TiO₂ nanocomposites have been published to display enhanced photocatalytic characteristics. A rising number of researchers are currently attempting to advance manufacturing techniques to achieve the heterostructure of MoS₂/TiO₂ possessing uniform distribution, influential interaction, and singular structures for numerous utilizations. These strategies to synthesize the MoS₂/TiO₂ heterostructure can be classified into two sections: ex situ synthetic approaches and in situ synthetic approaches (Chen et al. 2018).

Development of the N and Ti³⁺ co-substituted TiO₂ incorporating with MoS₂ has been reported by (Liu et al. 2017). Moreover, after conjugation with MoS₂, the photocatalytic

activity of the sample is notably improved, ascribed to the production of the heterogeneous structure, that not only efficiently prevents recombination of electron–hole pairs but also affords rich catalytic sites for contaminants removal.

Also, (Zhang et al. 2016) have successfully prepared the heterostructure of $\text{MoS}_2/\text{TiO}_2$ via the hydrothermal approach. Remarkably, the heterostructure of $\text{MoS}_2/\text{TiO}_2$ presents a more excellent adsorption capacity to degrade the organic dyes in contrast to pure TiO_2 . Also, the enrichment in the adsorption capacity for the heterostructure of $\text{MoS}_2/\text{TiO}_2$ photocatalysts can be notably ascribable to the exceptional specific surface area of the heterostructure of $\text{MoS}_2/\text{TiO}_2$, which contributes to growing the active adsorption sites to degrade the organic dyes and promote the photocatalytic potential. All heterostructures of $\text{MoS}_2/\text{TiO}_2$ display remarkably better photocatalytic potential than both pure TiO_2 and MoS_2 after exposure to ultraviolet-light radiation.

Zinc oxide ZnO also has a broad bandgap and is active only under ultraviolet radiation. Besides, it is one n-type semiconductor, which is a desirable photocatalytic candidate ascribing to its direct bandgap (3.37 eV), extraordinary photostability, exceptional sensitivity, cost-effective, non-toxic characteristics, and unique exciting binding energy (60 meV). ZnO is further limited only to ultraviolet radiation, and besides, the fast recombination for the carriers restricts its possible utilizations. Diverse strategies have been established to address ZnO serving in the visible light zone and promote ZnO absorption under the energies with low value by performing electronic levels inside its bandgap (Ebrahimi et al. 2017; Colombo et al. 2017). Many investigations have examined the MoS_2 potential candidate as co-photocatalysts to promote the photocatalytic potential of ZnO in water purification utilization. MoS_2 is a p-type semiconductor material with a narrow bandgap, which presents exceptional absorption toward the visible area of the solar radiation and possesses the stable layered metal dichalcogenides, which are infirmly linked via van der Waals interactions, presenting the feasibility for the bulk phase MoS_2 , which exfoliated to thin nanolayers for an additional examination of the activity of MoS_2 (Benavente et al. 2018).

Also, (Rahimi et al. 2019) have reported the enrichment of the photocatalytic potential of ZnO under sunlight via incorporating it with thin layers of MoS_2 . In the case of uses sunlight radiation, MoS_2 increments the photocatalytic potential of ZnO by 75%. Nevertheless, in the case of use of ultraviolet-blocked radiation, MoS_2 lessens the photocatalytic potential of ZnO to 67% of its original value. If the photon energy $h\nu \geq 3.1\text{eV}$, i.e., $\lambda < 400\text{nm}$, both ZnO and MoS_2 would be excited, and MoS_2 promotes the separation/division of electrons and holes. If the photon energy ranged between 2.45 and 3.1 eV, i.e., the wavelength ranged between 400 and 507 nm, this energy is sufficient to excited electrons MoS_2 to its conduction

band. Also, this energy demanded the electrons of ZnO to be excited to its defect-energy level.

Consequently, the excited electrons in the conduction band of MoS_2 possess energy used to flow at the ZnO defect-energy level. Also, ascribing to the broad bandgap of ZnO and when the ultraviolet region of the light is missing, ZnO is just partially excited, and MoS_2 performs the chief photodegradation capacity, and ZnO works essentially in an electron–hole division/separation for the photoinduced electrons and holes. Finally, if the photon possesses energy equivalent to the bandgap of MoS_2 , i.e., the wavelength range between 507 and 751 nm, the MoS_2 would be excited, and the level of defect energy for ZnO supports their separation.

Since pure MoS_2 is unmanageable to perform free radicals for degrading the organic pollutants, ascribing to its valence band edge capability is not oxidative sufficient. Additionally, pure MoS_2 is not simple to be cyclic employed.

Spinel ferrites with superior magnetic features and small band gaps are a profitable procedure to defeat these shortcomings of MoS_2 , where spinel ferrites can stimulate the existence of photoinduced charge carriers and improve the photodegradation sensitivity to visible light (Abdel Maksoud et al. 2020; Lu et al. 2020; Marcelo et al. 2021).

Recently, (Atacan et al. 2021) have reported synthesizing a magnetic photocatalyst nanocomposite based on $\text{CuFe}_2\text{O}_4/\text{MoS}_2$ via the hydrothermal method. The outcomes show that the $\text{CuFe}_2\text{O}_4/\text{MoS}_2$ displays the greatest photodecomposition in Rhodamine B degradation than those for pure MoS_2 and Cu-ferrite. The charge transference procedure formed through the p-n ($\text{CuFe}_2\text{O}_4/\text{MoS}_2$) heterojunction positively influences the separation of photoinduced carriers. Also, the $\text{CuFe}_2\text{O}_4/\text{MoS}_2$ photocatalyst showed ferromagnetically performance, and hence, it will enable fast rescue from the Rhodamine B solution by utilizing an external magnetic field. After the 5th cycle, an insignificant reduction in the photocatalytic capability of $\text{CuFe}_2\text{O}_4/\text{MoS}_2$ photocatalyst was marked. The photodegradation for $\text{CuFe}_2\text{O}_4/\text{MoS}_2$ photocatalyst was reduced by 3.5% than those obtained in the 1st cycle. The outcomes present extraordinary photocatalytic performance for the $\text{CuFe}_2\text{O}_4/\text{MoS}_2$ photocatalyst.

Also, (Jia et al. 2019) have enhanced the Au-decorated $\text{CoFe}_2\text{O}_4/\text{MoS}_2$ photocatalyst against methyl orange with feasibility for magnetic recovery. Indeed, the presence of Au as decorating for the surface of cobalt ferrite can efficiently improve the interface conduction and stimulate the recombination process for the conduction band electrons for cobalt ferrite with the holes in the MoS_2 valence band. They found a negligible reduction in the photocatalytic capability until the 4th recycle, showing that the $\text{Au-CoFe}_2\text{O}_4/\text{MoS}_2$ composite is durable for possible applications. The composites can be available to recover by utilizing a magnet.

Perovskite oxides also give a unique functional material character with a novel crystal structure. Also, these materials possessed extraordinary photocatalysis potential. Besides, they have an excellent performance in energy and environmental areas (Hu et al. 2020; Grabowska 2016; Kumar et al. 2019).

Recently, (Jiang et al. 2020) have reported the synthesis of $\text{MoS}_2/\text{CaTiO}_3$ heterogeneous for degrading tetracycline in water. The $\text{MoS}_2/\text{CaTiO}_3$ shows a higher photocatalytic achievement toward tetracycline than to pure MoS_2 and CaTiO_3 . The photodegradation enhancement is attributable to the electron transportation for the Z-scheme of the heterogeneous and the stimulating interaction between the MoS_2 and the CaTiO_3 perovskite. Moreover, the Z-scheme $\text{MoS}_2/\text{CaTiO}_3$ heterogeneous possessed more suitable induced carrier separation, more active charge transportation, and a greater photoinduced carrier lifetime and considerably improved photodegradation activities.

MoS_2 -metal sulfide composites

MoS_2/CdS heterostructures have been extensively investigated for organic dyes degradation, for instance, methylene blue, methylene orange, and rhodamine B, due to their unique properties and narrow band gap (Wang et al., 2018a; Lian et al. 2018; Li et al. 2019a). The heterojunction between CdS and MoS_2 could facilitate photogenerated charge migration and separation, thereby boosting photocatalytic performance (Kumar et al. 2016; Jia et al. 2014). A single-step hydrothermal process was used to prepare CdS/ MoS_2 nanocomposite and tested it for methylene blue degradation under ultraviolet illumination. The percentage of methylene blue photodegradation using CdS/ MoS_2 was higher by 48% compared to CdS and MoS_2 (Darsara et al. 2018). Montmorillonite/ MoS_2/CdS demonstrated a potential photocatalytic activity for rhodamine B degradation and achieved 98.8% when exposed to visible light for 45 min (Peng et al. 2019). The large surface area, high visible light-harvesting capacity, and low electron–hole pairs recombination rate were credited to the high performance. They proposed the mechanism of rhodamine B degradation. Under the visible light illumination, the electrons in MoS_2 and CdS are excited to the conduction band, leaving positive holes (h^+) in the valence band. The photogenerated e^- and h^+ transferred from CdS to the conduction band and valence band of MoS_2 , respectively, because the MoS_2 has a lower conduction band and higher valence band than CdS. The charge reunion rate was less in MoS_2 with an indirect band gap which prolonged their lifetime. The photogenerated electrons reacted with O_2 to form O_2^- . The OH groups present in the montmorillonite surface worked as a hole trapper to generate OH \cdot inhibiting the recombination of the electron–hole pairs. The h^+ , O_2^- ,

and OH \cdot acted as a strong oxidizing agent for rhodamine B dye removal (Peng et al. 2019).

Also, MoS_2/CdS nanodots-on-nanorods structure demonstrated high photodegradation efficiency of rhodamine B with 99.11% within 45 min. The well-defined structure, which inhibited charge recombination and allowed many charge carriers to participate in the rhodamine B degradation, was credited with this high performance. They explained the detailed photocatalytic activity mechanism of MoS_2/CdS . The electrons leaped conduction band under light irradiation, producing positive h^+ in the valence band, and then, the electrons moved from CdS to MoS_2 conduction band. These electrons react with O_2 to form O_2^- combined with h^+ to degrade rhodamine B (Li et al. 2019a).

The MoS_2/CdS nanocomposite was prepared using a two-stage solvothermal process at different temperatures and investigated for its photocatalytic activity for methylene orange removal under visible light illumination (Alomar et al. 2019). The thinner MoS_2/CdS sheet, which was prepared at 220 °C, exhibited the highest performance for methylene orange degradation with high stability under visible light. Compared to pristine MoS_2 and CdS, this nanocomposite's narrow bandgap, excellent separation, and low recombination of e^- and h^+ were credited with the high performance.

$\text{Bi}_2\text{S}_3/\text{MoS}_2/\text{TiO}_2$ showed the highest photocatalytic efficiency of methylene blue degradation under sunlight up to 99% after 4 min compared to bare TiO_2 , MoS_2 , and Bi_2S_3 . This developed performance was ascribed to the large surface area and the construction of double Z-scheme heterojunction, which increased the active sites and charge separation efficiency (Drmosh et al. 2020).

Besides, (Zhang et al. 2018a) evenly distributed the MoS_2 nanosheets with different Cu_2S snowflake to form MoS_2 nanosheets/ Cu_2S snowflake nanocomposites and examined their photocatalytic activity for methylene orange degradation under visible light illumination. The nanocomposite with 50 wt% of MoS_2 demonstrated the highest performance for methylene orange photodegradation and reached to 90% after 60 min when exposed to visible light. This excellent efficiency was owed to the high specific surface area of the Cu_2S snowflake structure, which improved the light-trapping ability and enhanced charge separation in the composite heterojunction.

The $\text{MoS}_2/\text{Ag}_2\text{S}/\text{Ag}$ ternary nanocomposite (flower-like structure) has been designed and examined it for the photodegradation of Congo red. This nanocomposite achieved 97.01% of Congo red degradation after 120 min when exposed to visible light. This outstanding performance was ascribed to the MoS_2 flower-like structure, which supplied many active sites; the electron transporter function of Ag and Z-scheme constructed in the $\text{MoS}_2/\text{Ag}_2\text{S}/\text{Ag}$ interface

boosted charge separation and mitigated the recombination rate (Zeng et al. 2019a).

The $\text{Bi}_2\text{S}_3/\text{MoS}_2$ revealed the highest photocatalytic activity for red phenol degradation up to 83.4% in 60 min compared to the pristine MoS_2 nanosheets and Bi_2S_3 nanorods (Vattikuti and Byon 2016). This was due to the outstanding suppression of charge recombination rate and increase in charge carrier lifetime, which reinforced the redox reaction. They explained the phenol red photodegradation over $\text{Bi}_2\text{S}_3/\text{MoS}_2$ binary composite. When $\text{Bi}_2\text{S}_3/\text{MoS}_2$ was exposed to visible light, electrons are leaped to the conduction band with forming positive holes in the valence band of Bi_2S_3 and MoS_2 . Then, the excited electrons in Bi_2S_3 conduction band migrated to MoS_2 conduction band (Jiang et al. 2016; Long et al. 2016), while positive holes transferred to the valence band of Bi_2S_3 from the valence band of MoS_2 . This electron separation mechanism suppressed the charge recombination rate and rose the charge carrier's lifetime and thereby enhanced the phenol red photodegradation (Vattikuti and Byon 2016).

Also, the $\text{WS}_2/\text{MoS}_2/\text{BiOCl}$ achieved 99.36% of methylene blue degradation in 240 min (Qi et al. 2021). The construction of a heterojunction between WS_2 , MoS_2 , and BiOCl improved light-harvesting performance, created a narrow band gap, and facilitated charge transfer and separation, resulting in this outstanding efficiency.

The precipitation–deposition process was utilized to prepare PbS/MoS_2 binary nanocomposites with various PbS molar proportions (0.5%, 1.0%, and 1.5%) and investigated it for the methylene blue dye photodegradation under visible light. 1% $\text{PbS}-\text{MoS}_2$ achieved the highest activity for methylene blue removal and reached 83% in 180 min. The findings of characterization techniques indicated that 1% $\text{PbS}-\text{MoS}_2$ exhibited the largest surface area and the highest electron–hole pair separation efficiency, which explains its outstanding photocatalytic behavior (Raja et al. 2017).

The electrospinning method used to make $\text{MoS}_2/\text{CdS}/\text{TiO}_2$ ternary nanocomposites deposited on carbon nanofibers followed by calcination under nitrogen (Pant et al. 2019). This nanocomposite showed outstanding efficiency for methylene blue removal compared to the bare TiO_2 nanofibers. This was due to the high absorption efficiency of carbon nanofibers and their good synergy with other components. They explained the adsorption and removal mechanism of methylene blue dye over $\text{MoS}_2/\text{CdS}/\text{TiO}_2$. The heterojunction between MoS_2 , CdS , and TiO_2 distributed on carbon fibers extended the light absorption capacity to the visible light region. When the ternary nanocomposite was exposed to the visible light, the electrons are leaped to the conduction band with generating positive holes in the valence band in each component. The excited electrons in the CdS conduction band migrated to the TiO_2 conduction band mean, while positive holes transferred from the CdS valence band

to the MoS_2 valence band. This electron transfer mechanism prolonged the lifetime of charge carriers and decreased their combination. These photogenerated electrons reacted with oxygen to generates O_2^- , and the holes reacted with OH^- and generated OH . These radicals (O_2^- , and OH) degraded methylene blue dye to CO_2 and H_2O (Pant et al. 2019).

The binary composite consists of MnS and MoS_2 nanostructures and tested it for the photocatalytic degradation of methylene blue dye (Chen et al. 2019a). The MnS/MoS_2 nanocomposite exhibited the highest performance compared to the bare MnS and MoS_2 . Due to the difference in the conduction band and valence band energies of both MnS and MoS_2 , the excited electrons in the MnS conduction band migrated to the MoS_2 conduction band. However, holes at MoS_2 valence band transferred to the MnS valence band. This movement of charge carriers inhibited the charge recombination and thereby enhanced the photocatalytic efficiency (Chen et al. 2019a). A way for the wastewater purification and synchronous generation of valuable chemicals such as hydrogen was opened by (Zhang et al. 2017a). They investigated the photocatalytic efficiency of $\text{MoS}_2/\text{ZnIn}_2\text{S}_4$ @reduced graphene oxide for the degradation of methylene blue, rhodamine B, fulvic acid, eosin Y, and p-nitrophenol, and it showed photodegradation performance 98.5%, 98.8%, 92.2%, 98.6%, and 91%, respectively. This was due to reduced graphene oxide's efficient role in facilitating electron transfer, and a large number of active sites were provided by MoS_2 . The highest amount of hydrogen (45 μmol) was obtained during rhodamine B removal (Zhang et al. 2017a).

Heavy metal contamination has become a global problem. The ecosystem is significantly harmed by industrial wastewater containing heavy metals such as chromium $\text{Cr}(\text{VI})$. Carbon nanotubes/ $\text{MoS}_2/\text{SnS}_2$ hydride nanotubes composite was prepared and explored it for the $\text{Cr}(\text{VI})$ reduction under visible light subjection (Dong et al. 2019). The carbon nanotubes/ $\text{MoS}_2/\text{SnS}_2$ composite demonstrated 100% removal of $\text{Cr}(\text{VI})$ solution containing 50-mg/L in 90 min, while SnS_2 and carbon nanotubes/ MoS_2 exhibited 96.3% and 80%, respectively, under the same circumstances. Besides, within 90 min, carbon nanotubes/ $\text{MoS}_2/\text{SnS}_2$ completely eliminated $\text{Cr}(\text{VI})$ from a solution containing 120 mg/L. They proposed a reduction mechanism of $\text{Cr}(\text{VI})$ over carbon nanotubes/ $\text{MoS}_2/\text{SnS}_2$ composite under visible light subjection. The p–n heterojunction formed by MoS_2 (p-type) and SnS_2 (n-type) increased and decreased the Fermi energy level of MoS_2 and SnS_2 responsibly, respectively, and reached the same Fermi energy level (Swain et al. 2018; Bagherzadeh and Kaveh 2018). Under visible light illumination, the electrons in MoS_2 and SnS_2 are leaped to the conduction band, leaving positive holes in the valence band (Hu et al. 2018a; Zhang et al. 2018b; Zhang et al. 2018c). MoS_2 has a more

negative conduction band potential than SnS₂, and thus, the excited electrons in the MoS₂ conduction band transferred to the SnS₂ conduction band. Meanwhile, the positive holes migrated from the SnS₂ valence band to MoS₂, leading to excellent charge separation performance. These electrons reduced the adsorbed Cr(VI), and holes oxidized water to generate O₂.

MoS₂/Co₃S₄ core–shell dispersed on nanofiber aerogel by (Qiu et al. 2020). This nanocomposite reduced Cr(VI) with excellent efficiency reached 90% after 50 min. The MoS₂/SnS₂ with Mo/Sn ratio of 7.5% demonstrated the highest efficiency for Cr(VI) reduction up to 99.9% and 96.5% for methylene blue removal when subjected to visible light (Qiang et al. 2021). This outstanding performance due to the Z-Scheme and the heterojunction construction facilitated the charge transfer process and inhibited the charge carrier recombination rate. Further, the 2-Cu₂S-MoS₂ achieved the rapid Cr(VI) photoreduction performance which was 0.0058 min⁻¹ when subjected to visible light (Zhang et al. 2020b), which was about 8.3- and 2.9-fold greater than pristine MoS₂ and Cu₂S, respectively. They studied the Cr(VI) photoreduction mechanism in-depth. Due to the difference in the energy levels of the conduction band and valence band of MoS₂ and Cu₂S and the formation of π -type alignment, the photoexcited electrons transferred from Cu₂S conduction band to MoS₂ conduction band, while positive holes migrated to MoS₂ valence band from Cu₂S valence band under visible light illumination. This phenomenon mitigated the charge carriers recombination rate and prolonged their lifetime. These electrons in MoS₂ conduction band reduced Cr(VI) to Cr(III); meanwhile, the positive holes in the valence band of Cu₂S oxidized water to generate O₂ (Zhang et al. 2020b).

MoS₂-based nanocomposites for supercapacitors

Currently, the amalgamation of energy demand with the depletion of only accessible power and energy resources is triggering scientists to look for novel, clean, low-cost, and environmental energy outputs and storage devices with superior performance (Xia et al. 2018). Electrochemical capacitor shows a growing role in providing the demand for high-rate production, storing, and conveying electrical energy. As a result, the necessity for high-power, ever-present, and high-energy–density storage has increased (Simon and Gogotsi 2020). Owing to their swift charge/discharge rate, high-power density, ultra-long cycle life, relatively low-cost, environmental, and safe operation environments, supercapacitors exhibit superiority over traditional electrostatic capacitors and batteries (Yin et al. 2020). As a result, according to the Statista database, the automotive supercapacitors market worldwide is predicted to rise to 7 billion

US \$ by 2028, related to ~0.5 US \$ in 2018. According to the Scopus database, the number of “MoS₂ in energy storage” publications compared with “MoS₂ supercapacitors” from 2013 till 2020 is increased concern to MoS₂ as a likely material for energy storage strategies in general and supercapacitors in specific.

Principle of energy storage in electrochemical capacitors

Supercapacitors primarily obey two charge storage mechanisms based on supercapacitors' working mechanism: (1) electrochemical double-layer capacitors, EDLCs, and (2) pseudo-capacitors. The first mechanism is charge separation at the interface sandwiched between the electrode and the electrolyte (EDLCs), where energy is stored via the accumulation (electrostatic) of charges at the interface. The second one, up through redox reactions, endures a Faradaic process (pseudo-capacitors). Pseudo-capacitors allow high specific capacitance than EDLCs due to the high density of charge storage done in the redox process. Systematically energy is deposited near or at the electrode's surface by the electro-sorption and/or reversible redox reactions (Salanne et al. 2016).

In EDLCs, energy stored via charge adsorption at the electrode surface is deprived of faradaic reactions. Throughout the progression of charge–discharge, current resulted from the prearrangement of charges in the two oppositely charged layers (Helmholtz double layer). The EDLCs can bring energy swiftly, and the sum of the stored energy is restricted and much lower than that of pseudo-capacitors due to the endurance of the electrode surface. Electrochemical double-layer capacitance (C_{dl}) and the response current (I) are described in the following equations (Zhang and Zhao 2009; Conway et al. 1997):

$$C_{dl} = \frac{Q}{V} = \frac{\epsilon_r \epsilon_o A}{d} \quad (1)$$

$$I = \frac{dQ}{dt} = C_{dl} \frac{dV}{dt} \quad (2)$$

where Q , ϵ_o , ϵ_r , A , d , t are the total charge transferred at potential V , the dielectric constant of vacuum, the dielectric constant of the electrolyte, the electrode surface area, the charge separation distance, and the charge time, respectively. Generally, carbon and carbon-based materials occupied most of the electrode materials of EDLCs due to their first-rate electric conductivity and their large specific surface area. However, EDLCs' carbon-based electrodes meet a limitation in commercial application from a high energy density point of interest (Thakur et al. 2017; Lamberti 2018; Zhao et al. 2018).

Energy storage concerning pseudo-capacitance displays the transitional electrochemical behavior between solid-state diffusion and pure electrostatic EDLCs controlled by Faradaic reactions in bulk electrode materials. Faradic mechanisms is divided into: (1) underpotential deposition, in which ions are placed on a metal/electrolyte boundary at positive potentials to their reversible redox potentials (e.g., H^+ on platinum or Pd^{2+} on gold) (Sudha and Sangaranarayanan 2002). (2) Redox pseudo-capacitance, where there is some range of change in reduced species on the electrode surface or within a slight shallow surface region of oxidized species (or vice versa) in a Faradaic redox system (e.g., or MnO_2 , and conducting polymers) (Makino et al. 2015; Lang et al. 2011). (3) Intercalation pseudo-capacitance, in which ions intercalation into a redox-active material occur without any change in the crystallographic phase and in a timescale near to that of EDLCs (e.g., Nb_2O_5) (Kong et al. 2014; Kong et al. 2015). Many kinds of research work are intensive on transition metal oxide and sulfide-based materials as pseudo-capacitors, especially metal sulfides. This is because the interaction between the Li^+ , for example, as a guest ion and the sulfide mesh should be weakened compared to oxides.

Additionally, this faded interaction should lead to swift ion passage through the lattice. MoS_2 is an attractive material for pseudo-capacitive electrode due to their large van der Waals gap (6.2 Å) in μ -sized samples that touch (6.9 Å) for nanostructured systems. This large van der Waals space will be reflected on the guest–host interaction by reduction, making MoS_2 a perfect pseudo-capacitive material (Liang et al. 2011; Hwang et al. 2011). MoS_2 has another advantage; that is, lithium inset into the semiconducting (2H phase) boosts a phase transition to the metallic (1T phase) of MoS_2 (Cook et al. 2017).

Supercapacitors' electrode materials

Capacitors performance was mastered by the electrode materials, which commonly studied electrode materials: (1) carbon materials (e.g., carbon nanotubes, carbon nanofibers, activated carbon, graphene, carbon aerogel). They show a high specific surface area, making them a good choice for EDLCs electrodes. Unfortunately, they are imperfect in their minimal energy density and low specific capacitance. (2) Conducting polymers, the most common (polypyrrole

and polyaniline that covered some defects of MoS_2 as well as could maximize the electrochemical performances). (3) Transition metal oxides (such as RuO_2 , NiO_x , MnO_x , and iron oxides) which show 10 to tenfold (100) times superior specific capacitance than previously mentioned carbon materials. Inappropriately, conducting polymers were subjected to exhaustive degradation on swelling and shrinking through several charge/discharge cycles. (4) Metal dichalcogenides (e.g., MoS_2 and $MoSe_2$) are other electrode materials that will be covered in this work.

MoS_2 -based electrodes offer a tunable morphology, structure, and surface chemistry of supercapacitors electrode materials (Yang et al. 2015). Thus, MoS_2 exhibits high capacitance because, firstly, MoS_2 has a dual charge storage potency rendered by the double-layer structure and the faradic action taking place at its daggl edge and defects at the surface (da Silveira Firmiano et al. 2014; Soon and Loh 2007; Zhang et al. 2015). Secondly, the wide oxidation state ranges (+2 up to +6) drive participation in a redox reaction (Chhowalla et al. 2013). Then, the non-stop redox reactions eliminate dead time. The redox-reaction activity and the charge separation efficiency are predominately particular by the accessibility of the active surface area and the nature of surface chemistry. Henceforth, refining the active surface area of MoS_2 will meaningfully raise its specific capacitance when utilized as an electrode for supercapacitors applications (Zhu et al. 2015). Additionally, MoS_2 can store charges by both mechanisms (i.e., EDLCs and pseudo-capacitance within both negative and positive windows, respectively). Therefore, MoS_2 can act as cathode and anode (mixed-type) materials for supercapacitors (Sun et al. 2015; Wang et al. 2014a).

Electrochemical performance of unsupported MoS_2

Owing to MoS_2 ' high specific capacitance, MoS_2 is highly fortunate for supercapacitors. For instance, MoS_2 in both forms (homogenous ultrathin and petal-like structure) was stated to display a good specific capacitance of over 575 Fg^{-1} at (5 mV s^{-1} , scan rate) (Karade et al. 2016) and 811 Fg^{-1} at (0.1 A.g^{-1} , current density) (Mishra et al. 2018). Although MoS_2 displayed an excellent specific capacitance, its performance (electrochemical) is restricted by its intrinsic restacking feature. Previously reported specific capacitances

Table 1 Comparison of supercapacitor performances of different forms of unsupported molybdenum disulfide nanostructures

Material structure	Current density, ($A \cdot g^{-1}$)	Potential range (V)	Specific capacitance, ($F \cdot g^{-1}$)	Refs.
MoS ₂ nanosheets	1	−0.6: 0.4 V	34.6	(Thangappan et al. 2016)
MoS ₂ nanosheets	1	−0.8: −0.2 V	192.2	(Huang et al. 2014a)
Sphere-like MoS ₂	0.5 (mA · Cm ²)	−0.2: −0.5 V	92.85	(Krishnamoorthy et al. 2014)
Spherically clustered MoS ₂	1	−0.5: −0.5 V	122	(Ilanchezhiyan et al. 2015)
Layered MoS ₂	1	−1: 0 V	120	(Huang et al. 2013a)
Layered MoS ₂	1	−0.8: −0.2 V	149	(Huang et al. 2014b)
MoS ₂ nanowall films	1	−0.2: −0.7 V	100	(Soon and Loh 2007)
Flower-like MoS ₂	1	−0.8: −0.2 V	118.9	(Huang et al., 2015b)
Flower-like MoS ₂	1	−0.9: −0.2 V	168	(Wang et al. 2014a)
Layer expanded MoS ₂ nanorods	1	−1: 0 V	231	(Xiao et al. 2017b)
Metallic 1 T phase MoS ₂ petal-like nanostructure	0.1	–	811	(Mishra et al. 2018)
	10.0		400	
Layer expanded MoS ₂ nanorods	0.5	–	275	(Xiao et al. 2017b)
	1.0		231	

and cyclic stabilities of diverse morphologies of MoS₂ are tabulated in Table 1.

Among these structures, layered MoS₂, which bids a great charge storage affinity as a result of its inherent ionic conductivity as well as ions intercalation within the layers, permits an effective absorption of these ions on the MoS₂ exterior (Ramadoss et al. 2014; Zheng et al. 2003). Since the morphology is crucial for making effective supercapacitors, a plethora of effort laid to propose an enhanced morphology of MoS₂ for improved capacitance, such as microspheres, nanospheres, nanowires, nanorods, and nanofibers (Ma et al. 2008; Nagaraju et al. 2007; Li et al. 2003; Tian et al. 2005; Tang et al. 2013).

Consequently, a bit incompact arrangement of MoS₂ nanosheets might enhance capacitance since the enlarged active surface area (Xiao et al. 2017b). Incorporating MoS₂ with materials (electrically active) such as carbon materials, conductive polymers, transition metal oxides, and transition metal sulfides produces hybrids and/or composites possess excellent electrochemical features as electrode material. These materials could improve the conductivity as well as provide a supportive mate to MoS₂. This may be reflected in the enhanced structural stability and electrochemical performance (Xiao et al. 2017b; Radhakrishnan et al. 2021).

Electrochemical performance of carbon-based hybrids of MoS₂

For instance, carbon nanotubes, carbon aerogel, graphene, as examples of carbon-based materials, have a high surface area, controlled surface functionality, morphology, and excellent electrical conductivity, putting them together as promising candidates as electrode materials for supercapacitors. Still, low-energy storage capacity restricts them

for use in practical applications. Molybdenum disulfide can boost conductive features and afford support to expand the hybrid's electrochemical performance and structural firmness.

Many researchers seek to fascinate the supercapacitors' electrode materials, especially those based on MoS₂/carbon composites. In turn, hybridization of the previously mentioned materials with MoS₂ outcomes in amended morphology and MoS₂ eases the interconnected network of carbon materials. Table 2 shows the electrochemical performances of yet tested MoS₂/carbon hybrids.

Graphene, a representative of the most exciting carbon material, has drawn widespread consideration due to its physical/chemical features. It has a notable sizeable surface area, conductivity, good thermal tolerance, besides its robust mechanical strength (Liu et al. 2019; El-Kady and Kaner 2013; Guo and Dong 2011; Wu et al. 2013). The harmonizing action between MoS₂ and graphene (MoS₂/graphene) hybrids, which adjusts each material's imperfections, progresses the electrochemical performance, improves the conductivity, provides more active sites, and hastens the charges (electrons) transport as well as diffusion of the electrolyte inside the electrode material (Sarkar et al. 2019).

Precisely, the upgrading of the MoS₂/graphene's electrochemical performances composites can be due to three main factors: Electron transportation from MoS₂ to graphene, besides structural constancy of MoS₂ hybrids, results from C–O–Mo interfacial interaction; this leads to remarkable rate capacity and reversible capacity (Teng et al. 2016). Secondly, the coupling between MoS₂ and highly conductive graphene leads to a hybrid (MoS₂/graphene) with enhanced electrochemical performances. In this hybrid, graphene is robust to accumulate and delivers a large surface area to MoS₂ mounting. Hence, a homogenous electrode structure

Table 2 Previously reported electrochemical performance of carbon-based hybrids of MoS₂

Material structure	Electrolyte/Electrode composition, mass ratio	Specific capacitance, F. g ⁻¹	Current density, A. g ⁻¹	Number of cycles	Specific capacitance retained, %	Energy density, Wh. Kg ⁻¹ /Power density, kW.kg ⁻¹	Refs.
MoS ₂ /carbon aerogel	1 M Na ₂ SO ₄	260	1	1500	92.4	—	(Huang et al., 2015b)
MoS ₂ /graphene	1 M Na ₂ SO ₄	243	1	1000	92.3	73.5/19.8	(Huang et al. 2013a)
MoS ₂ /carbon nanotubes	1 M Na ₂ SO ₄	108	0.1			7.4/3.7	(Khawula et al. 2016)
MoS ₂ /carbon nanotubes		231	0.1			26/6.443	
Reduced graphene oxide/MoS ₂	—	334.21	5 mV/s	500	90	—	(Murugan et al. 2017)
Graphene wrapped carbon nanotubes / MoS ₂	—	498	1	10,000	94.3	—	(Sun et al. 2017)
Carbon nanotubes /MoS ₂	1 M Na ₂ SO ₄	350.6	1	10,000	85	—	(Sun et al. 2017)
Electrospun MoS ₂ /carbon nanofiber	6 M KOH	355.6	5 mV/s	2000	93	—	(Kumuthini et al. 2017)
MoS ₂ /three-dimensional graphene network	3 M KOH	1972.58	1	4000	110.57	—	(Zhou et al. 2017)
MoS ₂ /graphene nanobelts	—	445.71	0.8	1000	96.75	38.6/0.4	(Jia et al. 2017)
Carbon/MoS ₂ nanosphere	3 M KOH	1000	20	20,000	93	—	(Luo et al. 2018)

and adjusted frame of MoS₂ will result during the cycling progression (Teng et al. 2016; Yu et al. 2014; Sun et al. 2016; Liu et al. 2014b). Finally, the conductive voids and channels shaped inside the MoS₂/graphene hybrids increased surface area and numerous active sites. Thus, afford continuous pathways for ions intercalations and electrochemical reactions and, in turn, enhance the electrode's reaction kinetics and elevate the hybrid's electrocatalytic performance (Paul et al. 2019; Huang et al. 2013b; Liu et al. 2020b).

As known, maximizing the capacitance is a challenge. The MoS₂ micro-flowers were prepared via a cost-effective hydrothermal method and further electrospun over carbon nanofibers forming a three-dimensional network for robust charge transfer (Rajapriya et al., 2020). The hybrid shows a capacitance ($\approx 900 \text{ F g}^{-1}$, at 1 A g^{-1}) and only loss ($\approx 5\%$) in efficiency at 5×10^3 cycles in 1 M potassium chloride as an electrolyte (Rajapriya et al., 2020). The effect of MoS₂ concentration via microwave heating as a facile method to deposit MoS₂ with different concentrations over reduced graphene oxide was considered. The best result was for low concentration MoS₂ (MoS₂/reduced graphene oxide) achieved a specific capacitance

1316 F g^{-1} . This electrode displays that an energy density was 63 Wh.kg^{-1} and good cyclic stability ($> 90\%$) of the specific capacitance retained after 1000 cycles (da Silveira Firmiano et al. 2014).

The large volume change of MoS₂ and the depressed electrical conductivity is another challenge. An active encapsulation approach is applied to preparing a core-shell MoS₂/mesoporous hollow carbon spheres MHCS as a nanocomposite (Zheng et al. 2019). MHCS controlled the development of MoS₂ and upgraded both conductivity and structural stability. The electrode brings a reasonably elevated (capacitance $> 610 \text{ F g}^{-1}$, at 1 A g^{-1}) with respectable (rate performance $> 350 \text{ F g}^{-1}$, at ten A g^{-1}) and excellent cycle performance aqueous supercapacitors. More significantly, an ultrahigh (specific energy density $> 200 \text{ Wh kg}^{-1}$, at 200 W kg^{-1}) is confirmed for Li-ion capacitors in which the nanocomposite is the anode (Zheng et al. 2019).

Another challenge is maximizing the gravimetric and volumetric capacitances still another challenge. From that, the hybridization of MoS₂ with hollow carbon nanobowls is studied by (Wang et al. 2020a). The semi-concave shape of MoS₂ encourages rapid electrolyte penetration and offers

an excellent conductive path for both the tested electrode as a supercapacitor, the MoS₂ nanosheets inside hollow carbon nanobowls named MoS₂/hollow carbon nanobowls confirmed outstanding gravimetric capacitance and volumetric capacitance equal (560 F g⁻¹ at 0.2 A g⁻¹ and 874 F cm⁻³), respectively, and cycling performance of 94.4% capacitance retention next 5,000 cycles which is considerably higher than hollow carbon nanobowls/MoS₂ in which hollow carbon nanobowls' surface covered by two-dimensional MoS₂ nanosheets (Wang et al. 2020a). Hollow carbon–MoS₂–carbon nanoplatelets synthesized with excellent stability and dispersibility in water merit electrical conductivity based on morphology enhancement. The hollow nanoplate can provide a high surface area of 543 m² g⁻¹ with a total pore volume of 0.677 cm³ g⁻¹. The symmetric supercapacitors device exhibited a specific capacitance of 248 F/g⁻¹ at 0.1 A g⁻¹, signifying that the prepared nanoplates are talented candidates for supercapacitors (Quan et al. 2019).

Now, a new challenge directs the researchers into environmental, economic, and high performances electrodes for supercapacitors. In particular, lots of efforts made to yield low-cost and environmental carbons. For fascinating the outcome of performance accompanied by environmentally available material, a simplistic process to prepare MoS₂/graphene system based on an improved, environmental-friendly, and cost-effective, scalable ball milling process that resulted in MoS₂/graphene-based inks with few-layer MoS₂ is presented by (Wang et al. 2020b). This ink was used for fabricating two-dimensional sandwiched supercapacitor electrodes. The electrodes displayed a (specific capacitance > 390 F g⁻¹, at 5 mV s⁻¹) and depressed (equivalent resistance ≈ 0.40 Ω), which outpaces the features of graphene electrodes. The specific capacitance of a two-dimensional printed electrode using the as-prepared composite's ink was (≈ 76 F g⁻¹ (at the same scan rate) with (capacitance ≈ of 0.058 μF cm⁻², at 0.77 mg cm⁻²) signifying high energy storage potentiality. The MoS₂/graphene composites' performance and their inks highlight their capacity as suitable electrodes for energy storage devices (Wang et al. 2020b).

Seeking for enhancing the performance with an environmental approach to add more active points and excellent conductance properties, (Zhao et al. 2020) succeeded in synthesizing (MoS₂/carbon) using cornstalks as a bio-carbon source with a large surface area that showed a high (≈ 0.340 μF g⁻¹ as specific capacitance) and good stability as the anode in supercapacitors (Zhao et al. 2020). Molybdenum disulfide/activated carbon is prepared in which carbon is derived from corncob (Wang et al., 2020c). The nanoflower-like MoS₂ is developed on the nanoflakes biomass-derived carbon to increase the specific surface area and thus enhanced its performance and maximized its (specific capacitance ≈ 0.333 μF g⁻¹, at a current density of 0.001 μA g⁻¹) with the capacitance retention loss (≈ 20%)

over 7000 cycles, which is 16-fold and fourfold that of activated carbon and molybdenum disulfide, respectively. The as-assembled MoS₂/activated carbon “symmetric supercapacitor” owns (specific capacitance and energy density ≈ 800 μF g⁻¹ and 7.6 W h kg⁻¹), respectively. One-step and solvent-free ball-milling approach is to synthesize MoS₂/reduced graphene oxide tidy composite by (Ji et al. 2019). The prepared electrode delivers specific capacitance approximately twice that of pure MoS₂ (≈ 300 F g⁻¹ at 0.5 A g⁻¹; current density) (Ji et al. 2019). An innovative, highly flexible, environmental, lightweight, and all-solid-state supercapacitor nanocellulose-derived carbon nanosphere fibers/MoS₂/reduced graphene oxide aerogel nanocomposite is proposed by (Lv et al. 2019) that is derived from nanocellulose fibers in one-step pyrolysis tailed by freeze-drying. The electrode exhibited an excellent energy density and power density touches of 57.5 μW h cm⁻² (28.8 W h kg⁻¹) and 29.1 mW cm⁻² (14.5 kW kg⁻¹), with an excellent capacitance of 1114 F g⁻¹ at 2 mV s⁻¹ and stability loss (less than 2%) after 10 × 10³ cycles in an electrolyte made of H₂SO₄/polyvinyl alcohol gel (Lv et al. 2019).

Maximum utilization of the available sources, as well as waste management, succeeded achieved by (Sangeetha and Selvakumar 2018). Firstly, they used biomass–Tendu leaves as a source for activated carbon. The synthesized composite (MoS₂/activated carbon) was used for supercapacitors. The activated carbon displayed both micro/mesopore structures with (specific surface area of 1509 m² g⁻¹). 0.261 mF g⁻¹ and 0.193 mF g⁻¹ are the specific capacitance values for the tested symmetric and hybrid supercapacitors, respectively (Sangeetha and Selvakumar 2018). Secondly, they used polyethylene terephthalate bottles as an activated carbon source with a high specific surface area (≈ 900 m² g⁻¹). The sponge-like activated carbon network with a minor layer of molybdenum disulfide–carbon displayed a power density up to 469 W kg⁻¹ (Sangeetha et al. 2020).

Electrochemical performance of polymeric hybrids of MoS₂

Two-dimensional MoS₂ considered an auspicious electrode material for supercapacitors, owing to its good morphology (exposed surface area), outstanding electrical features, and attractive physical properties. Nevertheless, its bulk suffers from low capacity resulting from the layers' overlaying and poor electric conductivity.

The combination of conductive polymers with MoS₂ resulted in integrating pseudo-capacitive behavior of conductive polymers and interactive features of MoS₂ to frame highly stable electrodes with good performance (electrochemical) such as astonishing capacitance and decent cycling stability. Reversible transport of ions within electrolyte related to the multilayered MoS₂, while conductive

Table 3 Electrochemical performance of polymeric hybrids of MoS₂:

Material	Preparation method	Electrolyte	Current density, A.g ⁻¹	Capacitance, F.g ⁻¹	Specific capacitance retained, %	Cycling stability, cycles × 10 ³	Refs.
MoS ₂ /polyaniline	Solvochemical in situ oxidative polymerization	1 M H ₂ SO ₄	1	496	79	6	(Meng et al. 2015)
			0.5	552	79	6	(Ren et al. 2015)
MoS ₂ /polypyrrole	Hydrothermal and in situ oxidative polymerization	1 M KCl	1	553.7	90	0.5	(Ma et al. 2013)
			0.5	695	85	4	(Tang et al. 2015)
MoS ₂ /polyaniline/carbon	Chemical exfoliation and oxidative polymerization	1 M H ₂ SO ₄	1 mV s ⁻¹	678	80	10	(Yang et al. 2016)
1H-MoS ₂ /oleylamine	Hot-injection thermolytic decomposition	1 M Na ₂ SO ₄	0.37	50.65 mF cm ⁻²	100	5	(Savjani et al. 2016)

polymers cover these layers, will increase the specific surface area (Wazir et al. 2019). Table 3 shows the electrochemical performances of some conductive polymers (such as polyaniline and polypyrrole) that were previously studied and indicated that conductive polymers–MoS₂ hybrids are actually suitable supportive candidates for supercapacitor applications (Huang et al. 2013c; Ren et al. 2015; Ma et al. 2013; Tang et al. 2015; Savjani et al. 2016).

For polyaniline–MoS₂ hybrids, multifunctional MoS₂/polyaniline pseudo-supercapacitor electrodes was proposed by (Zhu et al. 2015). MoS₂ nanosheets and polyaniline nanoarrays were fabricated via a large-scale approach.

Capacitance retention retained for 4000 cycles ($\approx 91\%$). High energy density achieved ($\approx 0.106 \times 10^3 \text{ Wh.kg}^{-1}$ at $\approx 106 \text{ kW kg}^{-1}$; power density) (Zhu et al. 2015). Other MoS₂/polyaniline nanocomposites reported by (Huang et al. 2013c) proved the positive synergistic effect of the conductive polymer (polyaniline) on molybdenum disulfide through the enhancement of specific capacitance ($\approx 0.575 \text{ mF g}^{-1}$ at 1 A g^{-1}) with an outstanding long-term cyclic stability. Polyaniline–MoS₂ hybrid offers a larger specific surface area “contact” for the protons’ intercalation/deintercalation resulting from the MoS₂ nanohybrid with graphene-like form which was assisted as an excellent two-dimensional conductive skeleton that affords an extremely electrolytic accessible surface area of redox-active (polyaniline) and runs a straight pathway for electrons (Huang et al. 2013c). Optimized method of the capacitive performance through a controlled process of progress of polyaniline nanowires arrays on the tubular molybdenum disulfide surface proposed by (Ren et al. 2015). MoS₂/polyaniline hybrid showed both high specific capacitance ($\approx 0.55 \text{ mF g}^{-1}$ at 0.5 A g^{-1}) and an excellent rate capability (only loss = 18%) from (0.5 to 30 A g^{-1}).

Recently, (Zeng et al. 2019b) stated that the covalent linking MoS₂ with conducting polymers would boost the electrochemical performance and overcome the drawbacks. So, (Zeng et al. 2019b) synthesized MoS₂-NH₂/polyaniline via in situ growth of polyaniline over MoS₂-NH₂ patterns and found that the as-prepared composite revealed a high (capacitance $\approx 0.326 \text{ mF g}^{-1}$, at 0.5 A g^{-1}), with low rate retention loss ($\approx 27\%$) as current intensity elevated from (0.5 to $1 \times 10^3 \text{ A.g}^{-1}$) in the three-electrode model, while, in the symmetric supercapacitor devices, cycling stability retained

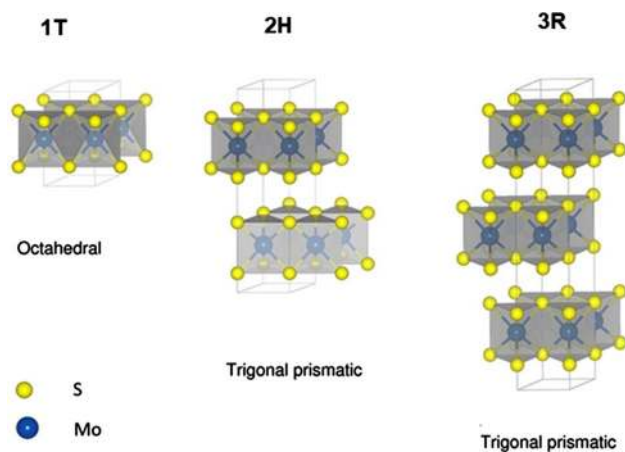


Fig. 1 Molybdenum disulfide crystal structure: octahedral, trigonal prismatic, and trigonal prismatic that abbreviated (1 T), (2H), and (3R), respectively. Reprinted with permission of John Wiley and sons from (Han and Hu 2016)

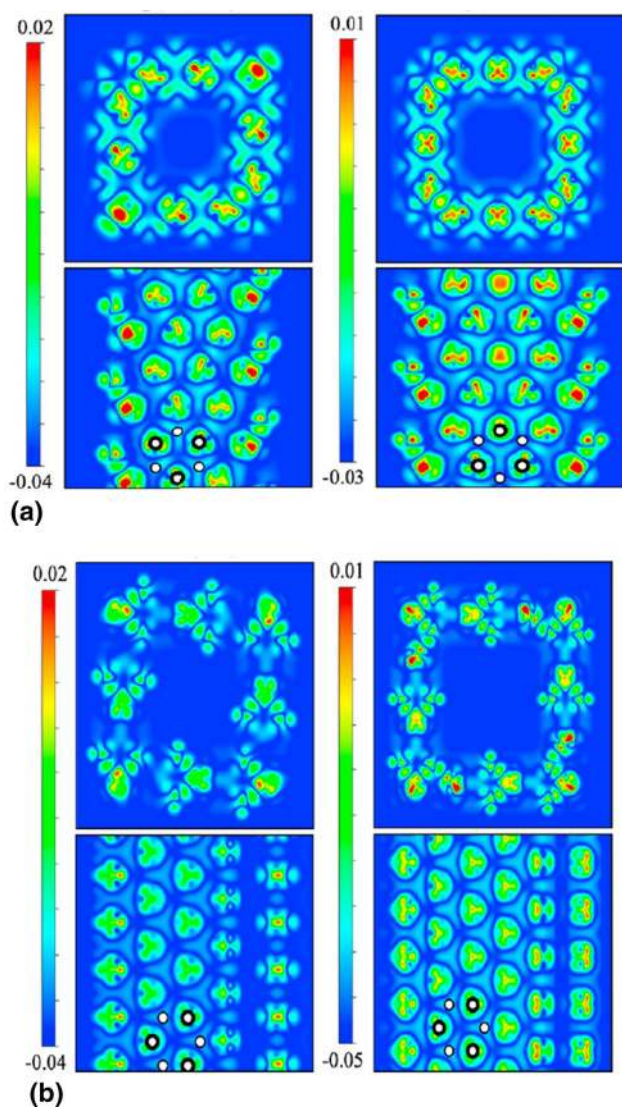


Fig. 2 **a** Zigzag structure of MoS₂ and **b** both square and cylinder nanotube. Reprinted with permission of Elsevier from (Zhang et al. 2021)

at 96.5% (subsequent 10,000 cycles at 5 A g⁻¹). This is also in agreement with the good impact of conducting polymers on MoS₂ and its capability as promising electrode materials for energy storage devices (Zeng et al. 2019b).

Another category of nanostructured polyaniline hybrids and polyaniline hydrogels has superior features such as flexible durability, good electrical conductivity, and astonishing electrochemical reactivity. So, (Das et al. 2019) used MoS₂ quantum dot and *N,N'*-dibenzoyl-L-cystine via in situ polymerization to make MoS₂/polyaniline hydrogel as a solid-state elastic supercapacitor electrode. The covalently linked hybrid achieved an enhanced energy storage performance and showed an excellent specific capacitance ($\approx 791 \text{ F g}^{-1}$ at 1 A g⁻¹) and ($\approx 331 \text{ F g}^{-1}$ at 1 A g⁻¹) for the

three-electrode and the stretchy all-solid-state supercapacitor device, respectively. Additionally, the energy and power densities were ($\approx 29.4 \text{ Wh kg}^{-1}$ and 398 W kg^{-1}), respectively, with capacitance retention ($\approx 84.2\%$ after 10,000 cycles). A tandem supercapacitor model consists of 4 (charged) solid-state supercapacitors connected together and linked to power different colored diode bulbs for a lengthy period, indicating their good capability as a storage device (Das et al. 2019).

According to MoS₂/polypyrrole hybrids, (Ma et al. 2013) reported a facile approach to synthesize MoS₂/polypyrrole as an electrode for high-performance supercapacitors. Firstly, a hydrothermal treatment was used to synthesize flower-like MoS₂ (graphene-like) and then in situ oxidation polymerization of polypyrrole in MoS₂ nanosheets suspension. The MoS₂/polypyrrole nanocomposite revealed a specific capacitance ($\approx 5.5 \times 10^2 \text{ F g}^{-1}$ at 1 A g⁻¹; current density) and (capacitance loss 10% after 5×10^2 cycles) (Ma et al. 2013). The polypyrrole ultrathin film grows on two-dimensional MoS₂ monolayer synthesized by (Tang et al. 2015). The hybrid MoS₂/polypyrrole exhibited a high specific capacitance reached ($\approx 700 \text{ F g}^{-1}$, at 0.5 A g⁻¹; discharge current) and ($5 \times 10^2 \text{ F g}^{-1}$, at 10 A g⁻¹; discharge current density). This signified the admirable rate of performance (Tang et al. 2015).

Also, (Savjani et al. 2016) synthesized high-quality and pure MoS₂ nanosheets covered by oleylamine through hot-injection thermolysis (one-pot synthetic route). MoS₂/oleylamine showed (0.05 F cm^{-2} ; specific capacitance, at 0.37 A g⁻¹). The cycling stability was excellent as it retained as much as 100% (up to 5000 cycles) (Savjani et al. 2016).

A comprehensive study between graphene oxide/polypyrrole and MoS₂/polypyrrole is fabricated via an easy and fast one-pot chronoamperometry procedure. The hybrids used to fabricate additive-free, scalable, and binder-free supercapacitors electrodes. Both the electrodeposited hybrids (graphene oxide-polypyrrole and molybdenum disulfide-polypyrrole) electrodes exhibited specific capacitance (nearly equal $\approx 2.7 \times 10^2 \text{ F g}^{-1}$ and $1.3 \times 10^2 \text{ F g}^{-1}$, at 1 A g⁻¹; current density), respectively. Reduced graphene oxide in polypyrrole mate presented high capacitance, while molybdenum disulfide upgraded the structural stability and a noticeable (2000 cycles; cycling stability). MoS₂/polypyrrole retains 82%, and graphene oxide/polypyrrole retains 64% of their initial capacitance (Prasankumar et al. 2019).

A facile strategy for in situ integrating two-dimensional molybdenum disulfide nanosheets into a three-dimensional polypyrrole network was proposed by (Tian et al. 2020). This was achieved via intercalation between MoS₂ nanosheets and (dodecylbenzene–sulfonate anions), allowing direct growth of polypyrrole in an ordered manner. The resulting orderly self-standing films of polypyrrole chains delivered a good areal capacitance and volumetric capacitance ($\approx 1.2 \text{ F cm}^{-2}$ and 325 F cm^{-3}), respectively, indicating the

Fig. 3 a–f Scanning electron microscope images, g mapping images for Red phosphorus coating MoS_2 @ reduced graphene oxide. Reprinted with permission of Elsevier from (Bai et al. 2018), showing the curly layers where the graphene oxide works as a scaffold to resulting in anchoring and stabilizing for the nanostructured sheets of MoS_2 and Red phosphorus and affirmed a consistent distribution of elements

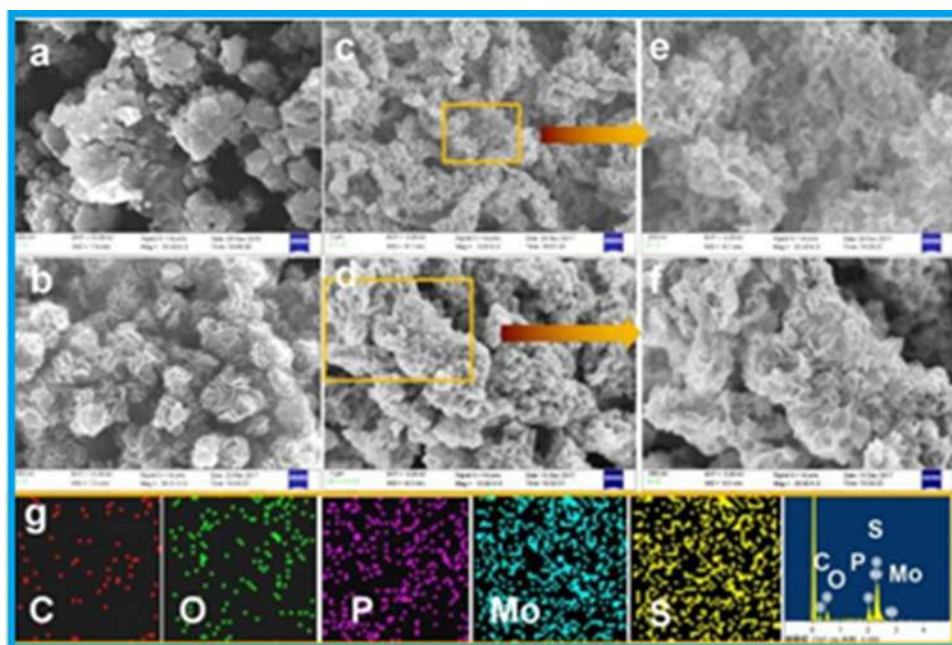
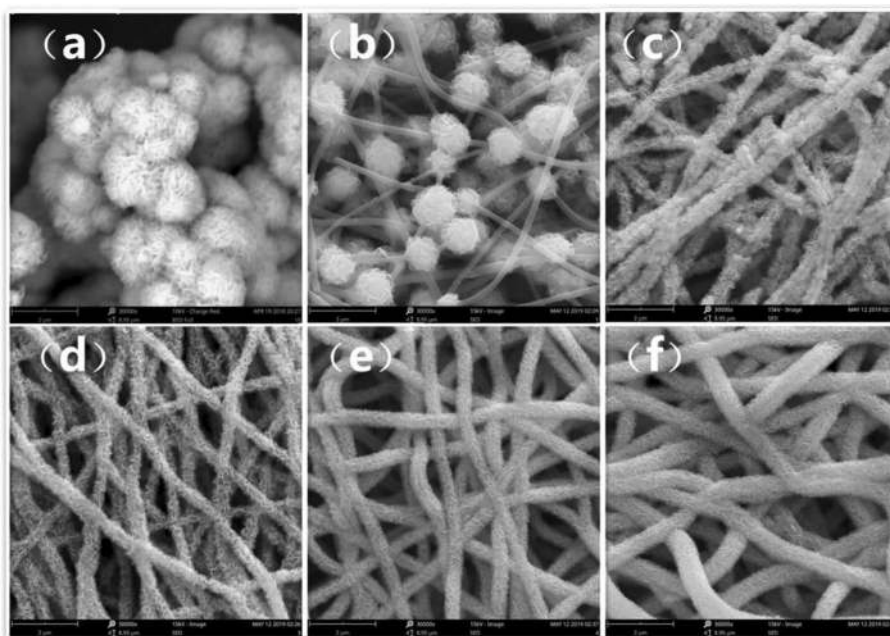


Fig. 4 Scanning electron microscope images of a pure MoS_2 , b–f different ratios of MoS_2 in MoS_2 /carbon nanofibers composite (0.1–0.5, step=0.1). Reprinted with permission of Elsevier from (Liang et al. 2020)



superiority of MoS_2 synergism effect with polypyrrole over pure polypyrrole and, as a result, imparting good applicability for stretchable supercapacitors with excellent performances (Tian et al. 2020).

Recent studies focus on ternary composites to cover the previously stated hybrids' defects, enhancing the composite characters and fascinating the electrode capacitance. In the same context, (Yang et al. 2016) synthesized (MoS_2 / polyaniline @carbon) ternary composite formed of MoS_2 (1 T phase) monolayers on which carbon shell-coated polyaniline grown up. The MoS_2 /polyaniline/carbon composite

electrode with a (~ 3.00 nm; carbon shell) and unveiled a notable specific capacitance ($\approx 678 \text{ F g}^{-1}$ at 1.0 mV s^{-1}), reserved only retention loss ($\approx 20\%$ after 10,000 cycles), and 19% at 10 mV s^{-1} , as good rate performance as a result of the combined effects of both 1 T MoS_2 substrates with polyaniline nanostructure and the protective cap of carbon shell (Yang et al. 2016).

Another research trend focused on inexpensive starting materials with the environmental manner; (Ma et al. 2014) succeeded to synthesize MoS_2 (flower-like) via sodium alginate as an additive for the annealing process via a facile route

(hydrothermal). The resulted MoS₂ was hexagonal phases with hierarchical morphology built on MoS₂ nanosheets. For the electrode for supercapacitors, the synthesized microsphere brought a good specific capacitance ($\approx 145 \text{ F g}^{-1}$, at 3 A g^{-1}) as well as exhibited good cycle stability (Ma et al. 2014).

Natural resources such as lignin were used by (Wang et al. 2019) as a renewable source for carbons. Laser irradiation and pyrolysis were the methods used to obtain tetrahedral amorphous carbon and graphitic carbon, respectively. They also mixed MoS₂ into the lignin/polyacrylonitrile hybrid polymers to optimize the capacities. Lignin/polyacrylonitrile compared to lignin/polyacrylonitrile doped with MoS₂ was found to fascinate the areal specific capacitance twice from (6.7 mF cm^{-2} (0.9 F cm^{-3}); at 10 mV s^{-1}) to (16 mF cm^{-2} (2.2 F cm^{-3}); and at 10 mV s^{-1}) (Wang et al. 2019). Also, (Ge et al. 2017) demonstrated a free-standing bendable MoS₂-based supercapacitor electrode. The poly (3,4-ethylene dioxythiophene)/poly (styrene sulfonate) highly conductive polymer was combined with robust MoS₂. The volumetric capacitance was ($\approx 1.41 \times 10^2 \text{ F cm}^3$), volumetric energy density was ($\approx 4.9 \text{ mWh cm}^3$), and capacitance retention was ($\approx 98.6\%$; after 5×10^3 cycles). The main reason for these enhanced results is that the fabricated film possesses remarkable mechanical features such as Young's modulus ($= 2.0 \text{ GPa}$) and fracture strength of 18.0 MPa (Ge et al. 2017).

Electrochemical performance of metal-based hybrids of MoS₂

Metal oxides (Ni, Co, and iron oxides) are abundant, environmental, chemically stable and have high theoretical capacitance. Besides, metal-MoS₂ hybrids/composites can be ascribed to their improved architecture and atomically sharp heterojunctions (Wazir et al. 2019). Transition metal oxides such as (Co₃O₄, Co(OH)₂, RuO₂, NiO, and NiCo₂O₄) can maximize specific capacities and perform swift redox kinetics. Therefore, they likely act as electrode materials for supercapacitors. Nevertheless, these oxides typically have a low surface area. Some have a poor electrical conductivity that increases the intrinsic resistance, hindering ions and electrons transfer, and restricted practical use. On the flip side, the transition metal oxides and sulfides engage a reversible faradaic reaction to stock charges. Their capacitance capabilities and energy densities are superior to those of carbon-based materials. Defects in commercial applications may result from their poor cycling stability from distortion in their microstructures and their original shape. So, the progress of highly porous transition metal oxides nanostructures having an excellent electrochemical performance is crucial.

Incorporating MoS₂ in MoS₂-transition metal oxides hybrids nanostructured will fascinate the energy-storage

performances associated with a high-rate capability. MoS₂-transition metal oxides hybrids are expected to have the following merits: low-cost, environmental, scalable, and facile synthesis approach with compatible and tunable morphologies. These heterostructures prevent restacking of the MoS₂ that will permit abundant active sites to be added due to enhanced ions permeability and electron interactions. The insertion of porous transition metal oxides (*e.g.*, Co₃O₄, NiO, and Fe₂O₃) into two-dimensional MoS₂ nanosheets using a facile strategy is studied by (Wang et al. 2017c). The resulting hybrid positively impacted enhanced electronic/ionic transport and confirmed an astonishing pseudo-capacitive performance (over 1×10^3 at 1 A g^{-1} and retained 101.9% after 9000 cycles at 2 A g^{-1}). MoS₂-NiO//MoS₂-Fe₂O₃ asymmetric supercapacitor achieved a high energy density ($\approx 40.0 \text{ W h kg}^{-1}$) (Wang et al. 2017c).

Another study presented by (Chai et al. 2018) used an in situ redox etching reaction to fabricate MnO₂ (hollow nanospheres) on a molybdenum disulfide (nanospheres) as a sacrificial matrix. The supercapacitor electrode verified (95.2%; capacitance retention after 5×10^3 cycles; at 5.0 A g^{-1}) and (394 F g^{-1} ; specific capacitance, at 1.0 A g^{-1}) (Chai et al. 2018).

Ternary composites will aid to cover the defects in the previously studied hybrids. Low-cost MoS₂/graphene coated on mesoporous MnO₂ nanocomposites that reveal (up to 527.0, 727.0, and 1160.0 F g^{-1} ; specific capacitance) escorted by continuous cyclic stability was fabricated by (Ramalingam et al. 2018).

Microwave-assisted, facile, and one-step methods are used to synthesize MoS₂/MoO_x nanocomposites that are grown on activated carbon (Sari and Ting 2018). The resulted composite supports the ions intercalation: MoO_{3-x}, monoclinic MoO₂, the conductive activated carbon. The cloth provides swift electron transport. On the contrary, molybdenum disulfide nanosheets/MoO_{3-x} nanoparticles will expand capacitance. Briefly, MoS₂/MoO_x-activated carbon cloth displayed an excellent specific capacitance ($\approx 230 \text{ F g}^{-1}$, at 5.0 mV s^{-1}) and showed steadiness over 125% and capacitance retention after 1500 cycles (Sari and Ting 2018).

The synergistic effect of Fe₃O₄, MoS₂, and reduced graphene oxide was considered by (Salarizadeh et al. 2020). The synthesized nanocomposite via a 2-step hydrothermal way demonstrated a respectable specific capacity ($\approx 527 \text{ F g}^{-1}$, at 0.5 mA cm^{-2}). This confirms that MoS₂ with iron oxides offers electroactive sites for electrolyte accessibility and faradic processes, and reduced graphene oxide provides conductivity (Salarizadeh et al. 2020).

The metal sulfides (NiS_x, CoS_x, CuS_x, and FeS₂) considered novel and suitable electrodes for supercapacitors because they have minor electronegativity and developed

electrochemical activity reflecting positively on specific capacities and energy/power densities. Specifically, metal sulfides-based hybrids can afford better redox reactions than monometal sulfides, expressing superior specific capacity. However, their poor conductivity retards rate capability and cycling stability. Introducing MoS₂ could reduce the previous defects, facilitate electron transport, and boost the electrochemical features (Li et al., 2020a). Owing to their low cost, good electrical conductivity, their activity, especially with their electrochemical stability, and the proper architecture of composites' metal sulfides is supposed to be very operative for abundantly exploiting their merits and breaking through their confines of the low-rate capability and lesser cycling stability in supercapacitors applications. The metal sulfides are widely tested and developed for supercapacitors with astonishing electrochemical performances.

This study presented a facile (in situ hydrothermal) approach to making high-performance binder-free electrodes (Zhao et al. 2020). The NiS₂/MoS₂ composite fabricated by (Yang et al. 2021) using a hydrothermal approach. Then the NiS₂/MoS₂ was decorated by graphene nanosheets. The obtained composite electrode owned imposing electrochemical performances such as a high specific capacity (over 230 F g⁻¹; at 1 A g⁻¹) with first-rate rate capability (over 60%; at 1 × 10² A g⁻¹) (Yang et al. 2021).

Additionally, other metal-MoS₂ hybrids that enhance electrode performance have been reported. For instance, (Wang and Xie 2020) designed an electro-active hybrid based on FeS₂/MoS₂. The hybrid tested theoretically and presented a high density of states (Fermi level) and a narrow bandgap. The hybrid revealed higher specific capacitance (394 mF cm⁻²) linked to that of MoS₂ (218.1 mF cm⁻²) and that of FeS₂ (286.5 mF cm⁻²) at 1.0 mA cm⁻² in 0.5 M Na₂SO₄. The capacity retention enhanced from 58 and 73% for MoS₂ and FeS₂, respectively, to be 76% for the hybrid in the same electrolyte. The cycling capacity retention for FeS₂/MoS₂ was 100.7% (5 × 10³ cycles; at 5.0 mA cm⁻²). For the asymmetric device, the anode was FeS₂/MoS₂, the cathode was exfoliated graphite carbon paper, and the electrolyte was NaMoO₄-Na₂SO₄-poly(vinyl alcohol) gel. The performance was 112.8 mF cm⁻² (at 1.0 mA cm⁻²) and 56.56 mWh cm⁻² for the specific capacitance and the energy density. Capacity retention lowered that ideal by 2% after (5000 cycles, at 5.0 mA cm⁻²) (Wang and Xie 2020).

Another strategy to improve the electrochemical performance and good stability and cyclability is fabricating a ternary composite based on metal sulfide and carbon materials along with MoS₂. Recently, (Li et al., 2020a) fabricated a ternary composite (MoS₂/NiCo₂S₄/carbon) composed of carbon-coated MoS₂/NiCo₂S₄ urchin-like micro-spheres via a self-template approach that achieved a high (≈250 mAh g⁻¹; specific capacity at 2 A g⁻¹) besides capability (≈ 91.1%; at 40 A g⁻¹). The asymmetric device with the as-prepared

composite as positive electrode and AC as negative electrode displayed an energy density of (≈ 53.01 Wh kg⁻¹) at power density (≈ 4.20 kW kg⁻¹) and stability of nearly ninety percent after ten thousand cycles at (10 10 A g⁻¹; current density) (as presented in Fig. 5) (Li et al., 2020a).

Reprinted with permission of Elsevier from (Li et al., 2020a). Among the studied electrodes, the discharging time of the MoS₂/NiCo₂S₄/C is the longest, which is in agreement with the cyclic voltammetry curves. Also, the MoS₂/NiCo₂S₄/C displays a lower equivalent series resistance than that of MoS₂/NiCo₂S₄ and NiCo₂S₄/C.

The synergistic effect of molybdenum disulfides with nickel sulfides on carbon nanotubes as a supportive mate was studied by (Yang et al. 2017). The composite (nickel sulfides/carbon nanotubes) was fabricated via a one-step hydrothermal approach. The asymmetric device assembled as nickel sulfides/carbon nanotubes achieved a specific capacitance over 107 F g⁻¹ at 0.5 A g⁻¹ with 100% cycling stability after ten thousand cycles. The network affords accessibility to the electrolyte and nickel sulfides nanoparticles encouraged the diffusion of ions onto the electrode surface, and nickel sulfides voids tolerate changes in volume while redox process (Yang et al. 2017).

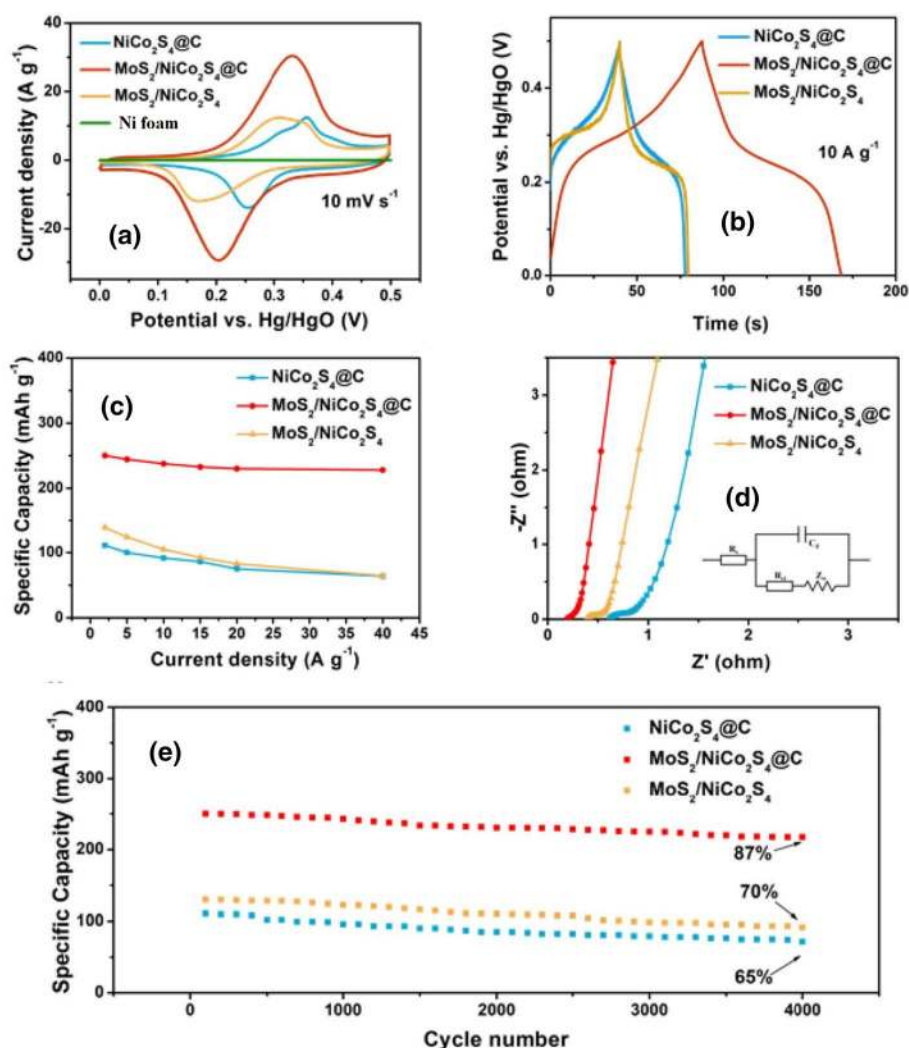
The NiCo₂S₄-C-MoS₂ composite structure was fabricated via hydrothermal and solvothermal techniques by (Wang et al., 2018). In the three-electrode system, the as-prepared electrode showed a specific capacitance of 1601 F g⁻¹ at 0.5 A g⁻¹, and the asymmetric device exhibited (energy density = 27.7 Wh kg⁻¹) at (power density = 400 W kg⁻¹) after one thousand cycles at 2 A g⁻¹ (Wang et al., 2018).

MoS₂-based nanocomposites for batteries

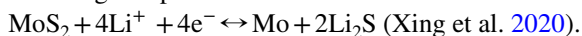
Lithium-ion batteries

Lithium-ion batteries played a master role in the past few years from both academic and industrialized energy storage societies because of their distinctive importance as the safest, low-cost, and widespread power/energy source for most portable electronics such as smartphones, digital cameras, laptop computers, and also as a talented power source for hybrid/electric vehicles (Scrosati et al. 2011). However, the hindrance is facing the current rechargeable batteries and their relatively low energy density, low stability, and sluggish charging rate (Xu et al. 2020). Therefore, discovering and tailoring innovative electrode materials are essential for improving the batteries' performance. However, the currently commercialized graphite anode in lithium-ion batteries is restricted by its theoretically low specific capacity and capacity fading over long-standing charge/discharge processing, which does not satisfy the request of high energy/power densities (Shen et al. 2018).

Fig. 5 **a** Cyclic voltammetry curves of the studied electrodes at 10 mVs^{-1} . **b** Galvanostatic charge–discharge curves of the studied electrodes at 10 A g^{-1} . **c** Specific capacities of the studied electrodes at different current densities. **d** Nyquist plots of the studied electrodes. **e** Cycling stability of the studied electrodes at 10 A



Moreover, the electrode volume will suffer from the increase in size during the lithiation/delithiation course in lithium-ion batteries, affecting the battery performance. In this regard, the energy storage field has witnessed a dramatic growth in the research efforts that are going on to accomplish new electrode materials for lithium-ion batteries. Owing to its remarkable properties and extensive potential applications, two-dimensional (graphene-like structure) materials have long been studied intensively (Cao et al. 2018). In this regard, the attractive advantages of rich abundance and low-cost transition metal sulfides play an essential part in the progress of electrode materials for batteries along with their energy-related performance. Among the two-dimensional transition metal sulfides, MoS₂ attracted the most attention due to its natural abundance and suburban stabilities (Wang et al. 2015). The layered-structure MoS₂ has a tremendous theoretical capacity of 0.67 Ah g^{-1} depending on the following lithiation storage response:



This lithiation mechanism is characterized by a fast diffusion rate of lithium ions, excluding volume expansion (Xing et al. 2020; Li et al., 2020b).

Practically, the low electrical conductivity of pristine MoS₂ inhibits the kinetic of electronic transfer, which impacts the behavior of lithium-ion batteries (Hu et al. 2015). Additionally, the bulk MoS₂ reveals slow kinetics of redox reaction, which decreases its electrochemical reactivity. Additional, poor cycle stability arises during the lithiation/delithiation process. Therefore, for practical application, pristine MoS₂ has drawback concerning with its cycling stability and conductivity. In this regard, structural modifications, including composite tailoring and/or atom doping, are often suggested to improve the desired features of MoS₂-based electrodes successfully.

Based on the layered structure of MoS₂ with sufficient interlayer distance, which allows for effective ion diffusion, (Teng et al. 2016) prepared nanosheets of molybdenum disulfide on the graphene sheets within a carbon–O–Mo bond via a feasible hydrothermal method. The growth of

MoS₂ on the graphene layers improved the mechanical stability and the electrical conductivity of the designed composite anode material for lithium-ion batteries, delivering outstanding rate capability and extensive cycle stability. The threefold electrode acquired additional advantages; for example, (1) the O-containing groups act as “connectors/collectors” leading to MoS₂ nanosheets to be spread vertically over the aligned graphene layers and thus provides frequent active edge sites for lithium reactivity as well as lessens the distance required for diffusion of both Li⁺ ions and electrons. (2) C–O–Mo bonds resulted in a stable MoS₂/graphene hybrid and an excellent path for electrons between the hybrid subunits. (3) Limited volume expansion is as a result of the robust graphene sheets. The previously mentioned features made MoS₂/graphene anodes have an astonishing performance.

Three dimensional-ordered microporous structure of MoS₂ combined with carbon cloth to impede the restacking of MoS₂ layers and regulate lithiation/delithiation volume expansion (Zhang et al. 2019a). The obtained electrode material maintains its structure even after 100 cycles.

Carbon-based/MoS₂ nanocomposite onion-like construction as an active material for the as-prepared anode electrode of lithium-ion batteries was designed by (Wang et al. 2014b). The nanocomposite showed a specific capacity ($\approx 853 \text{ mAh g}^{-1}$, at 50 mA g^{-1} ; current density) and can deliver for the first cycle an excellent coulombic efficiency of 97.6% (Wang et al. 2014b). More advance, (Wang et al. 2016b) have successfully prepared nanoleaves MoS₂ upon graphene nanosheets. This can not only stop the restacking of graphene layers but also improve the growth of MoS₂. The obtained electrode exhibited a specific capacity of 1277 mAh g^{-1} at 100 mA g^{-1} current density. Also, it can keep a capacity of 1109 mAh g^{-1} after even 100 consecutive cycles, reflecting its excellent cycling performance.

Other electrical active materials such as metal oxides (Pan et al. 2017), Mxene (Li et al. 2019b; Wu et al. 2017), and metal sulfides (Jiang et al. 2017) have been hybridized with MoS₂, in addition to carbon materials, to improve their lithium storage capacity. The synergistic effect between each part can improve favored the electrochemical performance of the prepared hybrids and/or composites by scheming the structure of the binary combinations rationally. Also, (Chen et al., 2014a) have prepared a MoS₂ with the help of a tiny Fe₃O₄ nanoparticle, using a two-step hydrothermal method. In the Fe₃O₄/MoS₂ hybrid, spacers Fe₃O₄ inhibited MoS₂ nanosheets restacking, while MoS₂ prevented Fe₃O₄ nanoparticles from aggregating. Consequently, Fe₃O₄/MoS₂-fabricated anodes showed superior capacities (≈ 224 and 1033 mAh g^{-1} at current densities (≈ 10 and 2 A g^{-1}), respectively.

Further, (Chen et al., 2014b) have prepared a composite anode material with great potential made from, SnO₂/MoS₂, with different ratios, where SnO₂ nanoparticles are used to

preclude the restacking of MoS₂ nanolayers, whereas MoS₂ nanolayers act as a substrate to provide accommodations with the SnO₂ nanoparticles. Four composites with different ratios of SnO₂/MoS₂ are prepared. One of them, SnO₂/MoS₂ composite with a mass ratio of 2: 1, achieved the best performance as anode material, providing the maximum and most stable reversible capacity within 230 cycles and a current density ($\approx 10^2$: 10^4 mA g^{-1}).

The Sn/SnO₂/C/MoS₂ as a novel anode material for lithium-ion batteries, contained nanosheets of Sn/SnO₂/C that combined with MoS₂ synthesized by (Huang et al. 2016). The composite revealed pronounced enhancement in the electrochemical response. They deliver outstanding cycling stability (exceeded 840.0 mAh g^{-1} at 1.0 A g^{-1} , after 4×10^2 cycles) and excellent rate capability (over 450 mAh g^{-1} at 10.0 A g^{-1}) to their practical combined effect among MoS₂ and Sn/carbon nanosheets.

Also, (Chen et al. 2019b) have fabricated the heterostructure of MoS₂–SnO₂ encapsulated inside carbon nanofibers and tested it as a negatively binder-free anode material (MoS₂–SnO₂/carbon nanofibers) for lithium-ion batteries. Such innovative architecture produced a 983 mAh g^{-1} discharge capacity at 200 mA g^{-1} after 100 cycles and 710 mAh g^{-1} after 800 cycles at 2000 mA g^{-1} .

Lately, (Li et al. 2019b) proposed synthesizing of molybdenum disulfide on Mxene structures via in situ sulfidation of Mo₂TiC₂T_x-Mxene designed for lithium storage (Li et al. 2019b). Mxene increased the electrical conductivity of MoS₂ and improved Li and polysulfide adsorption, which helped to enhance Coulombic efficiencies and cyclic performance. Molybdenum disulfide/TiO₂ nanotubes hybrid nanostructures are fabricated in a two-phase way. The prepared hybrid has demonstrated excellent lithium storage capacity and rate capabilities as an electrode in lithium-ion batteries (Xu et al. 2014).

The easy in situ conversion was used to transform molybdenum dioxide into MoS₂MoO₂ three-dimensional sulfur architectures (Xu et al. 2017). The obtained architectures from MoO₂/MoS₂ show explicitly increased Li⁺ storage and cycling capacity. The optimized composition was (91: 9%) of MoS₂ and MoO₂, respectively; the architectures of the MoO₂/MoS₂ are ready to have a reversible capacity of 1167 g^{-1} at the 2nd cycle of 1016 mAh g^{-1} after 2000 cycles.

Besides carbonaceous and metal oxides' electrodes, other electroactive electrode materials such as conducting polymers have gained a huge interest owing to their comparatively high energy density, inexpensive, facile manufacturing, and environmentally safe. However, the main challenge of conducting polymers lies in fading their performance after long-term cycling because of the swelling/shrinkage process of their bulk and consequent material destruction during the charging/discharging of ions. As a result, they are often

mixed with other electroactive materials such as carbon materials and/or metal oxide and/or sulfide. For example, nanosheets MoS_2 decorated polyvinylpyrrolidone as a surfactant (Liang et al. 2013), porous MoS_2 /polyaniline composite (Liu et al. 2015) as the template, and quasi-hollow hierarchical MoS_2 microspheres coated by monodisperse polystyrene sulfonates synthesized by (Wan et al. 2014). The polystyrene sulfonates have been working as a good template for carbon/ MoS_2 micro-shell preparation. The carbon/ MoS_2 microspheres, as prepared as an anode material, showed excellent cycling stability and high rates of performance (95% of the capacity retained after 100 cycles).

Three-dimensional hierarchical MoS_2 /polyaniline nanoflowers composite was fabricated using a feasible hydrothermal route (Hu et al. 2014). The as-prepared electrode of three-dimensional MoS_2 /polyaniline showed superb electrochemical performance. Moreover, the annealing of MoS_2 /polyaniline may lead to the development of three-dimensional hierarchical MoS_2 /C nanoflowers, as shown in Fig. 6. The produced MoS_2 /C sample revealed superior electrochemical performance (Fig. 7), more reversible capacity ($\approx 888.0 \text{ mAh g}^{-1}$), with the coulombic efficiency preserved with only a loss of 10% from the initial cycle, at a current density of 10^2 mA g^{-1} .

Also, (Yang et al., 2013b) integrate nanosheets of MoS_2 /polyaniline nanowires, showing adequate capacity and respectable cyclability, demonstrating promising anode material for lithium-ion batteries. The gained nanowires of MoS_2 /polyaniline with the optimum ratio of (MoS_2 /polyaniline) which was equal (66.7: 33.1%), respectively, show a high charge capacity of $1063.9 \text{ mAh g}^{-1}$ at 100 mA g^{-1} , holding over 90% of the initial capacity even after fifty cycles.

Fig. 6 Scanning electron microscopy with different magnifications imaged of three dimensional MoS_2 /polyaniline **a, b** and MoS_2 /carbon **d, e** with two photographs **c, f** of natural roses. Reprinted with permission of American Chemical Society from (Hu et al. 2014). The figure demonstrates that the hierarchical flower-like structures of the MoS_2 /polyaniline are successfully prepared

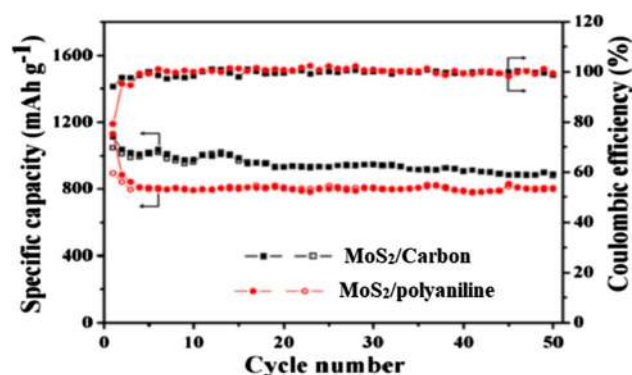
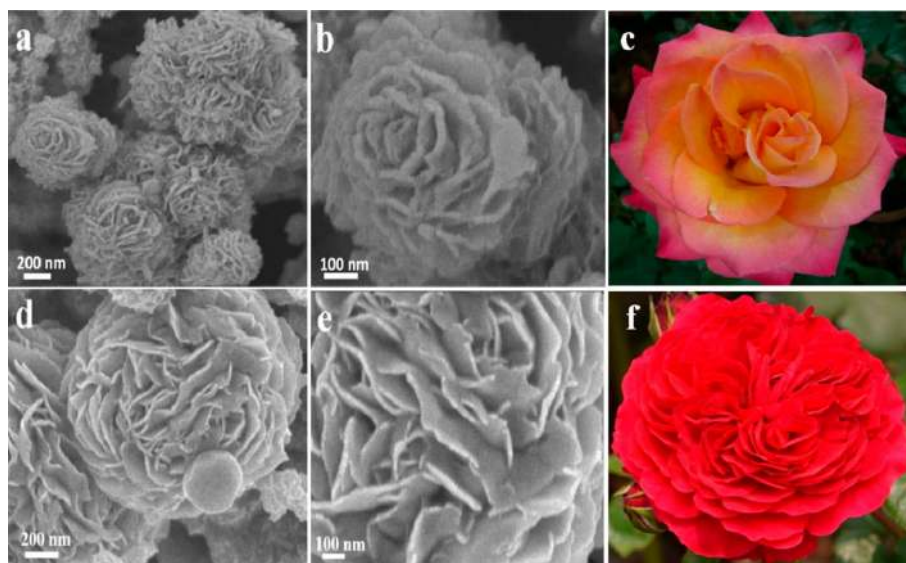


Fig. 7 Cycling performance and Coulombic efficiency of three-dimensional hierarchical MoS_2 /polyaniline and MoS_2 /C nanoflowers. Reprinted with permission of American Chemical Society from (Hu et al. 2014). Notably, both the MoS_2 /polyaniline and MoS_2 /C nanoflowers exhibit excellent cycling stability with high reversible specific capacities of 801.2 and 888.1 mAh g^{-1} after 50 cycles, respectively

Sodium-ion batteries

Besides its low redox potential and its outstanding rate capability, the vast abundance of sodium in nature lets the researchers more intensively interest sodium-ion batteries in being the coming generation of energy storage systems' market (Chen et al. 2020).

Nevertheless, the ionic radius (r) of ($\text{Na}^+ = 1.02 \text{ \AA}$), whereas ($\text{Li}^+ = 0.76 \text{ \AA}$) (Li et al., 2020b); sodium usually displays a slow reaction rate due to its relatively large radius. In this regard, it is important to examine new host electrode materials capable of accelerating and permitting sodiation/desodiation kinetics (Hwang et al. 2017). The large inter-layer spacing of molybdenum disulfide allows sodium ions to intercalate/deintercalate the layered arrays and offers a

larger surface area for Na^+ absorption, enhancing the electrochemical performance of sodium-ion batteries (Mao et al. 2018).

In this regard, (Hu et al. 2018b) developed a network structure constructed from a hybrid carbon base/ MoS_2 composite as active electrode material for both Li-ion batteries and Na-ion batteries. This construction helps the accommodation of volume enlargement and facilitates the diffusion of ions in/out the layers during battery operation.

The composite of MoS_2 /graphene microspheres was obtained by (Choi et al. 2015). The layers of MoS_2 have homogeneously surrounded the graphene microspheres. As a consequence of graphene microspheres porosity and the layered structure of MoS_2 , the diffusion process of Na^+ has been boosted.

The high coulombic efficiency value ($\approx 99.98\%$) was attained after 600 repeated cycles. The MoS_2 nanosheet have been grown on carbon paper (Nan et al. 2021). The obtained hierarchical structure of MoS_2 /carbon is favorable for the electrode/electrolyte interaction, reducing the electron transfer resistance. The obtained electrode exhibited an initial capacity of 0.556 and 0.442 Ah g^{-1} for discharge and charge. Moreover, it delivered an excellent initial coulombic efficiency of 79.5% compared to 38.3% for the pristine carbon paper.

Nanosized petals of MoS_2 micro-flowers for sodium-ion batteries display 0.595 Ah g^{-1} after 50 cycles (Kumar et al. 2015).

Also, (Kong et al. 2017) synthesized a new composite formed from ultrathin MoS_2 vertical nanosheets arrays with iron oxide (Fe_3O_4) that allowed growth over the surface of graphite paper and used it as an anode for sodium-ion batteries. The as-prepared anode of $\text{Fe}_3\text{O}_4/\text{MoS}_2$ delivered 468 and 0.231 Ah g^{-1} at 100 and 3.2 A g^{-1} , respectively, and 72.5% of its original capacitance retained after 300 cycles.

Poly(ethylene oxide)/intercalated MoS_2 nanocomposites were synthesized via a simple exfoliation/restacking route and evaluated as electroactive anode material for sodium-ion batteries (Li et al. 2015). The prepared anode revealed a specific capacity of 0.225 A h g^{-1} of 0.05 A g^{-1} current density, double that of commercial MoS_2 , and displayed better rate capability due to the enhancement of Na^+ ion diffusivity.

A nanostructure of nanoplates Sb anchored the ultrathin layered structure of MoS_2 (MoS_2/Sb) and tested it as anode material for sodium-ion batteries (Li et al., 2018b). The fabricated sodium-ion batteries delivered a superb reversible capacity of 0.666 Ah g^{-1} and 0.454 Ah g^{-1} at current densities of 0.1 A g^{-1} and 10 A g^{-1} , respectively, indicating its excellent cyclability and good rate performance.

Lithium–sulfur batteries

The economic sulfur cathode, respectable theoretical capacity (1.672 A h g^{-1}), and high energy density (1.672 kW h g^{-1}) (Xiang et al. 2019) have attracted much interest for lithium–sulfur batteries as a prospective energy storage market candidate. However, some problems face lithium–sulfur batteries, such as the non-conductivity of sulfur and its discharging products (Li_2S_2 and Li_2S), leading to a slow operating and low capacity (Chen et al. 2019c).

During the charging/discharging operations, polysulfide was formed as an intermediate product, which is easily soluble in electrolyte material and freely migrates between the two electrodes of lithium–sulfur batteries (Yuan et al. 2019). If the reactive lithium polysulfide is missing during the cycling process, it will lead to fast capacity fading. This problem is called “shuttle effects” (Zhang et al., 2020). Moreover, the shuttle effect will cause passivation to the lithium anode and induce low-rate behavior and sulfur consumption.

A device fabricated in which MoS_2 combined with a Celgard separator in lithium–sulfur batteries displayed a high conductivity and rapid diffusion rate of lithium (Zhang et al. 2019b). This separator can impede the diffusing rate of polysulfide. Therefore, the shuttle could be inhibited, which enhanced the battery’s performance, keeping a capacity of 0.401 Ah g^{-1} after 600 cycles and sustained 99.5% coulombic efficiency. An efficient protective coating layer of MoS_2 protects lithium metal anode from producing high-efficiency lithium–sulfur batteries (Cha et al. 2018).

Bibliometric analysis

Search methodology for TOPIC: (“ MoS_2 ” or “Molybdenum disulphide”) AND TOPIC: (capacitor OR wastewater OR “energy storage” OR “Water remediation” OR “ MoS_2 -based hybrids” OR “supercapacitors”). Timespan: All years from 1970 till 2021.

Figure 8a, b illustrates the bibliometric mapping created from the Web of Science core collection, where Fig. 8a shows the network visualization and Fig. 8b depicts the density visualization. Initially, the data from the web of science (2022 results) were exported and then plotted using VOS viewer software. The co-occurrence analysis was used in this study, including all keywords in the literature from 1970 till 2021, as well as the fractional counting method with a minimum number of occurrences of five keywords. Direct clusters connect identifiable keywords to broad topics such as molybdenum disulfide, wastewater, and supercapacitor in energy storage. This allowed for the visualization of the majority of the significant keywords associated with the use of MoS_2 in water remediation and energy storage

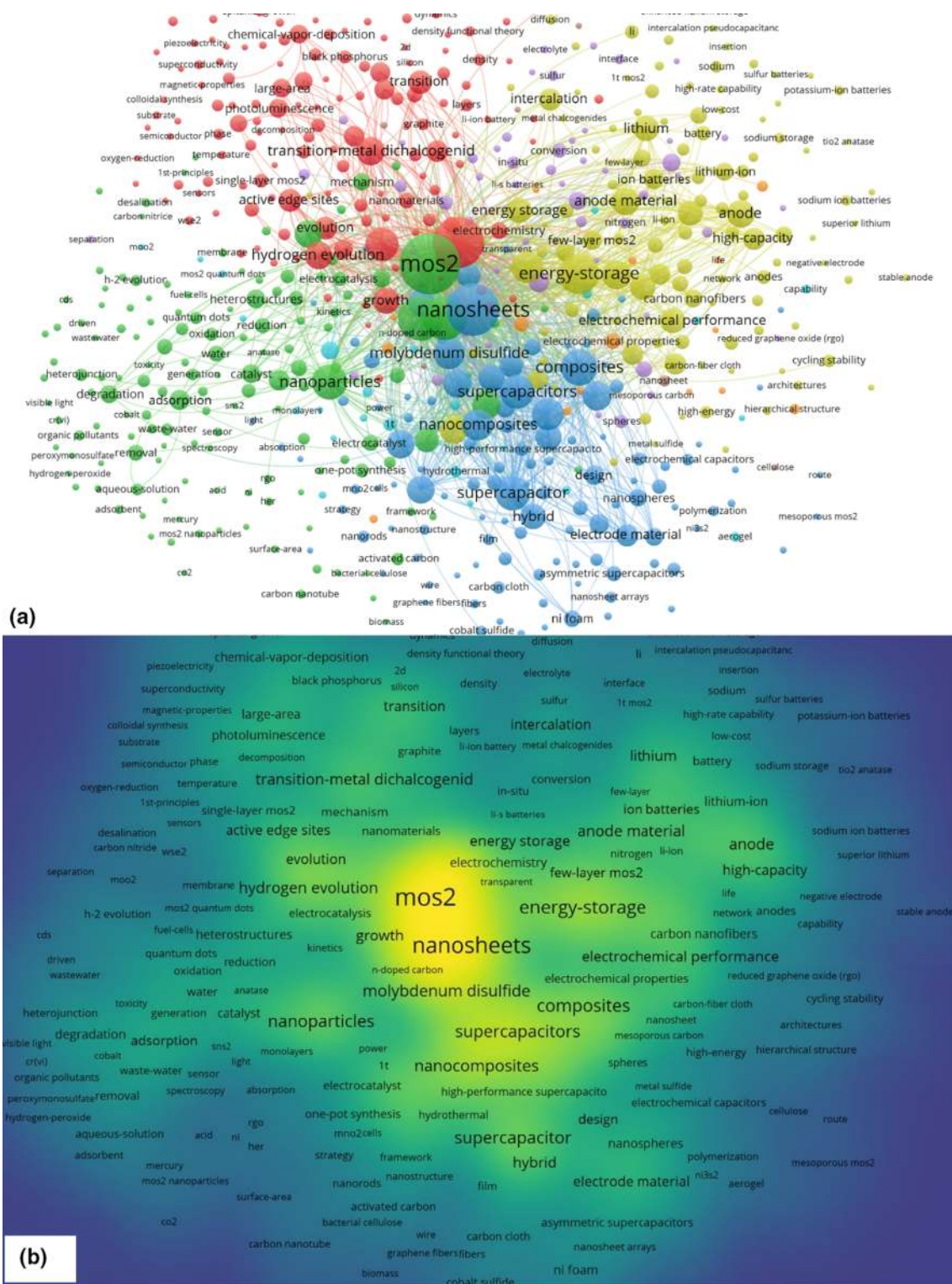


Fig. 8 The bibliometric mapping of MoS₂ utilization in water remediation and energy storage applications **a** network visualization and **b** density visualization maps. The bibliometric analysis was carried out in the timespan of 1970–2021

applications in publications from 1970 to 2021. Figure 8a, b clearly demonstrates that keywords such as supercapacitors, high capacity, composites, electrode material, nanosheet,

electrochemical performance, molybdenum disulfide, and transition metal dichalcogenides had seen a momentous increase in popularity and, as a result, progress in keyword

research. Besides, other associated keywords have shown in the bibliometric analysis, such as graphene and lithium-ion batteries. This implies that the utilization of MoS₂ in the energy storage route is at a mature stage in the research and development of water remediation application, as shown by the prominence of literature keywords over more than fifty years

On the other hand, the water treatment application of MoS₂ is still progressing and would require research and development in the near future. For instance, areas related to MoS₂ in water treatment include one-step synthesis, adsorbents, desalination, separation, and the mechanism. While bibliometric mapping is also shown in Fig. 8a, b, cyclic stability, asymmetric supercapacitors, pseudo-capacitance, flexible electrode, and stability are areas for MoS₂ energy storage application that need further investigation.

Conclusion

In this review, we critically reviewed the recent literature investigating molybdenum disulfide (MoS₂) material as a subclass of transition metal dichalcogenides, possessing a unique two-dimensional layered structure. This unique structure has granted MoS₂ promising electronic, physicochemical, optical, and electrical characteristics. These properties have attracted a lot of researchers' interests, directing them to investigate the versatile applications of these materials. Two of the main focus areas are environmental (water remediation) and energy storage applications (supercapacitors and ion batteries). As presented, MoS₂ can be prepared via many different synthetic approaches that can be divided into two main routes: top-down and bottom-up methods, through which their properties can be precisely tuned, giving researchers a significant advantage in how they are constructed. In addition, density-functional theory calculations can be used to analyze many electronic properties of MoS₂ materials, including their density of state, bandgap, HOMO–LUMO, charge density profiles, and work function. Then, we outlined the promising potential of MoS₂-based hybrids (MoS₂-carbon, MoS₂-metal oxides, and MoS₂-metal sulfides) to be employed as photocatalysts and absorbent materials due to their exceptional surface uptake, cost-effectiveness, and their small bandgap. MoS₂-based composites can be potential substitutes to complete the ongoing efforts toward clean accessible water due to the ease of conjugation with other active materials (small bandgap metal oxide semiconductors). Moreover, they can be used to satisfy the continuously increasing energy demand due to their outstanding electrical characteristics by acting in supercapacitors and ion batteries to save energy. This can potentially be achieved due to their high power density,

fast charge/discharge rates, and long cycle life. However, more investigations revealing and outlining their potential hybrids, subsequent properties, and available applications are still required.

Acknowledgements The authors wish to acknowledge the support of The Bryden Centre project (Project ID VA5048), which was awarded by The European Union's INTERREG VA Programme, managed by the Special EU Programmes Body (SEUPB), with match funding provided by the Department for the Economy in Northern Ireland and the Department of Business, Enterprise and Innovation in the Republic of Ireland.

Declarations

Disclaimer The views and opinions expressed in this review do not necessarily reflect those of the European Commission or the Special EU Programmes Body (SEUPB).

Open Access This article is licensed under a Creative Commons Attribution 4.0 International License, which permits use, sharing, adaptation, distribution and reproduction in any medium or format, as long as you give appropriate credit to the original author(s) and the source, provide a link to the Creative Commons licence, and indicate if changes were made. The images or other third party material in this article are included in the article's Creative Commons licence, unless indicated otherwise in a credit line to the material. If material is not included in the article's Creative Commons licence and your intended use is not permitted by statutory regulation or exceeds the permitted use, you will need to obtain permission directly from the copyright holder. To view a copy of this licence, visit <http://creativecommons.org/licenses/by/4.0/>.

References

- Abdel Maksoud MIA et al (2020) Insight on water remediation application using magnetic nanomaterials and biosorbents. *Coord Chem Rev* 403:213096. <https://doi.org/10.1016/j.ccr.2019.213096>
- Abdel Maksoud MIA et al (2021) Advanced materials and technologies for supercapacitors used in energy conversion and storage: a review. *Environ Chem Lett* 19:375–439. <https://doi.org/10.1007/s10311-020-01075-w>
- Acerce M et al (2015a) Metallic 1T phase MoS₂ nanosheets as supercapacitor electrode materials. *Nat Nanotechnol* 10:313–318. <https://doi.org/10.1038/nnano.2015.40>
- Acerce M et al (2015b) Metallic 1T phase MoS₂ nanosheets as supercapacitor electrode materials. *Nat Nanotechnol*. <https://doi.org/10.1038/nnano.2015.40>
- Algara-Siller G et al (2015) Square ice in graphene nanocapillaries. *Nature* 519:443–445. <https://doi.org/10.1038/nature14295>
- Al-Hossainy A et al (2018) Elucidation of electrical and optical parameters of poly (o-anthranilic acid)-poly (o-amino phenol)/copper oxide nanocomposites thin films. *J Inorg Organomet Polym Mater* 28:2572–2583. <https://doi.org/10.1007/s10904-018-0945-1>
- Ali BA et al (2018) Unveiling the effect of the structure of carbon material on the charge storage mechanism in MoS₂-based supercapacitors. *ACS Omega* 3:16301–16308. <https://doi.org/10.1021/acsomega.8b02261>

- Ali BA et al (2021) Towards Cs-ion supercapacitors: Cs intercalation in polymorph MoS₂ as a model 2D electrode material. *Chem Commun*. <https://doi.org/10.1039/D0CC07887E>
- Almeida DAL et al (2019) Flexible polyaniline/reduced graphene oxide/carbon fiber composites applied as electrodes for supercapacitors. *J Alloys Compd* 788:453–460. <https://doi.org/10.1016/j.jallcom.2019.02.194>
- Alomar M et al (2019) Controlling the growth of ultrathin MoS₂ nanosheets/CdS nanoparticles by two-step solvothermal synthesis for enhancing photocatalytic activities under visible light. *Appl Surf Sci* 480:1078–1088. <https://doi.org/10.1016/j.apsusc.2019.03.014>
- Ambrosi A et al (2015) 2H → 1T phase transition and hydrogen evolution activity of MoS₂, MoSe₂, WS₂ and WSe₂ strongly depends on the MX₂ composition. *Chem Commun* 51:8450–8453. <https://doi.org/10.1039/C5CC00803D>
- Arshad MM et al (2019) Current and future envision on developing biosensors aided by 2D molybdenum disulfide (MoS₂) productions. *Biosens Bioelectron* 132:248–264. <https://doi.org/10.1016/j.bios.2019.03.005>
- Atacan K et al (2021) Design and synthesis of magnetically separable CuFe₂O₄/MoS₂ p-n heterojunction for photocatalytic efficiency of Rhodamine B degradation. *Colloid Interface Sci Commun* 40:100359. <https://doi.org/10.1016/j.colcom.2020.100359>
- Azmi R et al (2016) Low-temperature-processed 9% colloidal quantum dot photovoltaic devices through interfacial management of p-n heterojunction. *Adv Energy Mater* 6:1502146. <https://doi.org/10.1002/aenm.201502146>
- Baghbanzadeh M et al (2011) Microwave-assisted synthesis of colloidal inorganic nanocrystals. *Angew Chem Int Ed* 50:11312–11359. <https://doi.org/10.1002/anie.201101274>
- Bagherzadeh M, Kaveh R (2018) A new SnS₂-BiFeO₃/reduced graphene oxide photocatalyst with superior photocatalytic capability under visible light irradiation. *J Photochem Photobiol A* 359:11–22. <https://doi.org/10.1016/j.jphotochem.2018.03.031>
- Bai X et al (2018) Synergy removal of Cr (VI) and organic pollutants over RP-MoS₂/rGO photocatalyst. *Appl Catal B Environ* 239:204–213. <https://doi.org/10.1016/j.apcatb.2018.08.016>
- Benavente E et al (2018) Heterostructured layered hybrid ZnO/MoS₂ nanosheets with enhanced visible light photocatalytic activity. *J Phys Chem Solids* 113:119–124. <https://doi.org/10.1016/j.jpcs.2017.10.027>
- Bindumadhavan K et al (2013) MoS₂-MWCNT hybrids as a superior anode in lithium-ion batteries. *Chem Commun* 49:1823–1825. <https://doi.org/10.1039/C3CC38598A>
- Cao Y et al (2018) Unconventional superconductivity in magic-angle graphene superlattices. *Nature* 556:43–50. <https://doi.org/10.1038/nature26160>
- Cha E et al (2018) 2D MoS₂ as an efficient protective layer for lithium metal anodes in high-performance Li–S batteries. *Nat Nanotechnol* 13:337–344. <https://doi.org/10.1038/s41565-018-0061-y>
- Chai C et al (2018) A MoS₂-templated oxidation-etching strategy to synthesize hollow δ-MnO₂ nanospheres as a high-performance electrode for supercapacitor. *Ceram Int* 44:16923–16930. <https://doi.org/10.1016/j.ceramint.2018.06.132>
- Chang K et al (2016) Targeted synthesis of 2H- and 1T-phase MoS₂ monolayers for catalytic hydrogen evolution. *Adv Mater* 28:10033–10041. <https://doi.org/10.1002/adma.201603765>
- Chen Y et al (2014) Ultrasmall Fe₃O₄ nanoparticle/MoS₂ nanosheet composites with superior performances for lithium ion batteries. *Small* 10:1536–1543. <https://doi.org/10.1002/sml.201302879>
- Chen L et al (2017) Fabrication of 3D quasi-hierarchical Zn-scheme RGO-Fe₂O₃-MoS₂ nanoheterostructures for highly enhanced visible-light-driven photocatalytic degradation. *Appl Surf Sci* 420:669–680. <https://doi.org/10.1016/j.apsusc.2017.05.099>
- Chen X, McDonald AR (2016) Functionalization of Two-Dimensional Transition-Metal Dichalcogenides. *Adv Mater* 28:5738–5746. <https://doi.org/10.1002/adma.201505345>
- Chen Y et al (2014) Synthesis of SnO₂/MoS₂ composites with different component ratios and their applications as lithium ion battery anodes. *J Mater Chem A* 2:17857–17866. <https://doi.org/10.1039/C4TA03770G>
- Chen B et al (2018) Preparation of MoS₂/TiO₂ based nanocomposites for photocatalysis and rechargeable batteries: progress, challenges, and perspective. *Nanoscale* 10:34–68. <https://doi.org/10.1039/C7NR07366F>
- Chen X et al (2019a) MnS coupled with ultrathin MoS₂ nanolayers as heterojunction photocatalyst for high photocatalytic and photoelectrochemical activities. *J Alloy Compd* 771:364–372. <https://doi.org/10.1016/j.jallcom.2018.08.319>
- Chen H et al (2019b) Correction: MoS₂ nanoflowers encapsulated into carbon nanofibers containing amorphous SnO₂ as an anode for lithium-ion batteries. *Nanoscale* 11:22134–22134. <https://doi.org/10.1039/C9NR90247C>
- Chen X et al (2019c) Combining theory and experiment in lithium-sulfur batteries: current progress and future perspectives. *Mater Today* 22:142–158. <https://doi.org/10.1016/j.mattod.2018.04.007>
- Chen B et al (2020) Transition metal dichalcogenide/multi-walled carbon nanotube-based fibers as flexible electrodes for electrocatalytic hydrogen evolution. *Chem Commun* 56:5131–5134. <https://doi.org/10.1039/D0CC00506A>
- Chenab KK et al (2020) Water treatment: functional nanomaterials and applications from adsorption to photodegradation. *Mater Today Chem* 16:100262. <https://doi.org/10.1016/j.mtchem.2020.100262>
- Cheriyian S et al (2018) Doping effect on monolayer MoS₂ for visible light dye degradation-A DFT study. *Superlattices Microstruct* 116:238–243. <https://doi.org/10.1016/j.spmi.2018.02.032>
- Chhowalla M et al (2013) The chemistry of two-dimensional layered transition metal dichalcogenide nanosheets. *Nat Chem* 5:263–275. <https://doi.org/10.1038/nchem.1589>
- Choi SH et al (2015) 3D MoS₂-graphene microspheres consisting of multiple nanospheres with superior sodium ion storage properties. *Adv Func Mater* 25:1780–1788. <https://doi.org/10.1002/adfm.201402428>
- Chou SS et al (2015) Understanding catalysis in a multiphase two-dimensional transition metal dichalcogenide. *Nat Commun* 6:1–8. <https://doi.org/10.1038/ncomms9311>
- Chua CK et al (2016) Top-down and bottom-up approaches in engineering 1 t phase molybdenum disulfide (MoS₂): towards highly catalytically active materials. *Chem A Eur J*. 22:14336–14341. <https://doi.org/10.1002/chem.201602764>
- Coleman JN et al (2011) Two-dimensional nanosheets produced by liquid exfoliation of layered materials. *Science* 331:568–571. <https://doi.org/10.1126/science.1194975>
- Colombo E et al (2017) Chitosan microspheres as a template for TiO₂ and ZnO microparticles: studies on mechanism, functionalization and applications in photocatalysis and H₂S removal. *RSC Adv* 7:19373–19383. <https://doi.org/10.1039/C7RA01227F>
- Conway BE et al (1997) The role and utilization of pseudocapacitance for energy storage by supercapacitors. *J Power Sources* 66:1–14. [https://doi.org/10.1016/S0378-7753\(96\)02474-3](https://doi.org/10.1016/S0378-7753(96)02474-3)
- Cook JB et al (2017) Pseudocapacitive Charge Storage in Thick Composite MoS₂ Nanocrystal-Based Electrodes. *Adv Energy Mater* 7:1601283. <https://doi.org/10.1002/aenm.201601283>
- da Silveira Firmiano EG et al (2014) Supercapacitor Electrodes Obtained by Directly Bonding 2D MoS₂ on Reduced Graphene Oxide. *Adv Energy Mater* 4:1301380. <https://doi.org/10.1002/aenm.201301380>
- Darsara SA et al (2018) One-step hydrothermal synthesis of MoS₂/CdS nanocomposite and study of structural, photocatalytic, and

- optical properties of this nanocomposite. *Optik* 169:249–256. <https://doi.org/10.1016/j.ijleo.2018.05.075>
- Das S et al (2019) Self-assembled nanostructured MoS₂ quantum dot polyaniline hybrid gels for high performance solid state flexible supercapacitors. *ACS Appl Energy Mater* 2:6642–6654. <https://doi.org/10.1021/acsaem.9b01171>
- Deng X et al (2019) Adsorption of formaldehyde on transition metal doped monolayer MoS₂: a DFT study. *Appl Surf Sci* 484:1244–1252. <https://doi.org/10.1016/j.apsusc.2019.04.175>
- Desai SB et al (2016) Gold-mediated exfoliation of ultralarge optoelectronically-perfect monolayers. *Adv Mater* 28:4053–4058. <https://doi.org/10.1002/adma.201506171>
- Ding Q et al (2016) Efficient Electrocatalytic and Photoelectrochemical Hydrogen Generation Using MoS₂ and Related Compounds. *Chem* 1:699–726. <https://doi.org/10.1016/j.chempr.2016.10.007>
- Dong R et al (2019) Morphology-controlled fabrication of CNT@MoS₂/SnS₂ nanotubes for promoting photocatalytic reduction of aqueous Cr (VI) under visible light. *J Alloy Compd* 784:282–292. <https://doi.org/10.1016/j.jallcom.2019.01.032>
- Drmosh Q et al (2020) Ternary Bi₂S₃/MoS₂/TiO₂ with double Z-scheme configuration as high performance photocatalyst. *Appl Surf Sci* 499:143938. <https://doi.org/10.1016/j.apsusc.2019.143938>
- Du H et al (2015) Solvothermal synthesis of MoS₂ nanospheres in DMF–water mixed solvents and their catalytic activity in hydrocracking of diphenylmethane. *RSC Adv* 5:79724–79728. <https://doi.org/10.1039/C5RA08424E>
- Ebrahimi M et al (2017) Improved solar-driven photocatalytic activity of hybrid graphene quantum Dots/ZnO nanowires: a direct Z-scheme mechanism. *ACS Sustain Chem Eng* 5:367–375. <https://doi.org/10.1021/acssuschemeng.6b01738>
- Eda G et al (2011) Photoluminescence from chemically exfoliated MoS₂. *Nano Lett* 11:5111–5116. <https://doi.org/10.1021/nl201874w>
- Eid MR, Al-Hossainy AF (2021) Combined experimental thin film, DFT-TDDFT computational study, flow and heat transfer in [PG-MoS₂/ZrO₂] C hybrid nanofluid. *Waves Random Complex Media* 23:1–26. <https://doi.org/10.1080/17455030.2021.1873455>
- El-Kady MF, Kaner RB (2013) Scalable fabrication of high-power graphene micro-supercapacitors for flexible and on-chip energy storage. *Nat Commun* 4:1475. <https://doi.org/10.1038/ncomms2446>
- Fageria P et al (2017) Decoration of MoS₂ on g-C₃N₄ surface for efficient hydrogen evolution reaction. *Electrochim Acta* 258:1273–1283. <https://doi.org/10.1016/j.electacta.2017.11.184>
- Fan X et al (2015) Fast and efficient preparation of exfoliated 2H MoS₂ nanosheets by sonication-assisted lithium intercalation and infrared laser-induced 1T to 2H phase reversion. *Nano Lett* 15:5956–5960. <https://doi.org/10.1021/acs.nanolett.5b02091>
- Fan X et al (2019) In situ photoelectrochemical activation of sulfite by MoS₂ photoanode for enhanced removal of ammonium nitrogen from wastewater. *Appl Catal B* 244:396–406. <https://doi.org/10.1016/j.apcatb.2018.11.061>
- Fang S et al (2018) Facile synthesis of novel ZnFe₂O₄/CdS nanorods composites and its efficient photocatalytic reduction of Cr(VI) under visible-light irradiation. *J Ind Eng Chem* 58:64–73. <https://doi.org/10.1016/j.jiec.2017.09.008>
- Fortin E, Sears W (1982) Photovoltaic effect and optical absorption in MoS₂. *J Phys Chem Solids* 43:881–884. [https://doi.org/10.1016/0022-3697\(82\)90037-3](https://doi.org/10.1016/0022-3697(82)90037-3)
- Ge Y et al (2017) A robust free-standing MoS₂/poly(3,4-ethylenedioxythiophene): poly(styrenesulfonate) film for supercapacitor applications. *Electrochim Acta* 235:348–355. <https://doi.org/10.1016/j.electacta.2017.03.069>
- Gourmelon E et al (1997) MS₂ (M= W, Mo) photosensitive thin films for solar cells. *Sol Energy Mater Sol Cells* 46:115–121. [https://doi.org/10.1016/S0927-0248\(96\)00096-7](https://doi.org/10.1016/S0927-0248(96)00096-7)
- Grabowska E (2016) Selected perovskite oxides: characterization, preparation and photocatalytic properties—a review. *Appl Catal B Environ* 186:97–126. <https://doi.org/10.1016/j.apcatb.2015.12.035>
- Guan G et al (2015) Protein induces layer-by-layer exfoliation of transition metal dichalcogenides. *J Am Chem Soc* 137:6152–6155. <https://doi.org/10.1021/jacs.5b02780>
- Guan Z et al (2018) A facile and clean process for exfoliating MoS₂ nanosheets assisted by a surface active agent in aqueous solution. *Nanotechnology* 29:425702. <https://doi.org/10.1088/1361-6528/aad676>
- Guo S, Dong S (2011) Graphene nanosheet: synthesis, molecular engineering, thin film, hybrids, and energy and analytical applications. *Chem Soc Rev* 40:2644–2672. <https://doi.org/10.1039/C0CS00079E>
- Gupta A et al (2015) Recent development in 2D materials beyond graphene. *Prog Mater Sci* 73:44–126. <https://doi.org/10.1016/j.pmatsci.2015.02.002>
- Gupta D et al (2020) A comprehensive review on synthesis and applications of molybdenum disulfide (MoS₂) material: past and recent developments. *Inorg Chem Commun* 121:108200. <https://doi.org/10.1016/j.inoche.2020.108200>
- Gusain R et al (2019) Efficient removal of Pb(II) and Cd(II) from industrial mine water by a hierarchical MoS₂/SH-MWCNT nanocomposite. *ACS Omega* 4:13922–13935. <https://doi.org/10.1021/acsomega.9b01603>
- Han B, Hu YH (2016) MoS₂ as a co-catalyst for photocatalytic hydrogen production from water. *Energy Sci Eng* 4:285–304. <https://doi.org/10.1002/ese3.128>
- Hebbbar RS et al (2017) Carbon nanotube- and graphene-based advanced membrane materials for desalination. *Environ Chem Lett* 15:643–671. <https://doi.org/10.1007/s10311-017-0653-z>
- Hu L et al (2014) Fabrication of 3D hierarchical MoS₂/polyaniline and MoS₂/C architectures for lithium-ion battery applications. *ACS Appl Mater Interfaces* 6:14644–14652. <https://doi.org/10.1021/am503995s>
- Hu X et al (2015) Nanostructured Mo-based electrode materials for electrochemical energy storage. *Chem Soc Rev* 44:2376–2404. <https://doi.org/10.1039/C4CS00350K>
- Hu J et al (2018a) Recyclable carbon nanofibers@ hierarchical I-doped Bi₂O₂CO₃–MoS₂ membranes for highly efficient water remediation under visible-light irradiation. *ACS Sustain Chem Eng* 6:2676–2683. <https://doi.org/10.1021/acssuschemeng.7b04270>
- Hu X et al (2018b) Three-dimensional network architecture with hybrid nanocarbon composites supporting few-layer MoS₂ for lithium and sodium storage. *ACS Nano* 12:1592–1602. <https://doi.org/10.1021/acsnano.7b08161>
- Hu Y et al (2020) Layered perovskite oxides and their derivative nanosheets adopting different modification strategies towards better photocatalytic performance of water splitting. *Renew Sustain Energy Rev* 119:109527. <https://doi.org/10.1016/j.rser.2019.109527>
- Huang K-J et al (2013a) Layered MoS₂–graphene composites for supercapacitor applications with enhanced capacitive performance. *Int J Hydrogen Energy* 38:14027–14034. <https://doi.org/10.1016/j.ijhydene.2013.08.112>
- Huang G et al (2013b) Graphene-Like MoS₂/Graphene Composites: Cationic Surfactant-Assisted Hydrothermal Synthesis and Electrochemical Reversible Storage of Lithium. *Small* 9:3693–3703. <https://doi.org/10.1002/sml.201300415>
- Huang K-J et al (2013c) Synthesis of polyaniline/2-dimensional graphene analog MoS₂ composites for high-performance supercapacitor. *Electrochim Acta* 109:587–594. <https://doi.org/10.1016/j.electacta.2013.07.168>

- Huang K-J et al (2014a) Hydrothermal synthesis of molybdenum disulfide nanosheets as supercapacitors electrode material. *Electrochim Acta* 132:397–403. <https://doi.org/10.1016/j.electacta.2014.04.007>
- Huang K-J et al (2014b) One-step preparation of layered molybdenum disulfide/multi-walled carbon nanotube composites for enhanced performance supercapacitor. *Energy* 67:234–240. <https://doi.org/10.1016/j.energy.2013.12.051>
- Huang K-J et al (2015) Synthesis of molybdenum disulfide/carbon aerogel composites for supercapacitors electrode material application. *J Electroanal Chem* 752:33–40. <https://doi.org/10.1016/j.jelechem.2015.06.005>
- Huang Y et al (2015) Reliable exfoliation of large-area high-quality flakes of graphene and other two-dimensional materials. *ACS Nano* 9:10612–10620. <https://doi.org/10.1021/acs.nano.5b04258>
- Huang Y et al (2016) Preparation of a Sn@ SnO₂@ C@ MoS₂ composite as a high-performance anode material for lithium-ion batteries. *J Mater Chem A* 4:7185–7189. <https://doi.org/10.1039/C6TA02080A>
- Hwang H et al (2011) MoS₂ Nanoplates consisting of disordered graphene-like layers for high rate lithium battery anode materials. *Nano Lett* 11:4826–4830. <https://doi.org/10.1021/nl202675f>
- Hwang J-Y et al (2017) Sodium-ion batteries: present and future. *Chem Soc Rev* 46:3529–3614. <https://doi.org/10.1039/C6CS00776G>
- Ilanchezhiyan P et al (2015) Electrochemical studies of spherically clustered MoS₂ nanostructures for electrode applications. *J Alloys Compd* 634:104–108. <https://doi.org/10.1016/j.jallcom.2015.02.082>
- Jayabal S et al (2017) Understanding the high-electrocatalytic performance of two-dimensional MoS₂ nanosheets and their composite materials. *J Mater Chem A* 5:24540–24563. <https://doi.org/10.1039/C7TA08327K>
- Ji H et al (2019) Directly scalable preparation of sandwiched MoS₂/graphene nanocomposites via ball-milling with excellent electrochemical energy storage performance. *Electrochim Acta* 299:143–151. <https://doi.org/10.1016/j.electacta.2018.12.188>
- Jia Y et al (2017) Hierarchical nanosheet-based MoS₂/graphene nanobelts with high electrochemical energy storage performance. *J Power Sources* 354:1–9. <https://doi.org/10.1016/j.jpowsour.2017.04.031>
- Jia Y et al (2019) Au nanoparticles enhanced Z-scheme Au-CoFe₂O₄/MoS₂ visible light photocatalyst with magnetic retrievability. *Appl Surf Sci* 463:854–862. <https://doi.org/10.1016/j.apsusc.2018.09.008>
- Jia T et al (2014) A graphene dispersed CdS–MoS₂ nanocrystal ensemble for cooperative photocatalytic hydrogen production from water. *Chem Commun* 50:1185–1188. <https://doi.org/10.1039/C3CC47301E>
- Jiang E et al (2020) Construction of a Z-scheme MoS₂/CaTiO₃ heterostructure by the morphology-controlled strategy towards enhancing photocatalytic activity. *Chem Eng J* 399:125721. <https://doi.org/10.1016/j.cej.2020.125721>
- Jiang Y et al (2016) Synthesis and visible light responded photocatalytic activity of Sn doped Bi₂S₃ microspheres assembled by nanosheets. *RSC Adv* 6:39810–39817. <https://doi.org/10.1039/C6RA02621D>
- Jiang Y et al (2017) Rationally incorporated MoS₂/SnS₂ nanoparticles on graphene sheets for lithium-ion and sodium-ion batteries. *ACS Appl Mater Interfaces* 9:27697–27706. <https://doi.org/10.1021/acsami.7b06572>
- Jilani A et al (2018) Graphene and its derivatives: synthesis, modifications, and applications in wastewater treatment. *Environ Chem Lett* 16:1301–1323. <https://doi.org/10.1007/s10311-018-0755-2>
- Joensen P et al (1986) Single-layer mos₂. *Mater Res Bull* 21:457–461. [https://doi.org/10.1016/0025-5408\(86\)90011-5](https://doi.org/10.1016/0025-5408(86)90011-5)
- Kalin M et al (2012) Mechanisms and improvements in the friction and wear behavior using MoS₂ nanotubes as potential oil additives. *Wear* 280:36–45. <https://doi.org/10.1016/j.wear.2012.01.011>
- Kam K, Parkinson B (1982) Detailed photocurrent spectroscopy of the semiconducting group VIB transition metal dichalcogenides. *J Phys Chem* 86:463–467. <https://doi.org/10.1021/j100393a010>
- Kang K et al (2015) High-mobility three-atom-thick semiconducting films with wafer-scale homogeneity. *Nature* 520:656–660. <https://doi.org/10.1038/nature14417>
- Karade SS et al (2016) MoS₂ ultrathin nanoflakes for high performance supercapacitors: room temperature chemical bath deposition (CBD). *RSC Adv* 6:39159–39165. <https://doi.org/10.1039/C6RA04441G>
- Kaushik S et al (2020) Study of sonication assisted synthesis of molybdenum disulfide (MoS₂) nanosheets. *Mater Today Proc* 21:1969–1975. <https://doi.org/10.1016/j.matpr.2020.01.313>
- Khawula TNY et al (2016) Symmetric pseudocapacitors based on molybdenum disulfide (MoS₂)-modified carbon nanospheres: correlating physicochemistry and synergistic interaction on energy storage. *J Mater Chem A* 4:6411–6425. <https://doi.org/10.1039/C6TA00114A>
- Kim YJ et al (2005) Electrical conductivity of chemically modified multiwalled carbon nanotube/epoxy composites. *Carbon* 43:23–30. <https://doi.org/10.1016/j.carbon.2004.08.015>
- Kolobov AV, Tominaga J (2016) Two-dimensional transition-metal dichalcogenides. Springer. <https://doi.org/10.1007/978-3-319-31450-1>
- Kong L et al (2014) High-power and high-energy asymmetric supercapacitors based on Li⁺-intercalation into a T-Nb₂O₅/graphene pseudocapacitive electrode. *J Mater Chem A* 2:17962–17970. <https://doi.org/10.1039/C4TA03604B>
- Kong L et al (2015) Free-standing T-Nb₂O₅/graphene composite papers with ultrahigh gravimetric/volumetric capacitance for Li-ion intercalation pseudocapacitor. *ACS Nano* 9:11200–11208. <https://doi.org/10.1021/acs.nano.5b04737>
- Kong D et al (2017) Fe₃O₄ quantum dot decorated MoS₂ nanosheet arrays on graphite paper as free-standing sodium-ion battery anodes. *J Mater Chem A* 5:9122–9131. <https://doi.org/10.1039/C7TA01172E>
- Krishnamoorthy K et al (2014) Supercapacitive properties of hydrothermally synthesized sphere like MoS₂ nanostructures. *Mater Res Bull* 50:499–502. <https://doi.org/10.1016/j.materresbull.2013.11.019>
- Kuc A et al (2011) Influence of quantum confinement on the electronic structure of the transition metal sulfide T S₂. *Phys Rev B* 83:245213. <https://doi.org/10.1103/PhysRevB.83.245213>
- Kumar PR et al (2015) High performance of MoS₂ microflowers with a water-based binder as an anode for Na-ion batteries. *RSC Adv* 5:79845–79851. <https://doi.org/10.1039/C5RA16297A>
- Kumar DP et al (2016) Noble metal-free ultrathin MoS₂ nanosheet-decorated CdS nanorods as an efficient photocatalyst for spectacular hydrogen evolution under solar light irradiation. *J Mater Chem A* 4:18551–18558. <https://doi.org/10.1039/C6TA08628D>
- Kumar A et al (2019) Carbon nitride, metal nitrides, phosphides, chalcogenides, perovskites and carbides nanophotocatalysts for environmental applications. *Environ Chem Lett* 17:655–682. <https://doi.org/10.1007/s10311-018-0814-8>
- Kumuthini R et al (2017) Electrochemical properties of electrospun MoS₂@C nanofiber as electrode material for high-performance supercapacitor application. *J Alloys Compd* 705:624–630. <https://doi.org/10.1016/j.jallcom.2017.02.163>
- Lamberti A (2018) Flexible supercapacitor electrodes based on MoS₂-intercalated rGO membranes on Ti mesh. *Mater Sci Semicond Process* 73:106–110. <https://doi.org/10.1016/j.mssp.2017.06.046>

- Lang X et al (2011) Nanoporous metal/oxide hybrid electrodes for electrochemical supercapacitors. *Nat Nanotechnol* 6:232–236. <https://doi.org/10.1038/nnano.2011.13>
- Late DJ et al (2012) Rapid characterization of ultrathin layers of chalcogenides on SiO₂/Si substrates. *Adv Func Mater* 22:1894–1905. <https://doi.org/10.1002/adfm.201102913>
- Lee JS, Jang J (2014) Hetero-structured semiconductor nanomaterials for photocatalytic applications. *J Ind Eng Chem* 20:363–371. <https://doi.org/10.1016/j.jiec.2013.11.050>
- Lee J et al (2017) Thermodynamically stable synthesis of large-scale and highly crystalline transition metal dichalcogenide monolayers and their unipolar n–n heterojunction devices. *Adv Mater* 29:1702206. <https://doi.org/10.1002/adma.201702206>
- Lee YB et al (2019) Facile microwave assisted synthesis of vastly edge exposed 1T/2H-MoS₂ with enhanced activity for hydrogen evolution catalysis. *J Mater Chem A* 7:3563–3569. <https://doi.org/10.1039/C8TA12080C>
- Li W-J et al (2003) Hydrothermal synthesis of MoS₂ nanowires. *J Crystal Growth* 250:418–422. [https://doi.org/10.1016/S0022-0248\(02\)02412-0](https://doi.org/10.1016/S0022-0248(02)02412-0)
- Li Y et al (2017) Glucose-assisted synthesis of 1D/2D nearly vertical CdS/MoS₂ heterostructures for efficient photocatalytic hydrogen evolution. *Chem Eng J* 321:366–374. <https://doi.org/10.1016/j.cej.2017.03.139>
- Li Y et al (2018) Engineering MoS₂ nanomesh with holes and lattice defects for highly active hydrogen evolution reaction. *Appl Catal B Environ* 239:537–544. <https://doi.org/10.1016/j.apcatb.2018.05.080>
- Li Q et al (2020) Hierarchical MoS₂/NiCo₂S₄@C urchin-like hollow microspheres for asymmetric supercapacitors. *Chem Eng J* 380:122544. <https://doi.org/10.1016/j.cej.2019.122544>
- Li H et al (2014) Preparation and applications of mechanically exfoliated single-layer and multilayer MoS₂ and WSe₂ nanosheets. *Acc Chem Res* 47:1067–1075. <https://doi.org/10.1021/ar4002312>
- Li Y et al (2015) Enhancing sodium-ion battery performance with interlayer-expanded MoS₂-PEO nanocomposites. *Nano Energy* 15:453–461. <https://doi.org/10.1016/j.nanoen.2015.05.012>
- Li C et al (2018) Two-dimensional coupling: Sb nanoplates embedded in MoS₂ nanosheets as efficient anode for advanced sodium ion batteries. *Mater Chem Phys* 211:375–381. <https://doi.org/10.1016/j.matchemphys.2018.03.010>
- Li L et al (2019a) Facile synthesized low-cost MoS₂/CdS nanodots-on-nanorods heterostructures for highly efficient pollution degradation under visible-light irradiation. *Sep Purif Technol* 212:135–141. <https://doi.org/10.1016/j.seppur.2018.11.032>
- Li G et al (2019b) Electrochromic Poly (chalcogenoviologen) s as anode materials for high-performance organic radical lithium-ion batteries. *Angew Chem Int Ed* 58:8468–8473. <https://doi.org/10.1002/ange.201903152>
- Li XL et al (2020) Controllable synthesis of two-dimensional molybdenum disulfide (MoS₂) for energy-storage applications. *ChemSuschem*. <https://doi.org/10.1002/cssc.201902706>
- Lian X et al (2018) MoS₂-CdS heterojunction with enhanced photocatalytic activity: a first principles study. *J Phys Chem Solids* 120:52–56. <https://doi.org/10.1016/j.jpcs.2018.04.020>
- Liang Y et al (2011) Rechargeable Mg Batteries with Graphene-like MoS₂ Cathode and Ultrasmall Mg Nanoparticle Anode. *Adv Mater* 23:640–643. <https://doi.org/10.1002/adma.201003560>
- Liang H et al (2020) Controllable growth of foxtail-like MoS₂ on one-dimensional carbon nanofibers with enhanced photocatalytic activity. *Vacuum* 172:109059. <https://doi.org/10.1016/j.vacuum.2019.109059>
- Liang S et al (2013) PVP-assisted synthesis of MoS₂ nanosheets with improved lithium storage properties. *CrystEngComm* 15:4998–5002. <https://doi.org/10.1039/C3CE40392K>
- Lin T et al (2015) Fe₃O₄@ MoS₂ core-shell composites: preparation, characterization, and catalytic application. *J Phys Chem C* 119:13658–13664. <https://doi.org/10.1021/acs.jpcc.5b02516>
- Liu X et al (2017) Fabrication of 3D flower-like black N-TiO₂-x@ MoS₂ for unprecedented-high visible-light-driven photocatalytic performance. *Appl Catal B Environ* 201:119–127. <https://doi.org/10.1016/j.apcatb.2016.08.031>
- Liu Y et al (2019) Nickel oxide/graphene composites: synthesis and applications. *Chem A Eur J* 25:2141–2160. <https://doi.org/10.1002/chem.201803982>
- Liu H et al (2020a) Promoting charge separation in dual defect mediated Z-scheme MoS₂/g-C₃N₄ photocatalysts for enhanced photocatalytic degradation activity: synergistic effect insight. *Colloids Surf A Physicochem Eng Aspects* 594:124668. <https://doi.org/10.1016/j.colsurfa.2020.124668>
- Liu C et al (2020b) MoS₂/graphene composites: fabrication and electrochemical energy storage. *Energy Storage Mater* 33:470–502. <https://doi.org/10.1016/j.ensm.2020.06.020>
- Liu J et al (2012) Preparation of MoS₂-polyvinylpyrrolidone nanocomposites for flexible nonvolatile rewritable memory devices with reduced graphene oxide electrodes. *Small* 8:3517–3522. <https://doi.org/10.1002/sml.201200999>
- Liu N et al (2014a) Large-area atomically thin MoS₂ nanosheets prepared using electrochemical exfoliation. *ACS Nano* 8:6902–6910. <https://doi.org/10.1021/nm5016242>
- Liu Y et al (2014b) A graphene-like MoS₂/graphene nanocomposite as a highperformance anode for lithium ion batteries. *J Mater Chem A* 2:13109–13115. <https://doi.org/10.1039/C4TA01644K>
- Liu H et al (2015) Porous tremella-like MoS₂/polyaniline hybrid composite with enhanced performance for lithium-ion battery anodes. *Electrochim Acta* 167:132–138. <https://doi.org/10.1016/j.electacta.2015.03.151>
- Liu Y et al (2016) Design, synthesis, and energy-related applications of metal sulfides. *Mater Horiz* 3:402–421. <https://doi.org/10.1039/C6MH00075D>
- Liu J et al (2018a) Molybdenum sulfide Co-catalytic Fenton reaction for rapid and efficient inactivation of Escherichia coli. *Water Res* 145:312–320. <https://doi.org/10.1016/j.watres.2018.08.039>
- Liu H et al (2018b) Production of mono-to few-layer MoS₂ nanosheets in isopropanol by a salt-assisted direct liquid-phase exfoliation method. *J Colloid Interface Sci* 515:27–31. <https://doi.org/10.1016/j.jcis.2018.01.023>
- Long L-L et al (2016) Layer-controlled growth of MoS₂ on self-assembled flower-like Bi₂S₃ for enhanced photocatalysis under visible light irradiation. *NPG Asia Mater* 8:e263–e263. <https://doi.org/10.1038/am.2016.46>
- Lu X et al (2019) Engineering MP_x (M = Fe, Co or Ni) interface electron transfer channels for boosting photocatalytic H₂ evolution over g-C₃N₄/MoS₂ layered heterojunctions. *Appl Catal B Environ* 252:250–259. <https://doi.org/10.1016/j.apcatb.2019.04.012>
- Lu Y et al (2020) Achieving effective control of the photocatalytic performance for CoFe₂O₄/MoS₂ heterojunction via exerting external magnetic fields. *Mater Lett* 260:126979. <https://doi.org/10.1016/j.matlet.2019.126979>
- Luciano AJR et al (2020) Manganese ferrite dispersed over graphene sand composite for methylene blue photocatalytic degradation. *J Environ Chem Eng* 8:104191. <https://doi.org/10.1016/j.jece.2020.104191>
- Lukowski MA et al (2013) Enhanced hydrogen evolution catalysis from chemically exfoliated metallic MoS₂ nanosheets. *J Am Chem Soc* 135:10274–10277. <https://doi.org/10.1021/ja404523s>
- Luo W et al (2018) One-pot synthesis of highly stable carbon-MoS₂ nanosphere electrodes using a co-growth mechanism for

- supercapacitors. *New J Chem* 42:10111–10117. <https://doi.org/10.1039/C8NJ01387J>
- Lv K et al (2017) Fabrication of TiO₂ nanorod assembly grafted rGO (rGO@TiO₂-NR) hybridized flake-like photocatalyst. *Appl Surf Sci* 391:218–227. <https://doi.org/10.1016/j.apsusc.2016.03.195>
- Lv Y et al (2019) Nanocellulose-derived carbon nanosphere fibers-based nanohybrid aerogel for high-performance all-solid-state flexible supercapacitors. *J Mater Sci Mater Electron* 30:8585–8594. <https://doi.org/10.1007/s10854-019-01180-9>
- Ma L et al (2008) Ionic liquid-assisted hydrothermal synthesis of MoS₂ microspheres. *Mater Lett* 62:797–799. <https://doi.org/10.1016/j.matlet.2007.06.062>
- Ma G et al (2013) In situ intercalative polymerization of pyrrole in graphene analogue of MoS₂ as advanced electrode material in supercapacitor. *J Power Sources* 229:72–78. <https://doi.org/10.1016/j.jpowsour.2012.11.088>
- Ma L et al (2014) Biopolymer-assisted hydrothermal synthesis of flower-like MoS₂ microspheres and their supercapacitive properties. *Mater Lett* 132:291–294. <https://doi.org/10.1016/j.matlet.2014.06.108>
- Ma D et al (2016) Formaldehyde molecule adsorption on the doped monolayer MoS₂: a first-principles study. *Appl Surf Sci* 371:180–188. <https://doi.org/10.1016/j.apsusc.2016.02.230>
- Maddinedi SB et al (2017) High reduction of 4-nitrophenol using reduced graphene oxide/Ag synthesized with tyrosine. *Environ Chem Lett* 15:467–474. <https://doi.org/10.1007/s10311-017-0610-x>
- Magda GZ et al (2015) Exfoliation of large-area transition metal chalcogenide single layers. *Sci Rep* 5:1–5. <https://doi.org/10.1038/srep14714>
- Majee BP et al (2020) Large area vertically oriented few-layer MoS₂ for efficient thermal conduction and optoelectronic applications. *J Phys Chem Lett* 11:1268–1275. <https://doi.org/10.1021/acs.jpcclett.9b03726>
- Makino S et al (2015) Towards Implantable Bio-Supercapacitors: Pseudocapacitance of Ruthenium Oxide Nanoparticles and Nanosheets in Acids, Buffered Solutions, and Bioelectrolytes. *J Electrochem Soc* 162:A5001–A5006. <https://doi.org/10.1149/2.0021505jes>
- Makvandi P et al (2021) Functionalization of polymers and nanomaterials for water treatment, food packaging, textile and biomedical applications: a review. *Environ Chem Lett* 19:583–611. <https://doi.org/10.1007/s10311-020-01089-4>
- Mamba BB et al (2007) Monofunctionalized cyclodextrin polymers for the removal of organic pollutants from water. *Environ Chem Lett* 5:79–84. <https://doi.org/10.1007/s10311-006-0082-x>
- Mao J et al (2018) Two-dimensional nanostructures for sodium-ion battery anodes. *J Mater Chem A* 6:3284–3303. <https://doi.org/10.1039/C7TA10500B>
- Marcelo LR et al (2021) Synthesis of iron-based magnetic nanocomposites and applications in adsorption processes for water treatment: a review. *Environ Chem Lett* 19:1229–1274. <https://doi.org/10.1007/s10311-020-01134-2>
- Matsumoto M et al (2002) Molecular dynamics simulation of the ice nucleation and growth process leading to water freezing. *Nature* 416:409–413. <https://doi.org/10.1038/416409a>
- Meng C et al (2015) Layered MoS₂ nanoparticles on TiO₂ nanotubes by a photocatalytic strategy for use as high-performance electrocatalysts in hydrogen evolution reactions. *Green Chem* 17:2764–2768. <https://doi.org/10.1039/C5GC00272A>
- Mishra RK et al (2018) Petal-like MoS₂ nanostructures with metallic 1 T phase for high performance supercapacitors. *Current Appl Phys* 18:345–352. <https://doi.org/10.1016/j.cap.2017.12.010>
- Miyake S, Wang M (2015) Nanoprocessing of layered crystalline materials by atomic force microscopy. *Nanoscale Res Lett* 10:1–16. <https://doi.org/10.1186/s11671-015-0811-9>
- Murugan M et al (2017) Synthesis and property studies of molybdenum disulfide modified reduced graphene oxide (MoS₂-rGO) nanocomposites for supercapacitor applications. *J Nanosci Nanotechnol* 17:5469–5474. <https://doi.org/10.1166/jnn.2017.13845>
- Nagaraju G et al (2007) Hydrothermal synthesis of amorphous MoS₂ nanofiber bundles via acidification of ammonium heptamolybdate tetrahydrate. *Nanoscale Res Lett* 2:461. <https://doi.org/10.1007/s11671-007-9087-z>
- Nan J et al (2021) Nanoengineering of 2D MXene-based materials for energy storage applications. *Small* 17:1902085. <https://doi.org/10.1002/sml.201902085>
- Nicolosi V et al (2013) Liquid exfoliation of layered materials. *Science* 340:1226419. <https://doi.org/10.1126/science.1226419>
- Novoselov KS et al (2004) Electric field effect in atomically thin carbon films. *Science* 306:666–669. <https://doi.org/10.1126/science.1102896>
- Novoselov K (2011) Nobel lecture: Graphene: Materials in the flatland. *Rev Mod Phys* 83:837. <https://doi.org/10.1103/RevModPhys.83.837>
- Novoselov KS et al (2005) Two-dimensional atomic crystals. *Proc Natl Acad Sci* 102:10451–10453. <https://doi.org/10.1073/pnas.0502848102>
- Oliveira JMS et al (2020) Intermittent aeration strategy for azo dye biodegradation: A suitable alternative to conventional biological treatments? *J Hazard Mater* 385:121558. <https://doi.org/10.1016/j.jhazmat.2019.121558>
- Onga L et al (2020) Oxidation of reactive azo-dyes with pulsed corona discharge: surface reaction enhancement. *J Electrostat* 103:103420. <https://doi.org/10.1016/j.elstat.2020.103420>
- Pan Q et al (2017) MoS₂ encapsulated SnO₂-SnS/C nanosheets as a high performance anode material for lithium ion batteries. *Chem Eng J* 316:393–400. <https://doi.org/10.1016/j.cej.2017.01.111>
- Panigrahi PK, Pathak A (2011) A novel route for the synthesis of nanotubes and fullerene-like nanostructures of molybdenum disulfide. *Mater Res Bull* 46:2240–2246. <https://doi.org/10.1016/j.materresbull.2011.09.003>
- Pant B et al (2019) MoS₂/CdS/TiO₂ ternary composite incorporated into carbon nanofibers for the removal of organic pollutants from water. *Inorg Chem Commun* 102:113–119. <https://doi.org/10.1016/j.inoche.2019.02.022>
- Patel KP et al (2020) Green transamidation catalysed by graphene oxide under concentrated solar irradiation. *Environ Chem Lett* 18:1731–1735. <https://doi.org/10.1007/s10311-020-01034-5>
- Paul R et al (2019) 3D heteroatom-doped carbon nanomaterials as multifunctional metal-free catalysts for integrated energy devices. *Adv Mater* 31:1805598. <https://doi.org/10.1002/adma.201805598>
- Peng K et al (2019) One-step hydrothermal growth of MoS₂ nanosheets/CdS nanoparticles heterostructures on montmorillonite for enhanced visible light photocatalytic activity. *Appl Clay Sci* 175:86–93. <https://doi.org/10.1016/j.clay.2019.04.007>
- Pirarath R et al (2021) Mercury removal from aqueous solution using petal-like MoS₂ nanosheets. *Front Environ Sci Eng* 15:1–10. <https://doi.org/10.1007/s11783-020-1307-0>
- Pramoda K et al (2017) Nanocomposites of C₃N₄ with layers of MoS₂ and nitrogenated RGO, obtained by covalent cross-linking: synthesis, characterization, and HER activity. *ACS Appl Mater Interfaces* 9:10664–10672. <https://doi.org/10.1021/acsami.7b00085>
- Prasankumar T et al (2019) 3D structures of graphene oxide and graphene analogue MoS₂ with polypyrrole for supercapacitor electrodes. *Mater Lett* 238:121–125. <https://doi.org/10.1016/j.matlet.2018.12.002>
- Py M, Haering R (1983) Structural destabilization induced by lithium intercalation in MoS₂ and related compounds. *Can J Phys* 61:76–84. <https://doi.org/10.1139/p83-013>

- Qi S et al (2021) Construction and photocatalytic properties of WS₂/MoS₂/BiOCl heterojunction. *Chem Phys Lett* 763:138203. <https://doi.org/10.1016/j.cplett.2020.138203>
- Qiang T et al (2021) Dual modified MoS₂/SnS₂ photocatalyst with Z-scheme heterojunction and vacancies defects to achieve a superior performance in Cr (VI) reduction and dyes degradation. *J Clean Prod* 291:125213. <https://doi.org/10.1016/j.jclepro.2020.125213>
- Qiu J et al (2020) A novel 3D nanofibrous aerogel-based MoS₂@Co₃S₄ heterojunction photocatalyst for water remediation and hydrogen evolution under simulated solar irradiation. *Appl Catal B* 264:118514. <https://doi.org/10.1016/j.apcatb.2019.118514>
- Quan T et al (2019) Highly dispersible hexagonal carbon–MoS₂–carbon nanoplates with hollow sandwich structures for supercapacitors. *Chem A Eur J* 25:4757–4766. <https://doi.org/10.1002/chem.201806060>
- Radhakrishnan S et al (2021) Energy storage performance of 2D MoS₂ and carbon nanotube heterojunctions in symmetric and asymmetric configuration. *Nanotechnology* 32:155403. <https://doi.org/10.1088/1361-6528/abd05b>
- Rahimi K et al (2019) Enhancement of sunlight-induced photocatalytic activity of ZnO nanorods by few-layer MoS₂ nanosheets. *Mater Lett* 234:134–137. <https://doi.org/10.1016/j.matlet.2018.09.103>
- Raja VR et al (2017) Facile fabrication of PbS/MoS₂ nanocomposite photocatalyst with efficient photocatalytic activity under visible light. *Solid State Sci* 67:99–108. <https://doi.org/10.1016/j.solidstasciences.2017.03.016>
- Rajapriya A et al (2020) Direct growth of MoS₂ hierarchical nanoflowers on electrospun carbon nanofibers as an electrode material for high-performance supercapacitors. *J Alloys Compd* 859:157771. <https://doi.org/10.1016/j.jallcom.2020.157771>
- Ramadoss A et al (2014) Enhanced activity of a hydrothermally synthesized mesoporous MoS₂ nanostructure for high performance supercapacitor applications. *New J Chem* 38:2379–2385. <https://doi.org/10.1039/C3NJ01558K>
- Ramalingam RJ et al (2018) Synthesis of MoS₂ nanoparticle deposited graphene/mesoporous MnOx nanocomposite for high performance super capacitor application. *Int J Hydrogen Energy* 43:17121–17131. <https://doi.org/10.1016/j.ijhydene.2018.07.061>
- Ren L et al (2015) Three-dimensional tubular MoS₂/PANI hybrid electrode for high rate performance supercapacitor. *ACS Appl Mater Interfaces* 7:28294–28302. <https://doi.org/10.1021/acsami.5b08474>
- Salanne M et al (2016) Efficient storage mechanisms for building better supercapacitors. *Nat Energy* 1:16070. <https://doi.org/10.1038/nenergy.2016.70>
- Salarizadeh P et al (2020) Synergistic effect of MoS₂ and Fe₃O₄ decorated reduced graphene oxide as a ternary hybrid for high-performance and stable asymmetric supercapacitors. *Nanotechnology* 31:435401. <https://doi.org/10.1088/1361-6528/aba1bd>
- Samadi M et al (2018) Group 6 transition metal dichalcogenide nanomaterials: synthesis, applications and future perspectives. *Nanoscale Horizons* 3:90–204. <https://doi.org/10.1039/C7NH00137A>
- Sangeetha DN et al (2020) Flower-like carbon doped MoS₂/Activated carbon composite electrode for superior performance of supercapacitors and hydrogen evolution reactions. *J Alloys Compd* 831:154745. <https://doi.org/10.1016/j.jallcom.2020.154745>
- Sangeetha DN, Selvakumar M (2018) Active-defective activated carbon/MoS₂ composites for supercapacitor and hydrogen evolution reactions. *Appl Surf Sci* 453:132–140. <https://doi.org/10.1016/j.apsusc.2018.05.033>
- Sari FNI, Ting J-M (2018) MoS₂/MoOx-Nanostructure-Decorated Activated Carbon Cloth for Enhanced Supercapacitor Performance. *Chemsuschem* 11:897–906. <https://doi.org/10.1002/cssc.201702295>
- Sarkar D et al (2019) Expanding interlayer spacing in MoS₂ for realizing an advanced supercapacitor. *ACS Energy Lett* 4:1602–1609. <https://doi.org/10.1021/acscenergylett.9b00983>
- Sarwar S et al (2020) Facile microwave approach towards high performance MoS₂/graphene nanocomposite for hydrogen evolution reaction. *Sci China Mater* 63:62–74. <https://doi.org/10.1007/s40843-019-9555-0>
- Savjani N et al (2016) Synthesis of lateral size-controlled monolayer 1H-MoS₂@Oleylamine as supercapacitor electrodes. *Chem Mater* 28:657–664. <https://doi.org/10.1021/acs.chemmater.5b04476>
- Scrosati B et al (2011) Lithium-ion batteries. A look into the future. *Energy Environ Sci* 4:3287–3295. <https://doi.org/10.1039/C1EE01388B>
- Seifert G et al (2000) Structure and electronic properties of MoS₂ nanotubes. *Phys Rev Lett* 85:146. <https://doi.org/10.1103/PhysRevLett.85.146>
- Shanker U et al (2017) Degradation of hazardous organic dyes in water by nanomaterials. *Environ Chem Lett* 15:623–642. <https://doi.org/10.1007/s10311-017-0650-2>
- Shen H et al (2017) Influence of interface combination of RGO-photosensitized SnO₂@RGO core-shell structures on their photocatalytic performance. *Appl Surf Sci* 391:627–634. <https://doi.org/10.1016/j.apsusc.2016.06.031>
- Shen X et al (2018) Beyond lithium ion batteries: higher energy density battery systems based on lithium metal anodes. *Energy Storage Mater* 12:161–175. <https://doi.org/10.1016/j.ensm.2017.12.002>
- Sheng B et al (2019) Pivotal roles of MoS₂ in boosting catalytic degradation of aqueous organic pollutants by Fe (II)/PMS. *Chem Eng J* 375:121989. <https://doi.org/10.1016/j.cej.2019.121989>
- Shi J et al (2016) Recent advances in controlling syntheses and energy related applications of MX₂ and MX₂/graphene heterostructures. *Adv Energy Mater* 6:1600459. <https://doi.org/10.1002/aenm.201600459>
- Shi L et al (2018) MoS₂ quantum dots embedded in g-C₃N₄ frameworks: a hybrid 0D–2D heterojunction as an efficient visible-light driven photocatalyst. *Appl Surf Sci* 457:30–40. <https://doi.org/10.1016/j.apsusc.2018.06.132>
- Sillanpää M et al (2018) Removal of natural organic matter in drinking water treatment by coagulation: a comprehensive review. *Chemosphere* 190:54–71. <https://doi.org/10.1016/j.chemosphere.2017.09.113>
- Simon P, Gogotsi Y (2020) Perspectives for electrochemical capacitors and related devices. *Nat Mater* 19:1151–1163. <https://doi.org/10.1038/s41563-020-0747-z>
- Singh S et al (2021) Mechanism and kinetics of adsorption and removal of heavy metals from wastewater using nanomaterials. *Environ Chem Lett* 19:2351–2381. <https://doi.org/10.1007/s10311-021-01196-w>
- Singh-Miller NE, Marzari N (2009) Surface energies, work functions, and surface relaxations of low-index metallic surfaces from first principles. *Phys Rev B* 80:235407. <https://doi.org/10.1103/PhysRevB.80.235407>
- Smith RJ et al (2011) Large-scale exfoliation of inorganic layered compounds in aqueous surfactant solutions. *Adv Mater* 23:3944–3948. <https://doi.org/10.1002/adma.201102584>
- Solomon G et al (2020) Microwave-assisted vs. conventional hydrothermal synthesis of MoS₂ nanosheets: application towards hydrogen evolution reaction. *Curr Comput-Aided Drug Des* 10:1040. <https://doi.org/10.3390/cryst10111040>
- Song I et al (2015) Synthesis and properties of molybdenum disulfide: from bulk to atomic layers. *RSC Adv* 5:7495–7514. <https://doi.org/10.1039/C4RA11852A>

- Soon JM, Loh KP (2007) Electrochemical Double-Layer Capacitance of MoS₂ Nanowall Films. *Electrochem Solid State Lett* 10:A250. <https://doi.org/10.1149/1.2778851>
- Splendiani A et al (2010) Emerging photoluminescence in monolayer MoS₂. *Nano Lett* 10:1271–1275. <https://doi.org/10.1021/nl903868w>
- Subramanian S et al (2020) Photophysics and electronic structure of lateral graphene/MoS₂ and metal/MoS₂ junctions. *ACS Nano* 14:16663–16671. <https://doi.org/10.1021/acsnano.0c02527>
- Sudha V, Sangaranarayanan MV (2002) Underpotential deposition of metals: structural and thermodynamic considerations. *J Phys Chem B* 106:2699–2707. <https://doi.org/10.1021/jp013544b>
- Sun G et al (2015) Hybrid Fibers Made of Molybdenum Disulfide, Reduced Graphene Oxide, and Multi-Walled Carbon Nanotubes for Solid-State, Flexible, Asymmetric Supercapacitors. *Angew Chem Int Edn* 54:4651–4656. <https://doi.org/10.1002/anie.20141533>
- Sun T et al (2016) Facile construction of 3D graphene/MoS₂ composites as advanced electrode materials for supercapacitors. *J Power Sources* 331:180–188. <https://doi.org/10.1016/j.jpowsour.2016.09.036>
- Sun T et al (2017) Graphene-wrapped CNT@MoS₂ hierarchical structure: synthesis, characterization and electrochemical application in supercapacitors. *New J Chem* 41:7142–7150. <https://doi.org/10.1039/C7NJ00623C>
- Sun D et al (2018) MoS₂/Graphene nanosheets from commercial bulky MoS₂ and graphite as anode materials for high rate sodium-Ion batteries. *Adv Energy Mater* 8:1702383. <https://doi.org/10.1002/aenm.201702383>
- Sun G et al (2019) Molybdenum disulfide nanoflowers mediated anti-inflammatory macrophage modulation for spinal cord injury treatment. *J Colloid Interface Sci* 549:50–62. <https://doi.org/10.1016/j.jcis.2019.04.047>
- Swain G et al (2018) Fabrication of hierarchical two-dimensional MoS₂ nanoflowers decorated upon cubic CaIn₂S₄ microflow-ers: facile approach to construct novel metal-free p–n heterojunction semiconductors with superior charge separation efficiency. *Inorg Chem* 57:10059–10071. <https://doi.org/10.1021/acs.inorgchem.8b01221>
- Tan C et al (2017) Recent advances in ultrathin two-dimensional nano-materials. *Chem Rev* 117:6225–6331. <https://doi.org/10.1021/acs.chemrev.6b00558>
- Tang G et al (2013) Hydrothermal synthesis and characterization of novel flowerlike MoS₂ hollow microspheres. *Mater Lett* 100:15–18. <https://doi.org/10.1016/j.matlet.2013.02.103>
- Tang H et al (2015) Growth of polypyrrole ultrathin films on MoS₂ monolayers as high-performance supercapacitor electrodes. *Adv Mater* 27:1117–1123. <https://doi.org/10.1002/adma.201404622>
- Tang W et al (2009) A grid-based Bader analysis algorithm without lattice bias. *J Phys Condens Matter* 21:084204. <https://doi.org/10.1088/0953-8984/21/8/084204>
- Tang D-M et al (2014) Nanomechanical cleavage of molybdenum disulphide atomic layers. *Nat Commun* 5:1–8. <https://doi.org/10.1038/ncomms4631>
- Teng Y et al (2016) MoS₂ nanosheets vertically grown on graphene sheets for lithium-ion battery anodes. *ACS Nano* 10:8526–8535. <https://doi.org/10.1021/acsnano.6b03683>
- Thakur AK et al (2017) Facile synthesis and electrochemical evaluation of PANI/CNT/MoS₂ ternary composite as an electrode material for high performance supercapacitor. *Mater Sci Eng B* 223:24–34. <https://doi.org/10.1016/j.mseb.2017.05.001>
- Thangappan R et al (2016) Graphene decorated with MoS₂ nanosheets: a synergetic energy storage composite electrode for supercapacitor applications. *Dalton Trans* 45:2637–2646. <https://doi.org/10.1039/C5DT04832J>
- Tian Y et al (2005) A facile route to synthesis of MoS₂ nanorods. *Mater Lett* 59:3452–3455. <https://doi.org/10.1016/j.matlet.2005.06.012>
- Tian Y et al (2020) Interface guide: In-situ integrating MoS₂ nanosheets into highly ordered polypyrrole film for high performance flexible supercapacitor electrodes. *Comp Sci Technol* 197:108263. <https://doi.org/10.1016/j.compscitech.2020.108263>
- Toh RJ et al (2017) 3R phase of MoS₂ and WS₂ outperforms the corresponding 2H phase for hydrogen evolution. *Chem Commun* 53:3054–3057. <https://doi.org/10.1039/C6CC09952A>
- Varrla E et al (2015) Large-scale production of size-controlled MoS₂ nanosheets by shear exfoliation. *Chem Mater* 27:1129–1139. <https://doi.org/10.1021/cm5044864>
- Vatamanu J et al (2015) Tailoring graphene-based electrodes from semiconducting to metallic to increase the energy density in supercapacitors. *Nanotechnology* 26:464001. <https://doi.org/10.1088/0957-4484/26/46/464001>
- Vattikuti SP, Byon C (2016) Bi₂S₃ nanorods embedded with MoS₂ nanosheets composite for photodegradation of phenol red under visible light irradiation. *Superlattices Microstruct* 100:514–525. <https://doi.org/10.1016/j.spmi.2016.10.012>
- Wan Z et al (2014) Core-shell structure of hierarchical quasi-hollow MoS₂ microspheres encapsulated porous carbon as stable anode for Li-ion batteries. *Small* 10:4975–4981. <https://doi.org/10.1002/sml.201401286>
- Wang D et al (2018) Kelp-like structured NiCo₂S₄-C-MoS₂ composite electrodes for high performance supercapacitor. *J Alloys Compd* 735:1505–1513. <https://doi.org/10.1016/j.jallcom.2017.11.249>
- Wang H et al (2020a) Improved preparation of MoS₂/graphene composites and their inks for supercapacitors applications. *Mater Sci Eng B* 262:114700. <https://doi.org/10.1016/j.mseb.2020.114700>
- Wang F et al (2020b) MoS₂/corn-cob-derived activated carbon for supercapacitor application. *Mater Chem Phys* 244:122215. <https://doi.org/10.1016/j.matchemphys.2019.122215>
- Wang Z, Mi B (2017) Environmental applications of 2D molybdenum disulfide (MoS₂) nanosheets. *Environ Sci Technol* 51:8229–8244. <https://doi.org/10.1021/acs.est.7b01466>
- Wang Y, Xie Y (2020) Electroactive FeS₂-modified MoS₂ nanosheet for high-performance supercapacitor. *J Alloys Compd* 824:153936. <https://doi.org/10.1016/j.jallcom.2020.153936>
- Wang QH et al (2012) Electronics and optoelectronics of two-dimensional transition metal dichalcogenides. *Nat Nanotechnol* 7:699–712. <https://doi.org/10.1038/nnano.2012.193>
- Wang X et al (2014a) High supercapacitor and adsorption behaviors of flower-like MoS₂ nanostructures. *J Mater Chem A* 2:15958–15963. <https://doi.org/10.1039/C4TA03044C>
- Wang Y et al (2014b) Pre-lithiation of onion-like carbon/MoS₂ nano-urchin anodes for high-performance rechargeable lithium ion batteries. *Nanoscale* 6:8884–8890. <https://doi.org/10.1039/C4NR01553C>
- Wang H et al (2015) Physical and chemical tuning of two-dimensional transition metal dichalcogenides. *Chem Soc Rev* 44:2664–2680. <https://doi.org/10.1039/C4CS00287C>
- Wang Z et al (2016a) Large-scale and controllable synthesis of graphene quantum dots from rice husk biomass: a comprehensive utilization strategy. *ACS Appl Mater Interfaces* 8:1434–1439. <https://doi.org/10.1021/acsmi.5b10660>
- Wang Y et al (2016b) MoS₂-coated vertical graphene nanosheet for high-performance rechargeable lithium-ion batteries and hydrogen production. *NPG Asia Mater* 8:e268–e268. <https://doi.org/10.1038/am.2016.44>
- Wang D et al (2017a) Phase engineering of a multiphase 1T/2H MoS₂ catalyst for highly efficient hydrogen evolution. *J Mater Chem A* 5:2681–2688. <https://doi.org/10.1039/C6TA09409K>
- Wang D et al (2017b) Swollen ammoniated MoS₂ with 1T/2H hybrid phases for high-rate electrochemical energy storage.

- ACS Sustain Chem Eng 5:2509–2515. <https://doi.org/10.1021/acssuschemeng.6b02863>
- Wang K et al (2017c) General solution-processed formation of porous transition-metal oxides on exfoliated molybdenum disulfides for high-performance asymmetric supercapacitors. *J Mater Chem A* 5:11236–11245. <https://doi.org/10.1039/C7TA01457K>
- Wang Y et al (2018) Effect of sulfur source on photocatalytic degradation performance of CdS/MoS₂ prepared with one-step hydrothermal synthesis. *J Environ Sci* 65:347–355. <https://doi.org/10.1016/j.jes.2017.07.004>
- Wang S et al (2019) All-solid-state supercapacitors from natural lignin-based composite film by laser direct writing. *Appl Phys Lett* 115:083904. <https://doi.org/10.1063/1.5118340>
- Wang L et al (2020) Carbon nanobowls filled with MoS₂ nanosheets as electrode materials for supercapacitors. *ACS Appl Nano Mater* 3:6448–6459. <https://doi.org/10.1021/acsnm.0c00924>
- Wazir MB et al (2019) Synergistic properties of molybdenum disulfide (MoS₂) with electro-active materials for high-performance supercapacitors. *Int J Hydrogen Energy* 44:17470–17492. <https://doi.org/10.1016/j.ijhydene.2019.04.265>
- Wu ZS et al (2013) Graphene-based in-plane micro-supercapacitors with high power and energy densities. *Nat Commun* 4:2487. <https://doi.org/10.1038/ncomms3487>
- Wu X et al (2017) Stabilizing the MXenes by carbon nanoplating for developing hierarchical nanohybrids with efficient lithium storage and hydrogen evolution capability. *Adv Mater* 29:1607017. <https://doi.org/10.1002/adma.201607017>
- Xia D et al (2018) Molybdenum and tungsten disulfides-based nanocomposite films for energy storage and conversion: a review. *Chem Eng J* 348:908–928. <https://doi.org/10.1016/j.cej.2018.04.207>
- Xiang K et al (2019) Rational fabrication of nitrogen and sulfur codoped carbon nanotubes/MoS₂ for high-performance lithium-sulfur batteries. *Chemsuschem* 12:3602–3614. <https://doi.org/10.1002/cssc.201900929>
- Xiao Y et al (2017a) The application of metal sulfides in sodium ion batteries. *Adv Energy Mater* 7:1601329. <https://doi.org/10.1002/aenm.201601329>
- Xiao H et al (2017b) Interlayer expanded molybdenum disulfide nanosheets assembly for electrochemical supercapacitor with enhanced performance. *Mater Chem Phys* 192:100–107. <https://doi.org/10.1016/j.matchemphys.2017.01.077>
- Xiao Z et al (2020) Adsorption of NO₂ on monolayer MoS₂ doped with Fe Co, and Ni, Cu: a computational investigation. *Chem Hys Letters*. 755:137768. <https://doi.org/10.1016/j.cplett.2020.137768>
- Xiao F-X et al (2014) Spatially branched hierarchical ZnO nanorod-TiO₂ nanotube array heterostructures for versatile photocatalytic and photoelectrocatalytic applications: towards intimate integration of 1D–1D hybrid nanostructures. *Nanoscale* 6:14950–14961. <https://doi.org/10.1039/C4NR04886E>
- Xing M et al (2018) Metal sulfides as excellent co-catalysts for H₂O₂ decomposition in advanced oxidation processes. *Chem* 4:1359–1372. <https://doi.org/10.1016/j.chempr.2018.03.002>
- Xing T et al (2020) Free-standing ternary metallic sulphides/Ni/C-nanofiber anodes for high-performance lithium-ion capacitors. *J Energy Chem* 42:108–115. <https://doi.org/10.1016/j.jechem.2019.06.002>
- Xu Z et al (2017) MoO₂@MoS₂ Nanoarchitectures for High-Loading Advanced Lithium-Ion Battery Anodes. *Part Part Syst Char* 34:1600223. <https://doi.org/10.1002/ppsc.201600223>
- Xu X et al (2014) Fabrication of MoS₂ nanosheet@ TiO₂ nanotube hybrid nanostructures for lithium storage. *Nanoscale* 6:5245–5250. <https://doi.org/10.1039/C3NR06736J>
- Xu J et al (2020) Recent progress in electrode materials for nonaqueous lithium-ion capacitors. *J Nanosci Nanotechnol* 20:2652–2667. <https://doi.org/10.1166/jnn.2020.17475>
- Xuan D et al (2017) Sodium alginate-assisted exfoliation of MoS₂ and its reinforcement in polymer nanocomposites. *Carbohydr Polym* 155:40–48. <https://doi.org/10.1016/j.carbpol.2016.08.052>
- Yang L et al (2013) Hierarchical MoS₂/polyaniline nanowires with excellent electrochemical performance for lithium-ion batteries. *Adv Mater* 25:1180–1184. <https://doi.org/10.1002/adma.201203999>
- Yang M et al (2015) Nitrogen-doped carbon-coated molybdenum disulfide nanosheets for high-performance supercapacitor. *Synth Met* 209:528–533. <https://doi.org/10.1016/j.synthmet.2015.09.007>
- Yang X et al (2017) Arrays of hierarchical nickel sulfides/MoS₂ nanosheets supported on carbon nanotubes backbone as advanced anode materials for asymmetric supercapacitor. *J Power Sources* 343:373–382. <https://doi.org/10.1016/j.jpowsour.2017.01.078>
- Yang X et al (2021) NiS₂/MoS₂ mixed phases with abundant active edge sites induced by sulfidation and graphene introduction towards high-rate supercapacitors. *Chemical Eng J* 406:126713. <https://doi.org/10.1016/j.cej.2020.126713>
- Yang W, Wang Y (2021) Enhanced electron and mass transfer flow-through cell with C₃N₄-MoS₂ supported on three-dimensional graphene photoanode for the removal of antibiotic and antibacterial potencies in ampicillin wastewater. *Appl Catal B Environ* 282:119574. <https://doi.org/10.1016/j.apcatb.2020.119574>
- Yang X et al (2013) Liquid-mediated dense integration of graphene materials for compact capacitive energy storage. *Science* 341:534–537. <https://doi.org/10.1126/science.1239089>
- Yang C et al (2016) Rational synthesis of carbon shell coated polyaniline/MoS₂ monolayer composites for high-performance supercapacitors. *Nano Res* 9:951–962. <https://doi.org/10.1007/s12274-016-0983-3>
- Yang P et al (2018) Batch production of 6-inch uniform monolayer molybdenum disulfide catalyzed by sodium in glass. *Nat Commun* 9:1–10. <https://doi.org/10.1038/s41467-018-03388-5>
- Yang P et al (2019) Thickness tunable wedding-cake-like MoS₂ flakes for high-performance optoelectronics. *ACS Nano* 13:3649–3658. <https://doi.org/10.1021/acsnano.9b00277>
- Yao Y et al (2012) Large-scale production of two-dimensional nanosheets. *J Mater Chem* 22:13494–13499. <https://doi.org/10.1039/C2JM30587A>
- Yin W et al (2020) Synthesis of tungsten disulfide and molybdenum disulfide quantum dots and their applications. *Chem Mater* 32:4409–4424. <https://doi.org/10.1021/acs.chemmater.0c01441>
- Yoo S et al (2009) On the phase diagram of water with density functional theory potentials: the melting temperature of ice I_h with the Perdew–Burke–Ernzerhof and Becke–Lee–Yang–Parr functionals. *Am Inst Phys*. <https://doi.org/10.1063/1.3153871>
- Yu L et al (2014) Graphene/MoS₂ hybrid technology for large-scale two-dimensional electronics. *Nano Lett* 14:3055–3063. <https://doi.org/10.1021/nl404795z>
- Yu H et al (2017) Wafer-scale growth and transfer of highly-oriented monolayer MoS₂ continuous films. *ACS Nano* 11:12001–12007. <https://doi.org/10.1021/acsnano.7b03819>
- Yuan H et al (2019) Sulfur redox reactions at working interfaces in lithium–sulfur batteries: a perspective. *Adv Mater Interfaces* 6:1802046. <https://doi.org/10.1002/admi.201802046>
- Yuwen L et al (2016) Rapid preparation of single-layer transition metal dichalcogenide nanosheets via ultrasonication enhanced lithium intercalation. *Chem Commun* 52:529–532. <https://doi.org/10.1039/C5CC07301D>
- Zeng Z et al (2011) Single-layer semiconducting nanosheets: high-yield preparation and device fabrication. *Angew Chem* 123:11289–11293. <https://doi.org/10.1002/ange.201106004>

- Zeng Y et al (2019a) Construction of flower-like MoS₂/Ag₂S/Ag Z-scheme photocatalysts with enhanced visible-light photocatalytic activity for water purification. *Sci Total Environ* 659:20–32. <https://doi.org/10.1016/j.scitotenv.2018.12.333>
- Zeng R et al (2019b) covalent connection of polyaniline with MoS₂ nanosheets toward ultrahigh rate capability supercapacitors. *ACS Sustain Chem Eng* 7:11540–11549. <https://doi.org/10.1021/acssuschemeng.9b01442>
- Zhang Y et al (2015) One-Pot Synthesis of Tunable Crystalline Ni₃S₄@Amorphous MoS₂ Core/Shell Nanospheres for High-Performance Supercapacitors. *Small* 11:3694–3702. <https://doi.org/10.1002/sml.201403772>
- Zhang X et al (2016) 3D MoS₂ nanosheet/TiO₂ nanofiber heterostructures with enhanced photocatalytic activity under UV irradiation. *J Alloys Compd* 686:137–144. <https://doi.org/10.1016/j.jallcom.2016.05.336>
- Zhang Z et al (2020) Synthesis of flower-like MoS₂/g-C₃N₄ nanosheet heterojunctions with enhanced photocatalytic reduction activity of uranium(VI). *Appl Surf Sci* 520:146352. <https://doi.org/10.1016/j.apsusc.2020.146352>
- Zhang LL, Zhao XS (2009) Carbon-based materials as supercapacitor electrodes. *Chem Soc Rev* 38:2520–2531. <https://doi.org/10.1039/B813846J>
- Zhang S et al (2017a) Photocatalytic wastewater purification with simultaneous hydrogen production using MoS₂ QD-decorated hierarchical assembly of ZnIn₂S₄ on reduced graphene oxide photocatalyst. *Water Res* 121:11–19. <https://doi.org/10.1016/j.watres.2017.05.013>
- Zhang Z et al (2017b) Noncovalent functionalization of monolayer MoS₂ with carbon nanotubes: tuning electronic structure and photocatalytic activity. *J Phys Chem C* 121:21921–21929. <https://doi.org/10.1021/acs.jpcc.7b06793>
- Zhang X et al (2018a) Controllable growth of MoS₂ nanosheets on novel Cu₂S snowflakes with high photocatalytic activity. *Appl Catal B* 232:355–364. <https://doi.org/10.1016/j.apcatb.2018.03.074>
- Zhang G et al (2018b) SnS₂/SnO₂ heterostructured nanosheet arrays grown on carbon cloth for efficient photocatalytic reduction of Cr (VI). *J Colloid Interface Sci* 514:306–315. <https://doi.org/10.1016/j.jcis.2017.12.045>
- Zhang L et al (2018c) Enhanced photocatalytic activity of CdS/SnS₂ nanocomposite with highly-efficient charge transfer and visible light utilization for selective reduction of 4-nitroaniline. *J Colloid Interface Sci* 532:557–570. <https://doi.org/10.1016/j.jcis.2018.08.017>
- Zhang H et al (2019a) Macroporous MoS₂/carbon hybrid film with superior ion/electron conductivity for superhigh areal capacity Li-ion batteries. *Chem Eng Sci* 207:611–618. <https://doi.org/10.1016/j.ces.2019.06.043>
- Zhang Y et al (2019b) Synergistic electrocatalysis of polysulfides by a nanostructured VS₄-carbon nanofiber functional separator for high-performance lithium–sulfur batteries. *J Mater Chem A* 7:16812–16820. <https://doi.org/10.1039/C9TA03516H>
- Zhang Y et al (2020a) Insight into l-cysteine-assisted growth of Cu₂S nanoparticles on exfoliated MoS₂ nanosheets for effective photo-reduction removal of Cr (VI). *Appl Surf Sci* 518:146191. <https://doi.org/10.1016/j.apsusc.2020.146191>
- Zhang S et al (2020b) In situ sulfur-doped graphene nanofiber network as efficient metal-free electrocatalyst for polysulfides redox reactions in lithium–sulfur batteries. *J Energy Chem* 47:281–290. <https://doi.org/10.1016/j.jechem.2020.01.033>
- Zhang M et al (2021) DFT calculation of square MoS₂ nanotubes. *Phys E* 130:114693. <https://doi.org/10.1016/j.physe.2021.114693>
- Zhao C et al (2018) Facile construction of MoS₂/RCF electrode for high-performance supercapacitor. *Carbon* 127:699–706. <https://doi.org/10.1016/j.carbon.2017.11.052>
- Zhao G et al (2020) Biocarbon based template synthesis of uniform lamellar MoS₂ nanoflowers with excellent energy storage performance in lithium-ion battery and supercapacitors. *Electrochim Acta* 331:135262. <https://doi.org/10.1016/j.electacta.2019.135262>
- Zheng L et al (2019) Core-shell structured MoS₂@Mesoporous hollow carbon spheres nanocomposite for supercapacitors applications with enhanced capacitance and energy density. *Electrochim Acta* 298:630–639. <https://doi.org/10.1016/j.electacta.2018.12.126>
- Zheng N et al (2003) Synthetic design of crystalline inorganic chalcogenides exhibiting fast-ion conductivity. *Nature* 426:428–432. <https://doi.org/10.1038/nature02159>
- Zheng J et al (2014) High yield exfoliation of two-dimensional chalcogenides using sodium naphthalenide. *Nat Commun* 5:1–7. <https://doi.org/10.1038/ncomms3995>
- Zhou R et al (2017) Hierarchical MoS₂-coated three-dimensional graphene network for enhanced supercapacitor performances. *J Power Sources* 352:99–110. <https://doi.org/10.1016/j.jpowsour.2017.03.134>
- Zhou H et al (2020) Molybdenum disulfide (MoS₂): A versatile activator of both peroxy monosulfate and persulfate for the degradation of carbamazepine. *Chem Eng J* 384:123264. <https://doi.org/10.1016/j.cej.2019.123264>
- Zhu J et al (2015) Multifunctional architectures constructing of pani nanoneedle arrays on mos₂ thin nanosheets for high-energy supercapacitors. *Small* 11:4123–4129. <https://doi.org/10.1002/sml.201403744>
- Zhu M et al (2019) High yield and concentration exfoliation of defect-free 2D nanosheets via gentle water freezing–thawing approach and stabilization with PVP. *Mater Res Express* 6:1150c9. <https://doi.org/10.1088/2053-1591/ab2de3>
- Zhu L et al (2020) Scalable salt-templated directed synthesis of high-quality MoS₂ nanosheets powders towards energetic and environmental applications. *Nano Res* 13:3098–3104. <https://doi.org/10.1007/s12274-020-2979-2>
- Zou X et al (2020) MoS₂/RGO composites for photocatalytic degradation of ranitidine and elimination of NDMA formation potential under visible light. *Chem Eng J* 383:123084. <https://doi.org/10.1016/j.cej.2019.123084>

Publisher's Note Springer Nature remains neutral with regard to jurisdictional claims in published maps and institutional affiliations.